Impaired mRNA splicing and proteostasis in preadipocytes in obesity-related metabolic disease

Julia Sánchez-Ceinos[1,2], Rocío Guzmán-Ruiz[1,2*], Oriol A. Rangel-Zúñiga[2,3], Elena Moreno-Caño[1], Mercedes del Río-Moreno[2,4], Elsa Maymo-Masip[5], Joan Vendrell[5], Sonia Fernández-Veledo[5], Jurga Laurencikiene[6], Mikael Rydén[6], Antonio Membrives[7], Raúl M. Luque[2,4], José López-Miranda[2,3], and María M. Malagón[1,2*]

[1]Department of Cell Biology, Physiology, and Immunology, Instituto Maimónides de Investigación Biomédica de Córdoba (IMIBIC)/University of Córdoba/Reina Sofia University Hospital, 14014 Córdoba, Spain. [2]CIBER Fisiopatología de la Obesidad y Nutrición (CIBERobn), Instituto de Salud Carlos III, Spain. [3]Lipids and Atherosclerosis Unit, Department of Internal Medicine, IMIBIC/Reina Sofia University Hospital/University of Córdoba, 14004, Spain. [4]OncObesity and Metabolism Group. Department of Cell Biology, Physiology and Immunology, IMIBIC/University of Cordoba/Reina Sofía University Hospital. Córdoba, 14004, Spain. [5]Hospital Universitari de Tarragona Joan XXIII, Institut d´Investigació Sanitària Pere Virgili Universitat Rovira i Virgili, Tarragona, Spain; CIBER de Diabetes y Enfermedades Metabólicas Asociadas (CIBERdem), Instituto de Salud Carlos III, Madrid, Spain.[6]Lipid Laboratory. Department of Medicine Huddinge/Karolinska Institute (KI)/Karolinska University Hospital. Stockholm, 14186, Sweden. [7]Unidad de Gestión Clínica de Cirugía General y Digestivo. Sección de Obesidad. IMIBIC/Reina Sofia University Hospital, Córdoba, 14004, Spain.

***For correspondence:**

Dr. María M. Malagón, Department of Cell Biology, Physiology, and Immunology, IMIBIC//University of Córdoba/Reina Sofia University Hospital, 14004 Córdoba, Spain, Tel: +34-957213777; E-mail: bc1mapom@uco.es. ORCID iD: 0000-0002-2419-2727.

Dr. Rocío Guzmán-Ruiz, Department of Cell Biology, Physiology, and Immunology, IMIBIC//University of Córdoba/Reina Sofia University Hospital, 14004 Córdoba, Spain, Tel: +34-957213778; E-mail: bc2gurur@uco.es. ORCID iD: 0000-0001-8020-4676.

Abstract Preadipocytes are crucial for healthy adipose tissue expansion. Preadipocyte differentiation is altered in obese individuals, which has been proposed to contribute to obesity-associated metabolic disturbances. Here, we demonstrate that impaired alternative splicing and dysregulated endoplasmic reticulum (ER)-associated protein degradation (ERAD) represent marker pathways of dysfunctional preadipocytes in obese individuals with insulin resistance (IR)/type 2 diabetes (T2D). Down-regulation of a key member of the major spliceosome, *PRFP8*/PRP8, as observed in IR/T2D preadipocytes from subcutaneous (SC) fat, prevented adipogenesis by altering both the expression and splicing patterns of adipogenic transcription factors and lipid droplet-related proteins, while adipocyte differentiation was restored upon recovery of *PRFP8*/PRP8 normal levels. Adipocyte differentiation was also compromised under conditions of ERAD hyperactivation, as occurs in SC and omental (OM) preadipocytes in IR/T2D obesity. Thus, targeting mRNA splicing and ER proteostasis in preadipocytes could improve adipose tissue function and thus contribute to metabolic health in obese individuals.

Introduction

Adipose precursor cells, the preadipocytes, are essential for the maintenance of adipose tissue homeostasis, regeneration, and expansion (***Berry et al., 2016***). Preadipocytes differentiation into adipocytes, i.e. adipogenesis, enables adipocyte turnover and adipose tissue growth and ensures adipose tissue plasticity to accommodate surplus energy ***(Arner et al., 2010; Sarjeant and Stephens, 2019***; ***Spalding et al., 2008***). It has been proposed that the inability for recruiting new adipose cells together with the functional impairment of hypertrophied adipocytes that occur in obesity contribute to lipid spillover from the adipose tissue (***Lessard and Tchernof, 2012***). Ectopic fat deposition and lipotoxicity in non-adipose organs have been associated with the development of insulin resistance (IR) and type 2 diabetes (T2D) (***Engin and Engin, 2017***). Thus, increasing adipogenesis appears as a valuable strategy to facilitate healthy adipose tissue expansion and ensure metabolic health (***Ghaben and Scherer, 2019***).

Adipocyte differentiation involves striking changes in size, metabolism, and responsiveness to signals. This process, in turn, relies on major changes in gene expression programs regulating mRNA and protein production (***de Sá et al., 2017***). An Increasing body of evidence shows that mRNA processing and, in particular, alternative splicing, is crucial for genome reprogramming during cell differentiation ***(Fiszbein and Kornblihtt, 2017***). In this line, the recent identification of PPARγ protein variants with opposing effects on preadipocyte differentiation, supports a role for alternative splicing in adipogenesis ***(Aprile et al., 2018***, ***2014***). However, the splicing components relevant to adipogenesis and the cellular events regulated by alternative splicing during adipocyte

differentiation have been scarcely explored (***Lin, 2015***), and it is yet to be established whether alternative splicing is modified in human obesity.

Another crucial mechanism preserving precursor cell function relates to protein homeostasis (i.e., proteostasis), which maintains the capacity of cells to expand in order to sustain tissue growth and regeneration (***Noormohammadi et al., 2018***). Several lines of evidence support an important role for the endoplasmic reticulum (ER) protein quality control system in the regulation of adipogenesis (***Lowe et al., 2011***). In fact, the unfolded protein response (UPR) is perturbed in the obese adipose tissue and has been proposed to contribute to the pathology of obesity (***Yilmaz, 2017***). By contrast, it is still unknown whether the other component of the protein control system, the ER-associated protein degradation (ERAD), which is crucial for protecting cells against accumulation of misfolded/unfolded proteins and proteotoxicity ***(Hwang and Qi, 2018***), is altered in the obese adipose tissue. Importantly, genetic ablation of the core ERAD protein, SEL1L, in mouse adipocytes causes lipodystrophy and postprandial hyperlipidaemia (***Sha et al., 2014***).

Here, we set out an iTRAQ-LC-MS/MS proteomic approach for the analysis of subcutaneous (SC) and omental (OM) preadipocytes from obese individuals with normoglycaemia (NG) and T2D in order to identify altered molecular pathways that may contribute to metabolic disease in obesity. Down-regulation of multiple components of the splicing machinery was observed in SC preadipocytes from obese individuals with insulin resistance (IR) or T2D, as compared to NG obesity. This, together with the observation that adipogenesis can be modulated by regulating the expression levels of a key spliceosome component, *PRFP8*/PRP8, support a role for alternative splicing in the development of obesity-associated

metabolic complications. In addition, our studies show that not only the UPR but also the ERAD system are altered in human SC and OM preadipocytes from IR/T2D obese subjects, and that this condition (i.e., hyperactivated ERAD), when mimicked *in vitro*, prevented adipogenesis. Our results provide novel mechanistic explanations for the impaired adipogenic capacity observed in IR/T2D obesity that relates to both mRNA and ER-proteostasis disturbance.

Results

Preadipocytes display distinct features in obesity-related IR/T2D

Preadipocytes from SC and OM adipose tissue were isolated from 69 morbidly obese subjects (BMI <40 kg/m^2) (hereinafter referred to as obese individuals) (***Table 1***), who were subclassified into three groups [normoglycemic (NG Obese): Glucose <100 mg/dL, HbA1c <5.7 %; impaired fasting glucose (IFG Obese): Glucose 100-126 mg/dL, HbA1c 5.7-6.5 %; and with type 2 diabetes (T2D Obese): Glucose >126 mg/dL, HbA1c >6.5 %], according to the criteria of the American Diabetes Association (***ADA, 2020***). IFG individuals exhibited significantly higher HOMA-IR values than NG individuals and they will be referred to as insulin-resistant (IR) subjects (***Díaz-Ruiz et al., 2015***; ***Tam et al., 2012***). No significant differences were found among groups in blood pressure, inflammation, or lipid parameters except triglycerides, whose levels were enhanced in T2D *vs.* NG obese groups.

Paired SC and OM adipose tissue samples were processed for the isolation of the stroma-vascular fraction (SVF) and mature adipocytes. Microscopic analysis

of freshly isolated mature adipocytes revealed that these cells were larger in IR/T2D than in NG obese individuals (***Figure 1—Figure supplement 1A***).

SC and OM preadipocytes were obtained after serial passaging (2-3 passages) of the corresponding SVFs following established methods (***Bunnell et al., 2008***; ***Palumbo et al., 2018***; ***Serena et al., 2016***; ***Zhu et al., 2013***). The purity of the preadipocyte cultures was confirmed by the presence of preadipocyte markers (DLK1/PREF1, ADIPOQ, CCL2, FABP4, PDGFRA, PPARγ, TGFβ2, UPK3B) and the absence of blood cell markers (CD45, CD14) (***Figure supplements 1B*** and ***1C***). Expression levels of the proliferation marker, *KI67*, and the proliferation rate, as assessed by cell count, were higher in SC than in OM preadipocytes, and both parameters decreased in IR/T2D (***Figure supplements 1D and 1E***). Preadipocyte proliferation rate negatively correlated with obesity and IR markers (BMI, glucose, insulin, and HbA1c) (***Supplementary file 1***).

Microscopic observation of lipid droplets (LDs) showed that both SC and OM preadipocytes from NG obese subjects differentiated well, while those from IR/T2D obese groups differentiated poorly (***Figure 1—Figure supplement 1F***). In this line, the mRNA levels of the adipocyte markers, *PPARG*, *FABP4,* and *ADIPOQ* were lower in IR obese subjects than in their NG counterparts throughout differentiation (***Figure 1—Figure supplement 1G***).

Comparative proteomics of human obese preadipocytes

In order to identify marker pathogenic pathways of dysfunctional preadipocytes in obesity-associated metabolic disease, we employed iTRAQ proteomics of SC and OM preadipocytes from obese individuals with extreme metabolic

phenotypes, NG *vs.* T2D. This study enabled the identification of a total of 1,758 proteins that were present in both SC and OM fat from NG and T2D obese individuals, thus defining the human obese preadipocyte proteome. According to GO Biological Process annotation, 55.5% of these proteins were related to cellular and metabolic processes (***Figure 1—Figure supplement 2A***), including metabolism of mRNA, proteins, glucose, and lipids (***Figure 1—Figure supplement 2B***). All the proteomic data related to this study are available at the ProteomeXchange Consortium via the Proteomics IDEntifications (PRIDE) partner repository ***(Perez-Riverol et al., 2019***) with the dataset identifier PXD015621.

Comparison of proteomic data from SC and OM preadipocytes revealed marked differences between the two types of cells regarding the number of differentially expressed proteins and protein-related functional pathways (***Figure 1—Figure supplement 3***, and ***Figure 1—source data 1***). To investigate enrichment for functional pathways in each depot, canonical pathway analysis of the proteomic data was performed using IPA. Among the top ten IPA canonical pathways that were overrepresented in SC preadipocytes in T2D obesity (***Figure 1—source data 2***), the highest ranked down-regulated pathway was the spliceosomal cycle (***Figure 1B***). The unfolded protein response (UPR) was also modified in SC preadipocytes from T2D obese group (***Figure 1B***), while pathways related to ER stress were up-regulated in OM preadipocytes (***Figure 1C***) in T2D *vs.* NG obesity.

Based on these findings, we next characterized the splicing machinery and ER control system in preadipocytes and their contribution to adipocyte differentiation.

Splicing dysregulation as a marker of SC preadipocytes in obesity-related metabolic disease

To complement our proteomic observations, we assessed the expression of splicing-related genes in human preadipocytes using a microfluidic-based dynamic qPCR array comprising 45 splicing-related components (***Gahete et al., 2018***). Preadipocytes isolated from the SC and OM fat pads of NG, IR, and T2D obese individuals were employed for this study. Analysis of gene expression profiles by hierarchical clustering revealed a marked gene expression shift between NG and IR/T2D SC preadipocytes, which was not evident for OM preadipocytes (***Figure 2A***). SC preadipocytes from IR/T2D obese individuals exhibited lower expression levels of splicing-related genes than NG obese subjects, including components of major spliceosome (*PRPF8*, *RNU5*, *SF3B1 tv1*, *TCERG1*, and *U2AF1*), and splicing factors (*CELF1*, *MAGOH*, *RBM3*, *RBM45*, *SFPQ*, and *SNW1*) (***Figure 2A, Figure 2C***, and ***Figure 2—Figure supplement 4***). Notably, only the minor spliceosome component, *RNU12*, was up-regulated in T2D *vs.* NG SC preadipocytes (***Figure 2B***). No differences in OM preadipocytes were observed among the three groups of obese individuals (***Figure 2—Figure supplement 4***). These observations were largely confirmed in a second independent subset of samples obtained from additional obese individuals using RT-PCR (***Figure 2—Figure supplement 5***).

PRPF8/PRP8 expression studies in human preadipocytes

One of the most highly expressed genes in SC preadipocytes from NG obese individuals that was significantly down-regulated in both IR and T2D obese

subjects as compared to NG SC preadipocytes, was *PRPF8*/PRP8. Specifically, mRNA and protein levels of this key component of the major spliceosome were reduced by 51% and 56%, respectively, in IR SC preadipocytes, and by 49% and 82% in T2D SC preadipocytes as compared to NG levels (***Figures 2A-C***). No differences in *PRPF8*/PRP8 expression were observed among groups in OM preadipocytes (***Figures 2A-C***).

Differentiation studies revealed that while *PRPF8* expression levels remained low throughout adipogenesis in IR preadipocytes, *PRPF8* levels peaked at day 3 (D3) of differentiation and thereafter remained above D0 levels in NG preadipocytes (***Figure 2D***). *PRPF8* mRNA remained constant or decreased at the end of differentiation of NG and IR OM preadipocytes, respectively (***Figure 2D***).

PRPF8/PRP8 was also investigated in a second cohort comprising lean subjects and NG and T2D individuals with simple obesity (BMI >30 kg/m^2) (cohort 2) (***Supplemental file 2***). These studies showed significantly higher *PRPF8* expression levels in SC preadipocytes from NG obese *vs.* lean individuals. Similar to that observed for morbidly obese individuals from cohort 1 (***Figure 2B***), significantly decreased *PRPF8* transcript levels were detected in T2D *vs.* NG individuals with simple obesity (***Figure 2E***). No differences were observed in OM preadipocytes among groups (***Figure 2E***).

***PRPF8*/PRP8 down-regulation in preadipocytes impairs adipogenesis**

We employed a siRNA strategy to down-regulate *PRPF8* gene expression levels in preadipocytes to mimic the conditions found in IR/T2D obese SC preadipocytes as compared to NG obesity. These studies were carried out using

the human SC adipocyte cell line, SGBS cells. As observed for NG SC human primary preadipocytes, *PRPF8* mRNA levels reached a peak at early stages of SGBS cell differentiation (D4) (***Figure 3A***).

siRNA treatment of SGBS preadipocytes (D4) decreased by 67% and 65% *PRPF8* mRNA and protein levels, respectively, at day 3 post-transfection (D7), without changing cell viability (***Figure supplements 6A-C***). Morphometric evaluation of Oil-Red O staining in confocal micrographs revealed that *PRPF8*-silenced preadipocytes accumulated more but smaller LDs than control cells, which resulted in an increase in the total lipid content in cells exposed to *PRPF8* siRNA (***Figure 3C***). *In silico* analysis of CLIP_Seq data using ENCORI (The Encyclopedia of RNA Interactomes) (***Li et al., 2013***) revealed both adipogenic (*PPARG* and *SREBF1)* and LD biogenesis and growth markers (*BSCL2*, *CIDEB*, and *CIDEC*) as PRP8 target genes (***Figure 3—source data 3***). Enrichment analysis of PRP8-RNA interactions revealed pathways such as insulin signalling, adipokine signalling, and fatty acid metabolism to be significantly overrepresented (***Figure 3—source data 3***). Similarly, the HumanBase tool (***Greene et al., 2015***) identified several adipogenesis-related genes, including *ADIPOQ*, *CAV1*, and *CD36*, among the Top10 genes showing functional interactions with *PRPF8* (***Figure 3—source data 4***). In accordance with the *in silico* data, expression of total *PPARG* and *SREBF1* transcript contents and the abundances of some of their isoforms were altered in *PRPF8*-silenced cells (***Figure 3C***). In particular, mRNA and protein levels of the fat specific *PPARG* isoform, *PPARG-2*, were up-regulated upon *PRPF8* silencing (***Figures 3D-E***). Decreased levels and/or altered splicing patterns of *BSCL2*, *CIDEB*, and *CIDEC,* were also observed in silenced cells (***Figure 3F***). Other genes showing significant

changes in *PRPF8*-silenced cells included enzymes involved in lipid synthesis (FAS and DGAT2), and the LD-associated protein, ADRP, while neither PLIN1 nor HSL/pHSL were modified (***Figure 3G***). *PRPF8* silencing also activated stress responses in SGBS adipocytes, as indicated by the increased protein levels of the ER stress marker, CHOP, the immunoproteasome component, PSMB8, and CASP3/Pro-CASP3 ratio (***Figure 3G***). Contrarily to control cells, *PRPF8*-silenced cells did not respond to an insulin challenge (***Figure 3H***). Most of the effects depicted for silenced SGBS cells at D7 remained significant at D10 (***Figure 3—Figure supplement 6***). Nevertheless, silenced cells at D10 still exhibited abundant LDs but of small size, thus resulting in a drastic decrease in the total amount of lipids stored in *PRPF8* siRNA-treated cells as compared with controls (***Figure 3I***). *PPARG-2* mRNA and protein, and the late adipocyte markers, *ADIPOQ* and *FABP4*, were down-regulated at D10 in *PRPF8*-silenced cells (***Figure supplements 6D-E*** and ***6H***).

Notably, recovery of PRP8 protein levels by co-transfection of *PRPF8*-silenced SGBS cells with an expression vector coding for this protein (*PRPF8*-pcDNA3.1) reverted the effects induced by *PRPF8* silencing on adipocyte and LD markers, both at D7 (data not shown) and D10 (***Figure supplements 6***). Silencing-induced changes in both LD number and size were also reverted in rescue experiments by *PRPF8* re-expression (***Figure 3I***).

Silencing experiments using human adipose-derived stem cells (hADSCs) gave similar results to those observed in SGSB cells (***Figure supplements 7D-F***).

The UPR is altered in preadipocytes of IR/T2D obese subjects

As mentioned earlier, pathway analysis of iTRAQ proteomic data indicated that ER stress-related pathways were altered in both SC and OM preadipocytes from T2D obese individuals when compared to NG obese subjects (***Figures 1B*** and ***1C***).

Immunoblotting studies of additional human preadipocyte samples to those employed for iTRAQ studies, confirmed and extended the proteomic data by demonstrating altered mRNA/protein levels of UPR components in both SC and OM preadipocytes from IR/T2D obese groups as compared to NG obesity (***Figures 1B*** and ***1C***, and ***Figure 4***). To be more specific, SC and OM preadipocytes from T2D obese individuals exhibited enhanced levels of the ER stress-inducible gene, BiP (***Figure 4A*** and ***Figure 1—source data 2***). IR/T2D modified the protein content of p90 and p50, and cleaved/full-length ATF6 ratio in OM preadipocytes, and decreased this ratio in SC preadipocytes in IR *vs*. NG (***Figure 4B***). In addition, pPERK and pPERK/PERK ratio were up-regulated in SC and OM preadipocytes in relation to IR and/or T2D (***Figure 4C***). However, peIF2α and peIF2α/eIF2α ratio as well as the eIF2α-target, CHOP, were significantly reduced in OM preadipocytes in relation to IR/T2D (***Figures 4C*** and ***4E***). We observed enhanced IRE1α levels and decreased pIRE1α/IRE1α ratio in IR *vs*. NG OM preadipocytes (***Figure 4F***). IR OM preadipocytes and IR/T2D SC preadipocytes also exhibited higher levels of the spliced form of *XBP1* than NG preadipocytes (***Figure 4G***). Finally, the ER chaperones, GRP94 and PDI, were more abundant in T2D preadipocytes than in NG preadipocytes from both SC and OM fat (***Figure 4H***). Our proteomic study revealed enhanced levels of 11 additional ER chaperones in T2D SC preadipocytes (***Figure 1—source data 2***).

Dysregulation of ER-associated protein degradation (ERAD) in IR/T2D obese preadipocytes

In association with the UPR, the ERAD represents a key quality-control machinery that recruits unfolded/misfolded ER proteins via ER chaperones and targets these proteins for cytosolic degradation by the proteasome ***(Christianson and Ye, 2014***; ***Qi et al., 2017***). Given our results on the UPR, we next explored the ERAD in human preadipocytes and observed a marked up-regulation of proteins involved in all the steps comprising this process, including protein recognition (*BIP*; ***Figure 5A***), retrotranslocation through the ER membrane (*DERL1*, *SEC61A1*, *STT3A*, and *STT3B*; ***Figure 5B***), ubiquitination (*HRD1* and *RNF185*; ***Figure 5C***), and targeting of misfolded proteins to the proteasome (*RAD23A* and *UBQLN1*; ***Figure 5D***) in IR/T2D *vs.* NG obesity. These changes occurred in both SC and OM preadipocytes, which split into two clusters (NG and IR/T2D) when ERAD data was represented in a two-way hierarchical clustering heatmap (***Figure 5E***). Interestingly, as we observed for IR/T2D preadipocytes *vs*. NG preadipocytes (either SC or OM), increasing BiP expression levels by overexpression of a vector coding for this ER chaperone, enhanced the mRNA content of ERAD-related genes in SGBS adipocytes (***Figure 5—Figure supplement 8A***). BiP overexpression also caused a concomitant decrease in the expression levels of several adipogenic markers (***Figure 5—Figure supplement 8B***).

Finally, the ERAD process was also explored during adipocyte differentiation. mRNA levels of ERAD genes increased during differentiation of human primary adipocytes, especially in IR, which resulted in higher overall transcript contents

of these genes in IR preadipocytes than in NG preadipocytes (measured as AUC) *(**Figure 5—Figure supplement 9**)*.

Hyperglycaemia/hyperinsulinemia alters preadipocyte ER proteostasis

In order to unveil the regulation of ERAD in response to obesogenic insults, SGBS preadipocytes were exposed to high concentrations of glucose and insulin (HGHI), TNFα, or fatty acids (palmitate or oleate), as *in vitro* models of hyperglycaemia/hyperinsulinemia, inflammation, and hypertrophy due to lipid overload, respectively (***Díaz-Ruiz et al., 2015***). None of the treatments compromised cell viability (data not shown) and, except for oleate, they impaired insulin-induced Akt phosphorylation (***Figure 5—Figure supplement 10C***). Exposure to HGHI increased the expression of BiP and nearly all the other ERAD components tested (***Figure 5F***). As shown in ***Figure 5G***, expression levels of ERAD genes enabled discrimination of HGHI-treated from control SGBS cells. Given these observations, we next examined the activity of the protein degradation machinery in the cytosol, the proteasome (***Bard et al., 2018***), in cells exposed to HGHI. These studies showed that hyperglycaemic/hyperinsulinemic conditions decreased the activity of the 26S proteasome while increasing the amount of ubiquitinated proteins in SGBS preadipocytes (***Figures 5H*** and ***5K***).

The naturally occurring bile acid, tauroursodeoxycholic acid (TUDCA), has been shown to restore ER homeostasis in ER-stressed cells (***Zhang et al., 2018***). We thus tested whether exposure of SGBS preadipocytes to TUDCA prior to HGHI treatment could prevent HGHI-induced up-regulation of ERAD genes and accumulation of ubiquitinated proteins in these cells, which was proven to be the case (***Figures 5I and 5J***). TUDCA also reverted HGHI inhibitory effects on PPARγ and FABP4 expression levels (***Figure 5K***). Notably, TUDCA also blocked

the effects induced by BiP overexpression on both ERAD genes and adipogenic markers (***Figure 5K***).

Discussion

We found that alternative splicing in the SC adipose tissue, and the ER stress-UPR-ERAD system in both SC and OM fat represent essential components of the adipogenic process that are altered in obese individuals with IR/T2D. Specifically, IR/T2D obesity is characterized by reduced expression levels of multiple members of the major and minor spliceosome, and splicing factors in SC preadipocytes. We provide experimental evidence demonstrating that decreasing the expression of a key component of the major spliceosome, *PRPF8*/PRP8, by siRNA is sufficient to hamper the expression of both markers of adipogenesis and regulators of LD biogenesis and growth, thus supporting a relevant role for this protein and the splicing machinery in the regulation of adipocyte differentiation. Our results are also indicative of IR/T2D-dependent ERAD hyperactivation in preadipocytes of the two major fat depots, SC and OM, in obese individuals. Maladaptative UPR and ERAD signalling upon ER stress induction may contribute to impair adipocyte differentiation and to the progression of metabolic disease in obesity.

Alternative splicing of mRNA enables cells to acquire protein diversity, which is essential for cell differentiation and tissue growth and identity ***(Baralle and Giudice, 2017***). It is accepted that both mRNA transcription and processing contribute to the changes in gene expression patterns leading to the transition of progenitor cells toward a mature phenotype (***Fiszbein and Kornblihtt, 2017***). In

this regard, recent reports suggest a role for alternative splicing in adipocyte differentiation (***Lin, 2015***). It has been shown that inhibition of the splicing factor, SF3B1, blocks 3T3-L1 adipocyte differentiation (***Kaida, 2019***), and recent RNA-seq studies support the occurrence of alternative splicing events during adipogenesis of bone marrow-derived human mesenchymal stem cells (***Yi et al., 2019***). Furthermore, certain naturally PPARγ isoforms generated by alternative splicing act as dominant-negative isoforms that prevent adipocyte differentiation (***Aprile et al., 2018***). However, few studies have addressed the relevance of the splicing machinery in human preadipocytes and whether this system is altered in obesity. To the best of our knowledge, this is the first study demonstrating the down-regulation of multiple members of the splicing machinery in human SC preadipocytes in relation to obesity-associated IR/T2D.

To analyse the relevance of alternative splicing on adipogenesis, we reduced the expression of a major spliceosome component found to be markedly down-regulated in SC preadipocytes from IR/T2D obese individuals, *PRPF8*/PRP8, by siRNA treatment of SGBS preadipocytes. In this context, recent work combining RNA-seq and proteomics demonstrated that PRP8 depletion altered the expression of more than 1,500 proteins in Cal51 breast cancer cells, supporting the relevance of this protein in defining the human proteome (***Liu et al., 2017***). In fact, as part of the core of the major spliceosome, PRP8 is potentially involved in the removal of most introns from precursor mRNAs (99.5% of non-coding regions are removed by the major spliceosome) (***Turunen et al., 2013***). Our studies showed that decreasing PRP8 protein levels by 2-fold (as observed in IR/T2D *vs*. NG obese SC preadipocytes) in SGBS preadipocytes evoked gene/protein expression changes indicative of altered adipogenesis, which was

confirmed by the decreased accumulation of lipids observed in SGBS cells at late stages of differentiation. These results were replicated in another SC adipocyte cell line, hADSCs, derived from a lean donor, reinforcing the key contribution of *PRPF8*/PRPR to human adipocyte differentiation.

Two different yet functionally interrelated pathways were impaired in *PRPF8*-silenced SGBS and hADSCs cells in terms of both total gene expression levels and isoform balance of the proteins involved, i.e., adipogenic transcriptional program, and LD biogenesis and growth (***Figure 3J***). Thus, PRP8 down-regulation altered the expression of PPARγ and SREBP1, as well as of seipin and two members of the CIDE family (CIDEB, CIDEC). In particular, the overall decrease in PPARγ and SREBP1 isoforms observed in SGBS cells upon PRP8 down-regulation may account for the reduction observed in mRNA and/or protein levels of known downstream target genes of these transcription factors (adiponectin, FABP4, CIDEC, and FAS) (Lowe et al., 2011; Slayton et al., 2019). Likewise, the dramatic changes in LD size and number observed in *PRPF8*-silenced adipocytes might be related to the low expression levels of the canonical seipin variant, seipin1 (***Craveiro Sarmento et al., 2018***), observed in these cells. Indeed, our observations in SGBS adipocytes are in line with previous data on seipin knockout A431 cells, which also exhibited more numerous but smaller LDs than controls (***Salo et al., 2016***). Interestingly, seipin knock-down has been shown to suppress *PPARG* and *SREBF1* expression (***Fei et al., 2011***), thus suggesting that the phenotype of SGBS cells silenced for PRP8 may be the result of the action of this spliceosome component on multiple key genes contributing to adipogenesis and lipogenesis. In line with this notion, analysis of CLIP-sep data in the ENCORI database revealed the presence of PRP8 binding sites in

PPARG, *SREBP1*, *BSCL2*, *CIDEB* and *CIDEC* mRNAs. Further research is needed to fully establish the splicing targets for PRP8 in preadipocytes and to characterize the relevance of the resulting protein isoforms (and/or their ratio) in adipogenesis. Notwithstanding this, the observation that PRP8 re-expression in *PRPF8*-silenced SGBS cells can restore the expression and/or isoform balance of genes such as *PPARG*, *BSCL2*, *CIDEB* or *CIDEC*, as well as normal LD content, supports a prominent role for this protein in lipid accumulation in adipocytes. In this scenario, it is reasonable to propose that the decreased expression of splicing-related genes in SC preadipocytes in IR/T2D obesity as compared to NG obesity could be responsible, at least in part, of the loss of adipogenic capacity displayed by SC preadipocytes from obese individuals with metabolic disease.

When viewed together, our data strongly support the notion that splicing deregulation in SC preadipocytes may represent a pathogenic factor that contributes to the development of obesity-related complications. Changes in splicing components between groups were negligible in OM preadipocytes as compared to their SC counterparts. These inter-depot differences, which appear to be cell autonomous, might contribute, at least partly, to the distinct differentiation capacity of SC and OM preadipocytes observed in this and other studies (***Martyniak and Masternak, 2017***). Future studies using human primary preadipocytes with altered expression levels of selected splicing-related genes will be important to elucidate the precise splicing events that are critical for adipogenesis.

Interestingly, along with altered splicing, SC preadipocytes in IR/T2D obesity also exhibited molecular features indicative of ER stress response failure, a

hallmark process associated with the development of metabolic diseases (***Bhattarai et al., 2020***). In fact, our data suggest that this pathogenic process also occurs in OM preadipocytes in IR/T2D obesity. In accordance with these findings, previous studies from our laboratory have established that IR obesity is associated with enhanced levels of ER stress markers in mature adipocytes isolated from either SC or OM fat (***Díaz-Ruiz et al., 2015***). Herein we report, for the first time, that the three UPR signal transducers, IRE1α, PERK, and ATF6 (***Hetz and Papa, 2018***), and two effector systems downstream the UPR branches, CHOP and *XBP1* splicing, are dysregulated in primary SC and OM preadipocytes in IR/T2D obesity with respect to NG obesity, in terms of total protein content and/or phosphorylation rate (i.e., activation). It is noteworthy that changes in these proteins did not always follow the same trends between SC and OM preadipocytes in response to IR/T2D, indicating the existence of depot-specific (mal)adaptative responses to obesity-associated ER stress. Notwithstanding this notion, a feature common to SC and OM preadipocytes was the up-regulation of both the master initiator of the UPR signalling pathway, BiP, and *XBP1s/ XBP1u* ratio, in IR/T2D obesity. Given the role of BiP in mediating the targeting of misfolded/unfolded ER proteins for cytosolic degradation via ERAD, and the stimulatory effect of *XBP1s* on the expression of ERAD components (***Karagöz et al., 2019***), these observations supported that IR/T2D obesity could not only alter the UPR but also the activity of this branch of the quality-control system in the ER ***(Hwang and Qi, 2018***). Interestingly, ERAD is activated when the protein folding capacity of the ER is exceeded ***(Hwang and Qi, 2018***), which seems to be the case for SC and OM preadipocytes of IR/T2D obese individuals according to their enhanced expression levels of ER

chaperones as compared to NG obesity. In fact, our studies show, for the first time, that SC and OM preadipocytes from IR/T2D obese individuals, as compared to NG obese individuals, display enhanced levels of proteins participating in all the steps comprising the ERAD, thus suggesting that this pathway is hyperactivated in preadipocytes during the progression to IR/T2D in obese individuals. An increase in the expression of ERAD genes was also observed in SGBS cells overexpressing BiP, further demonstrating the functional link between UPR and ERAD in preadipocytes.

In all, our data on the UPR and ERAD strongly support the notion that metabolic disease in obesity is characterized by the perturbation of ER proteostasis network components in preadipocytes. They also support the link between unresolved ER stress and adipogenesis dysregulation (***Longo et al., 2016***). Our studies using *in vitro* models mimicking different obesogenic inputs indicate that inflammation, adipocyte hypertrophy and, specially, hyperglycaemia/hyperinsulinemia (HGHI), as occurs in IR obese individuals, may contribute to alter ER proteostasis in preadipocytes. To be more specific, exposure to hyperglycaemic/hyperinsulinemic conditions represented the most active stimulus inducing ERAD hyperactivation, as well as BiP expression, in SGBS preadipocytes. Intriguingly, HGHI-induced ERAD expression was accompanied by a concomitant decrease in the activity of the cell machinery involved in misfolded/unfolded protein degradation, the proteasome, and the accumulation of ubiquitinated proteins in preadipocytes. These results suggest that the preadipocytes are unable to counteract the proteostatic stress evoked by HGHI-conditions, and proteotoxicity ensues. In agreement with these findings, we have reported the occurrence of proteotoxicity, i.e., decreased activity of the

proteasome and accumulation of ubiquitinated proteins, in *in vitro* differentiated preadipocytes and in mature adipocytes isolated from SC and OM fat of diet-induced obese mice as compared to lean animals, as well as in mature adipocytes isolated from IR *vs*. NG obese individuals (***Díaz-Ruiz et al., 2015***). Unfortunately, the limited amount of human preadipocytes available from adipose tissue biopsy samples, prevented to extend our experiments to primary cell cultures. Notwithstanding these limitations, in all, our studies strongly support the notion that dysregulated ERAD in preadipocytes represents a relevant pathological mechanism linked to the development of metabolic disease in obese individuals. In this line, altered ERAD expression levels in SGBS cells by exposure to HGHI or BiP overexpression were accompanied by changes in adipogenic markers demonstrative of impaired adipocyte differentiation. These effects were reverted by pre-exposure of SGBS cells to the ER stress-reducing agent, TUDCA (***Zhang et al., 2018***). Together, these findings suggest that TUDCA may represent a potentially useful treatment for preadipocyte damage prevention in obesity, as it has been proposed for this bile acid in other ER stress-related pathologies (***Kusaczuk, 2019***).

In summary, our results unveil an important role for alternative splicing in SC preadipocyte differentiation thus paving the way for the development of novel therapeutic strategies to modulate adipose tissue expansion. Our studies on altered ER dynamics, that affect not only the UPR but also the ERAD pathway, in SC and OM preadipocytes are in line with our previous results in mature adipocytes (***Díaz-Ruiz et al., 2015***) and, in all, indicate that the maintenance of ER proteostasis in adipose tissue cells is key to ensure metabolic health in obesity.

Materials and Methods

Subjects (Cohort 1)

A total of 69 morbidly obese subjects (BMI >40 kg/m^2) undergoing bariatric surgery were recruited at the General and Digestive Surgery Unit and the Lipids and Atherosclerosis Unit of the Reina Sofía University Hospital (HURS; Córdoba, Spain). Written consent was obtained from all the participants prior to recruitment, and the experimental protocol was approved by the Ethics and Research Committee of HURS following the Helsinki Declaration. Anthropometric and biochemical parameters were obtained as described (***Díaz-Ruiz et al., 2015***). Subjects are of Caucasian origin, aged 18-60 years. Type 2 diabetes mellitus (T2D) in treatment with insulin, serious systemic disease not related to obesity (infectious disease, cancer, kidney disease or severe liver disease) or major cardiovascular disease in the 6 months prior to the inclusion of the study, pregnancy, or breastfeeding and acute or chronic inflammatory diseases were considered as exclusion criteria.

Subjects were matched by age and BMI and subclassified into three groups [normoglycemic (NG Obese, n= 27; 13 females and 14 males): Glucose <100 mg/dL and HbA1c <5.7%; impaired fasting glucose (IFG Obese, n=25; 13 females and 12 males): Glucose 100–126 mg/dL and HbA1c 5.7-6.4%; and diagnosed with type 2 diabetes (T2D Obese, n=17; 11 females and 6 males): Glucose >126 mg/dL and HbA1c >6.4%], according to the criteria of the American Diabetes Association (***ADA, 2019***). The clinical characteristics of the subjects are shown in ***Table 1***. IFG individuals exhibited significantly higher HOMA-IR values than NG individuals, as well as other clinical and plasma parameters that are within the cut-off points for identifying insulin resistance in hyperinsulinemia-

euglycemic clamp studies (***Tam et al., 2012***). Thus, they will be referred to hereinafter as insulin-resistant (IR) subjects (***Díaz-Ruiz et al., 2015***).

Subjects (Cohort 2)

43 subjects were recruited by the Endocrinology and Surgery departments at the University Hospital Joan XXIII (Tarragona, Spain) as reported previously (***Ejarque et al., 2017***). All subjects were of Caucasian origin and reported that their body weight had been stable for at least 3 months before the study. They had no systemic disease other than obesity, and all had been free of infection in the previous month before the study. Primary liver disease, cardiovascular disease, arthritis, acute inflammatory disease, infectious disease, neoplastic and renal diseases were specifically excluded by biochemical work-up. Subjects were classified by BMI according to World Health Organization criteria as lean (n=18, BMI<25 kg/m^2) and obese (n=25, BMI>30 kg/m^2). Obese subjects were subclassified into NG (n=15) and T2D (n=10) groups, as previously described (***Serena et al., 2016***). OM and SC adipose tissue samples were obtained during scheduled non-acute surgical procedures including laparoscopic surgery for hiatus hernia repair or cholecystectomies in non-morbid obese population. Anthropometric and biochemical variables from the cohort are presented in ***Supplemental file 2***.

The hospital ethics committee approved the study and informed consent for biobanking surgically removed tissue was obtained from all participants in accordance with the Declaration of Helsinki.

Adipose tissue processing

Paired abdominal subcutaneous (SC) and omental (OM) adipose tissue biopsies were obtained during bariatric surgery and processed as previously described (***Díaz-Ruiz et al., 2015***; ***Peinado et al., 2010***). Samples were washed with Dulbecco`s phosphate buffered saline (D-PBS) to remove blood contaminants and mechanically dispersed in DMEM/F-12 (1:1). Next, samples were enzymatically dispersed by incubation in DMEM/F-12 (1:1) containing 400 units/mL of collagenase type V at 37 ºC for 30 min in a shaking bath. Undigested tissue was removed by filtering through a sterile 100 µm pore Cell Strainer (BDFalcon, Cat#352360) and the remaining was centrifuged at 600 x g for 10 min to separate the floating mature adipocyte layer and the pelleted stromal-vascular fraction (SVF). SVF was resuspended in DMEM/F-12 (1:1), filtered through a 40 µm pore Cell Strainer (BDFalcon, Cat#352340) and centrifuged at 400 x g for 5 min. Then, pelleted SVF was resuspended in 500 µL of RBC Lysis Buffer and incubated for 3 min at room temperature (RT). After centrifugation at 400 x g for 10 min, SVF was frozen in liquid nitrogen and stored at -80 ºC for further analysis and/or seeded onto culture flasks.

Freshly isolated mature adipocytes were washed with DMEM/F-12 (1:1) and added to lipolysis buffer [Krebs Ringer Phosphate (KRP) buffer: 0.9 % NaCl, 15 mM NaH_2PO_4, 6 mM KCl, 1.5 mM MgSO4, 1.6 mM $CaCl_2$ supplemented with 2% bovine serum albumin (BSA), 1 mg/mL glucose and 0.1 mg/mL ascorbic acid; pH 7.4]. Fat cell volume and weight was determined as described (***Tchoukalova et al., 2003***) and discussed (***Lundgren et al., 2007***). In brief, light microscopy images of 100 cells were captured with a coupled camera (Moticam 1080; Motic, Barcelona, Spain) and their diameters (d) were measured in micrometres using

ImageJ 1.50b. Mature adipocytes are assumed to be spheres so that their volume (expressed in picolitres) was calculated as ([$\pi \times d^3$]/6) where d is the cell diameter in micrometres.

Human primary preadipocytes

Human primary preadipocytes were cultured as previously described (***Serena et al., 2016***; ***Guzmán-Ruiz et al., 2014***). SVF cells obtained from fresh SC and OM adipose tissue samples were seeded in preadipocyte-proliferation medium DMEM/F-12 (1:1) supplemented with 8 mM biotin, 18 mM d-pantothenate acid, 100 mM ascorbate, and 1% penicillin-streptomycin, and 10% new-born calf serum (NCS) at 37 ºC in a humidified atmosphere with 95% air: 5% CO2. Medium was replaced every 48 h until confluence. Once in confluence (>80%), the cells were detached with trypsin- EDTA solution and subcultured at 4,000 cells/cm^2 2-3 times to purify and amplify the cell culture following established methods (***Bunnell et al., 2008***; ***Palumbo et al., 2018***; ***Zhu et al., 2013***). Thereafter, preadipocytes were collected and frozen in liquid nitrogen and stored at -80 ºC for immunophenotyping analysis, proliferation studies, or directly induced for adipogenic differentiation, as indicated in detail in the following sections.

Immunophenotyping analysis

Freshly isolated SVF cells and cell cultures derived from SVF at passages 2-3 were processed for detection of preadipocyte markers and immune cell markers to assess the purity of the cell preparations employed for further analysis. To be more specific, the protein content of DLK1/PREF1 (preadipocyte marker), CD45 (leukocyte marker), and CD14 (macrophage marker) was assessed in extracts from the SVF and preadipocytes that were obtained from the same SC and OM

adipose tissue samples following the procedures indicated in the “Quantitative immunoblotting” section below.

In vitro differentiated human adipocytes

Preadipocytes were seeded at 4.000 cells/cm^2 in preadipocyte proliferation medium until they reached 70-80% of confluence. Then (day 0 of differentiation), primary preadipocytes were differentiated keeping them in differentiation medium: preadipocyte-proliferation medium with 3% NCS and 17.5 mM glucose, supplemented with 10 µg/mL insulin, 0.1 µM dexamethasone, 1 µM rosiglitazone, and 0.5 mM IBMX for the first 3 days. Then, medium was removed and replaced by differentiation medium supplemented with 10 µg/mL insulin and 0.1 µM dexamethasone for 4 more days (day 6), when the medium was refreshed and maintained until day 10. The adipogenic process was monitored by the appearance of doubly refractile lipid inclusions by light microscopy and images of the cultures were taken with a coupled camera (Moticam 1080; Motic, Barcelona, Spain). Experiments were carried out using cells from passages 3 to 4.

Human adipose tissue cells lines

In this study we employed SGBS cells, a human-derived preadipocyte cell line isolated from the SVF of SC adipose tissue from a 3-months male infant with Simpson-Gobali-Behmel syndrome, was kindly donated by Prof. Dr. José Manuel Fernández-Real (Institut d'Investigació Biomèdica of Girona, Spain). This cell model has been largely used in studies pertaining to preadipocytes and differentiated adipocytes (***Allott et al., 2012***; ***Fischer-Posovszky et al., 2008***; ***Kalkhof et al., 2020***; ***Li et al., 2016***; ***Newell et al., 2006***; ***Zandbergen et al., 2005***). SGBS cells growth and differentiation into adipocytes were performed as

previously described (***Moure et al., 2016***). Cells were seeded at a density of 4,000 cells/cm2 and proliferated to 80% confluence in basal medium: DMEM/F12 (1:1) supplemented with 32.7 µM biotin, 16.78 µM d-panthothenic acid, and 1% penicillin-streptomycin.

Confluent SGBS cells (day 0 of differentiation) were differentiated keeping them in differentiation medium: serum-free basal medium, supplemented with 0.01 mg/mL human transferrin, 20 nM human insulin, 100 nM hidrocortisone, 0.2 nM 3,3',5-triiodo-l-thyronine (T3), 25 nM dexamethasone, 0.5 mM IBMX, and 2 µM rosiglitazone for the first 4 days. Next, medium was removed and replaced by differentiation medium supplemented with medium 0.01 mg/mL human transferrin, 20 nM human insulin, 100 nM hidrocortisone, and 0.2 nM T3 for 6 days (day 10). Then, medium was refreshed, and cells were maintained in culture until day 14. The differentiation process was monitored by microscopic observation of LDs and expression analysis of known markers of adipogenesis and LD biogenesis (data not shown).

We also employed an adipose-derived stem cell line (hADSCs) that was isolated from SC adipose tissue of a male lean donor (aged 16 years, BMI 24 kg/m^2). This cell model was developed and validated in our previous works (***Acosta et al., 2017***; ***Ehrlund et al., 2017b***, ***2017a***; ***Petrus et al., 2020***). Cells were isolated, propagated, and differentiated into adipocytes as described (***Gao et al., 2014***, ***2017***). Cells were cultured at 20.000 cells/cm^2 in proliferation medium [DMEM low glucose (1 g/L glucose), pyruvate supplemented with 1% hepes buffer 1M, 0.5% penicillin/streptomycin (10,000 U/mL), and 10% FBS] with 2.5 ng/mL human FGF2. Cells were then proliferated until 80% of confluence and

the medium was replaced for proliferation medium without FGF2 for one more day.

Cells at day 0 of differentiation were differentiated keeping them in differentiation medium [serum-free proliferation medium:Ham's F-12 Nutrient Mix (1:1)] supplemented with 5 µg/mL human insulin, 10 µg/mL transferrin, 0.2 nM T3, 1 µM rosiglitazone, 100 µM IBMX, and 1 µM dexamethasone for the first 3 days. Next, at day 3 of differentiation, medium was removed and replaced by differentiation medium supplemented with 5 µg/mL human insulin, 10 µg/mL transferrin, 0.2 nM T3, and 1 µM rosiglitazone. The medium was refreshed each 2-3 days until day 6 and day 10 of differentiation. Differentiation process were monitored by microscopic observations of LDs.

iTRAQ labelling and high-resolution LC-MS/MS

$1x10^6$ human SC and OM preadipocytes from NG and T2D obese subjects were homogenized in lysis buffer containing 8 M urea, 4% CHAPS, 30 mM Tris base, sonicated, and quantified by RcDc assay kit. Reduction and alkylation were done by addition of 2 mM 1,4-dithiothreitol (DTT) and 7 mM iodoacetamide (IAA), respectively, for 15 min at RT. Then, samples from 2-3 individuals per group and fat depot were pooled and used for two separate iTRAQ experiments (n=5-6 subjects per group and fat depot). Protein samples were precipitated using 10% trichloroacetic acid (TCA), diluted in tetraethylammonium bromide (TEAB) with 0.1% sodium dodecyl sulphate (SDS) and quantified. Samples were diluted 1:2 with TEAB and digested with 2% trypsin. Tryptic peptides (240 µg per group and fat depot) were employed for proteomic analysis using 4-plex isobaric tags for iTRAQ according to the manufacturer's instructions. Samples were tagged with

the corresponding iTRAQ reagent, mixed, desalted and fractionated by strong cation exchange (SCX).

Six fractions were collected, and each fraction was desalted, evaporated to dryness, and diluted in 20 µL of injection phase. Then, 8 µL of extract were diluted with 5% methanol (MeOH)/1% formic acid and analysed by liquid chromatography-tandem mass spectrometry (LC-MS/MS). The MS system used was an Orbitrap XL (Thermo Scientific) equipped with a microESI ion source (Proxeon; Madrid, Spain) and coupled to an Agilent 1200 series LC-system (Agilent Technologies; Madrid, Spain). The SCX-fractions were loaded onto a chromatographic system consisting of a C18 preconcentrating cartridge (Agilent Technologies) connected to a 15 cm long, 100 µm i.d. C18 column (Nikkyo Technos Co., Ltd.; Tokyo, Japan). The separation was performed at 0.4 µL/min in a 90-min acetonitrile gradient from 3 to 40% [solvent A: 0.1% formic acid, solvent B: acetonitrile with 0.1% formic acid]. The Orbitrap XL was operated in the positive ion mode with a spray voltage of 2 kV. The scan range for full scans was m/z 400-1800. The spectrometric analysis was performed in a data dependent mode, acquiring a full scan followed by 8 MS/MS scans of the 4 most intense signals detected in the MS scan. For each MS signal, two MS/MS spectra were acquired using higher energy collisional dissociation (HCD) and ion-trap-based collision-induced dissociation (CID) as fragmentation devices. The HCD spectra were used to measure the intensity of iTRAQ fragments and the CID spectra were used for database search and peptide identification. An exclusion time of 30 sec and a spectral count of 2 were included to avoid repetitive MS/MS analysis of the dominant MS signals.

Database search and protein identification

Peak lists were searched against the complete human proteome (UniProt release 2014_08, with 68.049 proteins) using SEQUEST (Proteome Discoverer 1.3, ThermoFisher) as search engine. The search tolerances were set as follows: peptide mass tolerance 10 ppm, fragment tolerance 0.8 Da, with trypsin as enzyme (allowing up to two missed cleavages), methionine oxidation (+15.995 Da) and 4-plex iTRAQ (K, Y, N-terminal, +144.102) as variable modifications, and cysteine carbamidomethylation (+57.021 Da) as fixed modification. Peptide identifications were filtered for 0.5% FDR and only proteins identified with two or more peptides were considered. All the raw data of mass spectrometry measurements, together with protein identification have been deposited to the ProteomeXchange Consortium via the PRIDE (***Perez-Riverol et al., 2019***) partner repository with the dataset identifier PXD015621.

Data normalization and statistical analysis

Protein intensities, for each of the two iTRAQ experiments, were normalized using protein median intensities in each comparison (iTRAQ reagents 115/116: 0.987, 115/117: 0.958, 116/114: 1.142, 117/114: 1.191 for replicate 1; and 115/116: 1.026, 115/117: 0.933. 116/114: 1.090, 117/114: 1.180 for replicate 2). Protein identified in the two replicates were matched. To discard duplicate proteins between replicates, the following parameters were considered: absence of missing values, # unique peptides, # peptide and coverage (the higher, the better). Proteins showing quantification values within a fixed average ratio (±1.5) and a coefficient of variation (CV) under 20% were considered for further statistical analysis. Specifically, the Perl module “Statistic R” was used to calculate the average, the standard deviation (SD), the coefficient of variation

(CV), and the fold change ratios for each protein between groups. Data normality was tested by Shapiro-Wilk test, and a Student's t test was performed to obtain the statistical significance (*p-value*).

Bioinformatics analysis

Gene Ontology (GO) analysis of the proteomic results was conducted using online open-source software PANTHER (Protein ANalysis THrough Evolutionary Relationships) classification system 14.1 that annotated proteins to biological processes (***Mi et al., 2019a***, 2***019b***). Significant over- and under-represented GO terms and pathways were identified by Fisher's Exact with FDR multiple test correction < 0.05 taking all the Homo sapiens genes in the data set as a reference list. To determine quantitative changes in this study, a ±1.5-fold change, with p<0.05 (determined by t-test) in two replicates, was set as the threshold for categorizing up-regulated and down-regulated proteins. Pathway and upstream regulator analysis were performed using IPA (Ingenuity Pathways Analysis) software 49309495. Canonical pathway analysis identified the pathways from the IPA library of canonical pathways that were most significant to the data set. The significance of the association between the data set and the canonical pathway was measured in 2 ways: 1) A ratio of the number of proteins from the data set that mapped to the pathway divided by the total number of proteins that mapped to the canonical pathway displayed. 2) Fisher's exact test was used to calculate a p-value determining the probability that the association between the proteins in the dataset and the canonical pathway was explained by chance alone, and p<0.05 was considered statistically significant. The authors thankfully acknowledge the computer resources, technical expertise and assistance provided by the PAB (Andalusian Bioinformatics Platform) centre located at the

University of Málaga (www.scbi.uma.es). mRNA binding sites and adipose tissue-specific functional interactions of PRPF8 were investigated using ENCORI (The Encyclopedia of RNA Interactomes; http://starbase.sysu.edu.cn/index.php) (***Li et al., 2013***) and HumanBase tool (https://hb.flatironinstitute.org/) (***Greene et al., 2015)***, respectively.

***PRPF8* silencing**

SGBS preadipocytes, cultured on 6-wells or 12-wells plates, were stably transfected at day 4 of differentiation with targeted double stranded siRNA oligonucleotides against the splicing factor *PRPF8* or a specific negative control siRNA using Lipofectamine RNAiMAX Transfection Reagent following manufacturer's instructions. Transfection efficiency was checked by RT-PCR, western blotting and, when possible, by cotransfecting cells with N-terminal end of phrGFP-N1, as a reporter (***Moreno-Castellanos et al., 2017***) using Lipofectamine 2000 Transfection Reagent. Briefly, the cells were washed twice with D-PBS and submerged into 1 mL of OPTI-MEMTM medium containing 100 nM of the corresponding siRNA and, when required, 3 µg of phrGFP-N1 during 24 h. Thereafter, the transfection medium was removed, and fresh culture medium was added. Finally, after 3-5 days of transfection, silenced cells were stained with Oil Red-O. The effects of *PRPF8* silencing were also explored by RT-PCR and quantitative immunoblotting. In another series of experiments, siRNA-treated cells were exposed to 100 mM insulin for 15 min.

hADSCs were transfected one day before differentiation induction through electroporation by Kit Neon™ Transfection System (***Kim et al., 2008***). The cells were trypsinised and washed with D-PBS (without Ca^{2+} and Mg^{2+}) and resuspended in Resuspension Buffer R at a final density of $1x10^6$ cells/mL. The

NEON system (Invitrogen) 10-µL electroporation tips were used with 10^6 cells per reaction. One pulse (1,200 V, 40 ms) was used to transfect a final concentration of 40 nmol/L siRNA to cells, which were seeded in medium without antibiotic/antimycotic. Twenty-four h after electroporation, the medium was replaced, and differentiation started following the standard protocol. Finally, the effects of PRPF8 silencing were evaluated at different days of differentiation (0, 3, 6 and 10 days of differentiation).

***PRPF8* and *BIP* overexpression**

SGBS preadipocytes, cultured on 6-wells or 12-wells plates, were stably transfected at day 4 of differentiation with a plasmid vector coding for *PRPF8* (*PRPF8*-pcDNA3.1), its corresponding empty plasmid vector alone (pcDNA3.1) as a negative control or co-transfected with *PRPF8*-pcDNA3.1 and *PRPF8*-siRNA (*PRPF8*-pcDNA3.1+*PRPF8*-siRNA) using Lipofectamine 2000 Transfection Reagent following manufacturer's instructions. In another sets of experiments, SGBS preadipocytes were stably transfected with a plasmid vector coding for *BIP* (pCMV *BiP*-Myc-KDEL-wt) or its corresponding empty vector (pCMV-Myc), Transfection efficiency was checked by RT-PCR, western blotting and, when needed, by co-transfecting cells with N-terminal end of phrGFP-N1, as a reporter (***Moreno-Castellanos et al., 2017***). Briefly, the cells were washed twice with D-PBS and submerged into 1 mL of OPTI-MEMTM medium containing 3 µg of corresponding plasmid vector and 100 nM of the siRNA during 24 h. Thereafter, the transfection medium was removed, and fresh culture medium was added. Finally, after 3-5 days of transfection, silenced cells were stained with Oil Red-O. The effects of PRPF8 overexpression and recovery were also explored

by RT-PCR and quantitative immunoblotting. All constructs were verified by DNA sequencing.

Lipid droplet (LD) morphometric analysis

Oil Red-O staining of cellular lipids was performed in SGBS cells grown on glass coverslips under different conditions as previously described (***Pulido et al., 2011***). Cells were washed with D-PBS and fixed with 4% paraformaldehyde for 8 min at RT. Coverslips were washed with 60% isopropanol and then left to dry completely. Subsequently, an Oil Red-O stock solution was prepared: 0.35 g Oil Red-O was dissolved in 100 mL 100% isopropanol. Before use, the solution was diluted 6:4 with distilled water, allowed to stand for 10 min, and then filtered through Whatman no. 1 paper. Cells were exposed to this solution for 30 min at RT in darkness and the unbound dye was rinsed with distilled water. Images were captured with an inverted light microscope coupled to a camera. For morphometric studies of the lipid droplets (LDs), coverslips were mounted on slides with fluorescent mounting medium containing 1 µg/mL DAPI, to visualize the nuclei, and examined by confocal microscopy as described previously (***Pulido et al., 2011***). At least 30 cells were randomly selected for each experimental condition and the LD number and size were then estimated by using ImageJ 1.50b (***Deutsch et al., 2014***; ***Mohan et al., 2019***). Analysis was performed by converting the 8-bit image into a binary image, that consists of the pixels comprising the LDs. Following binarization, the image was subjected to watershed object separation for image processing, which is used to identify borders of adjacent LDs (***Abdolhoseini et al., 2019***). After separation, the binary image was manually compared with the original image for consistency and correct binary conversion. After setting the scale of the image, the amount and

individual size of the LDs in the image, displayed by ImageJ as surface area in µm2, were measured. Incomplete LDs located at the edge of the image were excluded. The sum of the areas of all the LDs present in a cell was used as the total lipid content.

Staining of neutral lipid and DNA was performed in hADSCs cultured on 96-wells plates under PRPF8-silencing as previously described (***Pettersson et al., 2015***). hADSCs were washed with PBS and fixed with 4% paraformaldehyde solution (PFA) containing 0.123 mol/L $NaH_2PO_4x2H_2O$, 0.1 mol/L NaOH and 0.03 mol/L glucose for 10 min at RT. Fixed cells were washed with PBS and stained with Bodipy 500/510 (0.2 µg/ml PBS) and Hoechst (2 µg/ml PBS, Molecular probes) for 20 min at RT. After washing with PBS, accumulation of intracellular lipids (Bodipy staining) and cell number (Hoechst staining for nuclei) were quantified with Cell Insight CX5 High-Content Screening (HCS) Platform (Thermo Fisher Scientific) and High-Content Screening (HCS) Studio Cell Analysis Software 2.0. Total lipid content, LD number and size were normalised by cell number.

Experimental treatments

SGBS preadipocytes at day 4 of differentiation were exposed for 30 h to different treatments inducing IR as previously described (***Díaz-Ruiz et al., 2015***): the inflammatory cytokine tumor necrosis factor alpha (TNFα, 5 nM), a combination of high glucose (4.5 g/L) and high insulin (100 nmol/L) (HGHI), palmitic acid (sodium salt; 500 µM), or oleic acid (500 µM). Palmitic and oleic acid solutions contained 2% fatty acid-free BSA. One sample per experiment was used to obtain control responses in the presence of the solvent. After the treatments, control and TNFα-, HGHI-, palmitic, and oleic acid-treated SGBS

cells were stimulated with insulin (100 nM) for 15 min. At the end of the experiments, SGBS cells were processed for immunoblotting, RNA isolation, and Oil Red-O staining.

In a second series of experiments, the effect of a bile acid known to reduce ER stress, tauroursodeoxycholic acid (TUDCA) (***Uppala et al., 2017***; ***Xia et al., 2017***; ***Zhang et al., 2018***), was tested in SGBS cells exposed to HGHI conditions. To this end, SGBS cells at day 4 were exposed to 0.5 mg/mL TUDCA for 14 h before culture in medium alone or in the presence of glucose (4.5 g/L) and insulin (100 nmol/L) (HGHI) for 30 h. Then, SGBS cells were processed for RNA isolation and dot-blot.

Confocal immunofluorescence microscopy

Samples were visualized by confocal microscopy under an LSM 5 Exciter confocal microscope fitted with Immersol^{TM} immersion oil. Depending on the cell depth, 5-8 stacks per channel were collected and projected in a single image. After acquisition, images underwent a deconvolution process with the software package Huygens Professional 2.4.4.

RNA extraction and real-time PCR (RT-PCR)

Total RNA isolation and purification from human preadipocytes were performed using the RNeasy Kit and RNA from SGBS cells was isolated using TRIzol Reagent following the manufacturers' protocols, and subsequently treated with DNase. Quantification of recovered RNA was assessed using NanoDrop2000 spectrophotometer. One µg of RNA was retrotranscribed to cDNA as previously described (***Peinado et al., 2010***) using with the Revertaid First Strand cDNA Synthesis kit. Transcript levels were quantified by RT-PCR

with GoTaq qPCR Master Mix kit. Previously validated specific primers (***Supplemental file 3***) were designed using Primer3 Input 4.1.0 and purchased from Metabion (Steinkirchen, Germany). Primers or encompassing fragments of the areas from the extremes of two exons were designed to ensure the detection of the corresponding transcripts avoiding genomic DNA amplification. The cDNA was amplified with a thermal profile at the following conditions: hot-start activation at 95 ºC for 2 min, followed by 40 cycles of denaturation (95 ºC for 15 sec), then annealing/extension (60 ºC for 60 sec), and finally, a dissociation cycle (melting curve; 60 ºC to 95 ºC, increasing 0.5 ºC / 30 sec) to verify that only one product was amplified, using the Light-Cycler 96 instrument (Roche; Basilea, Switzerland). The primer concentrations were 500 nM. To allow for variation in the amount of RNA used and the efficiency of the reverse-transcription reaction, all results were normalized by the expression of three house-keeping genes (*ACTB*, *GAPDH* and *HPRT*) and relative quantification was calculated using the ΔCT formula (***Catalán et al., 2007***). All samples for each experiment were run in the same plate in triplicate and the average values were calculated.

qPCR dynamic array

A qPCR dynamic array based on microfluidic technology for simultaneous determination of the expression of 45 transcripts in 36 samples (Fluidigm; San Francisco, CA) was employed (***del Río-Moreno et al., 2019***). Specific primers for human transcripts including components of the major (n=13) and minor spliceosome (n=4), associated splicing factors (n=28), and three housekeeping genes (*ACTB*, *GAPDH*, and *HPRT*) were specifically designed with the Primer3 software and StepOneTM Real-Time PCR System software v2.3 (Applied Biosystems, Foster City, CA). Preamplification, exonuclease treatment, and

qPCR dynamic array based on microfluidic technology were implemented as recently reported (***Gahete et al., 2018***; ***del Río-Moreno et al., 2019***), following manufacturer's instructions using the Biomark System and the Real-Time PCR Analysis Software (Fluidigm). The panel of splicing machinery components was selected on the basis of two main criteria: 1) the relevance of the given spliceosome components in the splicing process (such as the components of the spliceosome core), and 2) their demonstrated participation in the generation of splicing variants implicated in the pathophysiology of metabolic diseases (as is the case of the 28 splicing factors selected in this study) (***Gahete et al., 2018***; ***del Río-Moreno et al., 2019***)

Briefly, following manufacturer's instructions, 12.5 ng of cDNA of each sample were pre-amplified using 1 µL of all primers mix (500 nM) in a T100 Thermal cycler (BioRad, Hercules, CA), using the following program: 1) 2 min at 95 ºC; 2) 15 sec at 94 ºC and 4 min at 60 ºC (14 cycles). Then, samples were treated with 2 µL of 4 U/µL Exonuclease I solution following the manufacturer's instructions. Next, samples were diluted with 18 µL of TE Buffer, and 2.7 µL were mixed with 3 µL of EvaGreen Supermix and 0.3 µL of cDNA Binding Dye Sample Loading Reagent. Primers were diluted to 5 µM with 2 X Assay Loading Reagent. Control line fluid was charged in the chip and Prime script program was run into the IFC controller MX. Finally, 5 µL of each primer and 5 µL of each sample were pipetted into their respective inlets on the chip and the Load Mix script in the IFC controller software was run. Thereafter, the qPCR was run in the Biomark System following the thermal cycling program: 1) 9 ºC for 1 min; 2) 35 cycles of denaturing (95 ºC for 5 sec) and annealing/extension (60 ºC for 20 sec); and 3) a last cycle where final PCR products were subjected to graded temperature-dependent

dissociation (60 ºC to 95 ºC, increasing 1 ºC/3 sec). Data were processed with Real-Time PCR Analysis Software 3.0.

Finally, to control for variations in the efficiency of the retrotranscription reaction, mRNA copy numbers of the different transcripts analysed were adjusted by normalization factor (NF), calculated with the expression levels of the three housekeeping genes mentioned above using GeNorm 3.3 software. This selection was based on the stability of these housekeeping genes among the experimental groups to be compared, wherein the expression of these housekeeping genes was not significantly different among groups.

Quantitative immunoblotting

Human preadipocytes isolated from SC and OM adipose tissue of NG, IR and T2D obese individuals were disrupted in BLC buffer containing 150 mM NaCl, 20 mM Tris-HCl pH 7.4, 1% Triton-X-100, 1 mM EDTA, and 1 µg/mL anti-protease cocktail CLAP (Chymostatin, Leupeptin, Antipain and Pepstatin A). Protein content was measured by Bradford assay and 30 mg of protein per sample were loaded into 4-20 % precast SDS-PAGE gels (Bio-Rad) under denaturing conditions. SGBS cells were homogenized in SDS-DTT buffer containing 62.5 mM Tris-HCL pH 7.6, 2 % SDS, 100 mM DTT, 20% Glycerol. Protein content was separated by 10 % SDS-PAGE under denaturing conditions. In both cases, samples were transferred to nitrocellulose membranes (Bio-Rad), stained with Ponceau to ensure equal sample loading, and blocked in Tris-buffer saline (TBS) consisting of 25 mM Tris, 150 mM NaCl with 0.05% Tween 20 (TTBS) containing 5 % non-fat dry milk for 1 h at RT. Blots were then incubated overnight at 4 ºC with the corresponding primary antibody (***Appendix 1—key resource table***). The antigen-antibody complexes were visualized using horseradish peroxidase

(HRP)-conjugated secondary antibodies (***Appendix 1—key resource table***) and the enhanced chemiluminescence ECL Plus detection system. The intensity of the bands was determined by densitometric analysis with the LAS4000 gel documentation system (GE Healthcare; Barcelona, Spain) and ImageJ software 1.50b, and normalized with Ponceau density values as previously described (***Jimenez-Gomez et al., 2013***; ***Peinado et al., 2011***). All comparative experiments were performed under identical conditions.

Proteasome activity assay

The 26S proteasome (ATP stimulated) and 20S (SDS stimulated) activities were measured in SGBS preadipocytes after a 4 day-exposure to HGHI (***Díaz-Ruiz et al., 2015***; ***Li et al., 2008***). Assays for proteasome activity were performed using Suc-LLVY-AFC product, which is proteolyzed by the chymotrypsin-like (ChT-L) active site of the proteasome forming a fluorogenic substrate (AFC) (***Keita et al., 2014***).

Cells were washed with D-PBS and scraped from plates in BLC buffer without DTT, TX-100 or protease inhibitors because these compounds interfere with the assay. The reaction was conducted in 250 µL of activity assay buffer in a 96-well plate containing 50 µg/ml protein lysate in Proteasome buffer (20 mM Tris–HCl, pH 7.8, 1 mM EDTA, 0.5 mM DTT, 5 mM MgCl2, and 50 µM Suc-LLVY-AFC) plus 2 mM ATP or 0.02% SDS for the determination of the 26S or 20S proteasome, respectively. In order to confirm the specificity of the findings for proteasome activity, parallel reactions containing the proteasome inhibitor, MG-132 (25 µM), were run as controls. The reaction mixture was incubated for 3 h at 37 ºC and the fluorescence of the released AMC product was kinetically followed each 10 min in a Flex Station 3 at an emission wavelength of 355 nm and an excitation

wavelength of 460 nm. The background fluorescence values obtained by incubating the lysates with MG132 were subtracted from activity values. Results were analysed with the SoftMax Pro 2.2.1 and the values reported for proteasome peptidase activity are expressed as relative fluorescence arbitrary units/min/mg of total protein.

Cell viability and cytotoxicity assays

Cell viability of SGBS cell cultures was assessed by the MTT assay. Briefly, cells were incubated for 2 h with 0.1 mg/ml of (3-(4,5-dimetililtiazol-2-ilo)-2,5-difeniltetrazol de bromuro (MTT), dissolved in D-PBS. Washing with D-PBS (1 mL) was followed by the addition of DMSO (1 mL) and gentle shaking for 10 min so that complete dissolution was achieved. Aliquots (200 µL) of the resulting solutions were transferred to 96-well plates and absorbance was recorded at 570 nm using a Flex Station 3. Results were analysed with the SoftMax Pro 2.2.1 and are presented as percentage of the control siRNA values.

Cytotoxicity of PRPF8-silencing in hADSCs was evaluated by Cytotoxicity Detection Kit Plus. The culture medium was aspirated and centrifugated at 3,000 rpm for 10 min to obtain a cell free supernatant. Aliquots of media and warm reagent were mixed in a 96-well plate and absorbance was recorded using a microplate reader (Tecan Infinite 2000; Männedorf, Switzerland). Results were analysed with Magellan software 7.2 SP1.

Measurement of cell proliferation rate

Cell counting in culture flasks was carried out to monitor growth rates of the preadipocytes in culture. At passage 3, cells were detached from the culture flasks and an aliquot was stained with trypan blue and cells were counted in a

Neubauer chamber. Cell proliferation was calculated as the total number of live cells per initial seeding number (***Morten et al., 2016***).

Statistical analysis

For *in vitro* experiments, at least four replicates were obtained for each condition. Data are presented as mean ± standard error of the mean (S.E.M.) and statistical analysis was performed using GraphPad Prism 7. To determine the normality distribution of the samples, Shapiro-Wilk normality test was used. To determine significance, either unpaired t test for parametric data or Mann Whitney test for non-parametric data were employed for comparisons between two groups. For comparison of more than two groups either one-way ANOVA with Tukey's multiple comparisons test for parametric data or Kruskal-Wallis with Dunn's multiple comparisons test for non-parametric were used. A two-way ANOVA was used to identify significant differences between experimental conditions in the response to insulin or during differentiation. Values were considered significant at $P<0.05$. Statistical details and significance can be found in the figure legends.

Acknowledgments

The authors are grateful to the Proteomics Facilities of the SEPBIO/Autonomous University of Barcelona (UAB; Spain) and David Ovelleiro (Proteomics Unit, IMIBIC) for the iTRAQ-LC-MS/MS analysis and the Andalusian Bioinformatics Platform (PAB) centre located at the University of Málaga (Spain) for the Ingenuity Pathway Analysis (IPA) software. We thank Prof. Dr. José Manuel

Fernández-Real (Institut d'Investigació Biomèdica of Girona, Spain) for providing the SGBS cell line.

Additional information

Funding

Funder	Grant reference number	Author
Ministerio de Ciencia, Innovación y Universidades/FEDER	BFU2013-44229-REDT; BFU2016-76711-REDT; BFU2017-90578-REDT	M.M.M.
Ministerio de Ciencia, Innovación y Universidades/FEDER	RTI2018-093919-B-I00	S.F.-V.
Consejería de Salud y Bienestar Social/Junta de Andalucía/FEDER	PI-0200/2013	M.M.M.
Consejería de Salud y Bienestar Social/Junta de Andalucía/FEDER	PI-0159-2016	R.G.-R.
Instituto de Salud Carlos III (ISCIII)/FEDER	PIE14/00005	J.L.-M. and M.M.M.
Instituto de Salud Carlos III (ISCIII)/FEDER	PI16/00264	R.M.L.
Instituto de Salud Carlos III (ISCIII)/FEDER	PI17/0153	J.V.
Fondo de Investigación Sanitaria/ISCIII/FEDER Miguel Servet tenure-track program	CP10/ 00438 and CPII16/00008	S.F.-V.
Research Plan of University of Córdoba	Mod 2.5, 2019	R.G-R.
Co-funded by European Regional Development Fund/European Social Fund "Investing in your future"); and Consejería de Economía, Conocimiento, Empresas y Universidad/Junta de Andalucía/FEDER (BIO-0139). CIBEROBN is an initiative of the ISCIII, Spain.		
The funders had no role in study design, data collection and interpretation, or the decision to submit the work for publication.		

Author contributions

M.M.M. and R.G.-R. designed research. J.L.-M., OA.R.-Z., and A.M. selected the patients from cohort 1. E.M.-M., S.F.-V., and J.V. selected the patients from cohort 2 and performed preadipocyte isolation. J.S.-C., E.M.-C., and M.d.R.-M. performed research and analysed data. D.O. coordinated the iTRAQ/LC-MS/MS study. R.M.L. coordinated the splicing array study. M.R. and J.L. coordinated the

transcriptomic analysis studies. R.G.-R., S.F.-V., J.L.-M., R.M.L., M.R., and J.L. reviewed/edited the manuscript. M.M.M. and J.S.-C. wrote the manuscript. All the authors discussed the results and the manuscript.

Author ORCIDs

María M. Malagón, ORCID iD: 0000-0002-2419-2727.

Rocío Guzmán-Ruiz, ORCID iD: 0000-0001-8020-4676.

Ethics

Human subjects: Written consent was obtained from all the participants prior to recruitment, and the experimental protocol was approved by the Ethics and Research Committee of Reina Sofía University Hospital (HURS; Córdoba, Spain), and University Hospital Joan XXIII (Tarragona, Spain) following the Helsinki Declaration.

Data availability

The proteomic dataset generated during this study are available at ProteomeXchange Consortium via the PRIDE partner repository with the dataset identifier PXD015621. All other data generated during the study are included in the manuscript and supporting files. Source data has been provided for ***Figure 2*** and ***4***.

References

ADA. 2020. 2. Classification and Diagnosis of Diabetes: Standards of Medical Care in Diabetes—2020. *Diabetes Care* **43**:S14 LP-S31. doi:10.2337/dc20-S002

Aprile M, Ambrosio MR, D'Esposito V, Beguinot F, Formisano P, Costa V, Ciccodicola A. 2014. PPARG in human adipogenesis: Differential contribution of canonical transcripts and dominant negative isoforms. *PPAR Research* **2014**:18–20. doi:10.1155/2014/537865

Aprile M, Cataldi S, Ambrosio MR, D'Esposito V, Lim K, Dietrich A, Blüher M, Savage DB, Formisano P, Ciccodicola A, Costa V. 2018. PPARγΔ5, a Naturally Occurring Dominant-Negative Splice Isoform, Impairs PPARγ Function and Adipocyte Differentiation. *Cell Reports* **25**:1577-1592.e6. doi:10.1016/j.celrep.2018.10.035

Arner E, Westermark PO, Spalding KL, Britton T, Rydén M, Frisén J, Bernard S, Arner P. 2010. Adipocyte turnover: Relevance to human adipose tissue morphology. *Diabetes* **59**:105–109. doi:10.2337/db09-0942

Baralle FE, Giudice J. 2017. Alternative splicing as a regulator of development and tissue identity. *Nature Reviews Molecular Cell Biology* **18**:437–451. doi:10.1038/nrm.2017.27

Bard JAM, Goodall EA, Greene ER, Jonsson E, Dong KC, Martin A. 2018. Structure and Function of the 26S Proteasome. *Annual Review of Biochemistry* **87**:697–724. doi:10.1146/annurev-biochem-062917-011931

Berry DC, Jiang Y, Graff JM. 2016. Emerging Roles of Adipose Progenitor Cells

in Tissue Development, Homeostasis, Expansion and Thermogenesis. *Trends in Endocrinology and Metabolism* **27**:574–585. doi:10.1016/j.tem.2016.05.001

Bhattarai KR, Chaudhary M, Kim H-R, Chae H-J. 2020. Endoplasmic Reticulum (ER) Stress Response Failure in Diseases. *Trends in Cell Biology* **30**:672–675. doi:https://doi.org/10.1016/j.tcb.2020.05.004

Bunnell BA, Flaat M, Gagliardi C, Patel B, Ripoll C. 2008. Adipose-derived stem cells: isolation, expansion and differentiation. *Methods (San Diego, Calif)* **45**:115–120. doi:10.1016/j.ymeth.2008.03.006

Chong J, Soufan O, Li C, Caraus I, Li S, Bourque G, Wishart DS, Xia J. 2018. MetaboAnalyst 4.0: Towards more transparent and integrative metabolomics analysis. *Nucleic Acids Research* **46**:W486–W494. doi:10.1093/nar/gky310

Christianson JC, Ye Y. 2014. Cleaning up in the endoplasmic reticulum: Ubiquitin in charge. *Nature Structural and Molecular Biology* **21**:325–335. doi:10.1038/nsmb.2793

Craveiro Sarmento AS, de Azevedo Medeiros LB, Agnez-Lima LF, Lima JG, de Melo Campos JTA. 2018. Exploring Seipin: From Biochemistry to Bioinformatics Predictions. *International Journal of Cell Biology* **2018**:5207608. doi:10.1155/2018/5207608

de sá PM, Richard AJ, Hang H, Stephens JM. 2017. Transcriptional regulation of adipogenesis. *Comprehensive Physiology* **7**:635–674. doi:10.1002/cphy.c160022

Díaz-Ruiz A, Guzmán-Ruiz R, Moreno NR, García-Rios A, Delgado-Casado N, Membrives A, Túnez I, El Bekay R, Fernández-Real JM, Tovar S, Diéguez C, Tinahones FJ, Vázquez-Martínez R, López-Miranda J, Malagón MM. 2015. Proteasome Dysfunction Associated to Oxidative Stress and Proteotoxicity in Adipocytes Compromises Insulin Sensitivity in Human Obesity. *Antioxidants & Redox Signaling* **23**:597–612. doi:10.1089/ars.2014.5939

Ejarque M, Ceperuelo-Mallafré V, Serena C, Pachón G, Núñez-Álvarez Y, Terrón-Puig M, Calvo E, Núñez-Roa C, Oliva-Olivera W, Tinahones FJ, Peinado MA, Vendrell J, Fernández-Veledo S. 2017. Survivin, a key player in cancer progression, increases in obesity and protects adipose tissue stem cells from apoptosis. *Cell death & disease* **8**:e2802. doi:10.1038/cddis.2017.209

Engin AB, Engin A. 2017. Obesity and Lipotoxicity. doi:10.1007/978-3-319-48382-5

Fei W, Li H, Shui G, Kapterian TS, Bielby C, Du X, Brown AJ, Li P, Wenk MR, Liu P, Yang H. 2011. Molecular characterization of seipin and its mutants: implications for seipin in triacylglycerol synthesis. *Journal of lipid research* **52**:2136–2147. doi:10.1194/jlr.M017566

Fiszbein A, Kornblihtt AR. 2017. Alternative splicing switches: Important players in cell differentiation. *BioEssays* **39**:1–11. doi:10.1002/bies.201600157

Gahete MD, del Rio-Moreno M, Camargo A, Alcala-Diaz JF, Alors-Perez E, Delgado-Lista J, Reyes O, Ventura S, Perez-Martínez P, Castaño JP, Lopez-Miranda J, Luque RM. 2018. Changes in Splicing Machinery

Components Influence, Precede, and Early Predict the Development of Type 2 Diabetes: From the CORDIOPREV Study. *EBioMedicine* **37**:356–365. doi:10.1016/j.ebiom.2018.10.056

Gao H, Mejhert N, Fretz JA, Arner E, Lorente-Cebrián S, Ehrlund A, Dahlman-Wright K, Gong X, Strömblad S, Douagi I, Laurencikiene J, Dahlman I, Daub CO, Rydén M, Horowitz MC, Arner P. 2014. Early B Cell Factor 1 Regulates Adipocyte Morphology and Lipolysis in White Adipose Tissue. *Cell Metabolism* **19**:981–992. doi:https://doi.org/10.1016/j.cmet.2014.03.032

Gao H, Volat F, Sandhow L, Galitzky J, Nguyen T, Esteve D, Åström G, Mejhert N, Ledoux S, Thalamas C, Arner P, Guillemot JC, Qian H, Rydén M, Bouloumié A. 2017. CD36 Is a Marker of Human Adipocyte Progenitors with Pronounced Adipogenic and Triglyceride Accumulation Potential. *Stem Cells* **35**:1799–1814. doi:10.1002/stem.2635

Ghaben AL, Scherer PE. 2019. Adipogenesis and metabolic health. *Nature Reviews Molecular Cell Biology* **20**:242–258. doi:10.1038/s41580-018-0093-z

Greene CS, Krishnan A, Wong AK, Ricciotti E, Zelaya RA, Himmelstein DS, Zhang R, Hartmann BM, Zaslavsky E, Sealfon SC, Chasman DI, Fitzgerald GA, Dolinski K, Grosser T, Troyanskaya OG. 2015. Understanding multicellular function and disease with human tissue-specific networks. *Nature Genetics* **47**:569–576. doi:10.1038/ng.3259

Hetz C, Papa FR. 2018. The Unfolded Protein Response and Cell Fate Control. *Molecular Cell* **69**:169–181. doi:10.1016/j.molcel.2017.06.017

Hwang J, Qi L. 2018. Quality Control in the Endoplasmic Reticulum: Crosstalk between ERAD and UPR pathways. *Trends in Biochemical Sciences* **43**:593–605. doi:10.1016/j.tibs.2018.06.005

Kaida D. 2019. Spliceostatin A treatment inhibits mitotic clonal expansion and adipogenesis. *Biochemical and Biophysical Research Communications* **514**:848–852. doi:10.1016/j.bbrc.2019.04.180

Karagöz GE, Acosta-Alvear D, Walter P. 2019. The Unfolded Protein Response: Detecting and Responding to Fluctuations in the Protein-Folding Capacity of the Endoplasmic Reticulum. *Cold Spring Harbor Perspectives in Biology* **11**:a033886. doi:10.1101/cshperspect.a033886

Krämer A, Green J, Pollard J, Tugendreich S. 2014. Causal analysis approaches in ingenuity pathway analysis. *Bioinformatics* **30**:523–530. doi:10.1093/bioinformatics/btt703

Kusaczuk M. 2019. Tauroursodeoxycholate-Bile Acid with Chaperoning Activity: Molecular and Cellular Effects and Therapeutic Perspectives. *Cells* **8**:1471. doi:10.3390/cells8121471

Lessard J, Tchernof A. 2012. Depot- and obesity-related differences in adipogenesis. *Clin Lipidol* **7**:587–596.

Li J-H, Liu S, Zhou H, Qu L-H, Yang J-H. 2013. starBase v2.0: decoding miRNA-ceRNA, miRNA-ncRNA and protein–RNA interaction networks from large-scale CLIP-Seq data. *Nucleic Acids Research* **42**:D92–D97. doi:10.1093/nar/gkt1248

Lin JC. 2015. Impacts of alternative splicing events on the differentiation of

adipocytes. *International Journal of Molecular Sciences* **16**:22169–22189. doi:10.3390/ijms160922169

Liu Y, Gonzàlez-Porta M, Santos S, Brazma A, Marioni JC, Aebersold R, Venkitaraman AR, Wickramasinghe VO. 2017. Impact of Alternative Splicing on the Human Proteome. *Cell Reports* **20**:1229–1241. doi:10.1016/j.celrep.2017.07.025

Longo M, Spinelli R, D'Esposito V, Zatterale F, Fiory F, Nigro C, Raciti GA, Miele C, Formisano P, Beguinot F, Di Jeso B. 2016. Pathologic endoplasmic reticulum stress induced by glucotoxic insults inhibits adipocyte differentiation and induces an inflammatory phenotype. *Biochimica et Biophysica Acta - Molecular Cell Research* **1863**:1146–1156. doi:10.1016/j.bbamcr.2016.02.019

Lowe CE, O'Rahilly S, Rochford JJ. 2011. Adipogenesis at a glance. *Journal of Cell Science* **124**:3726. doi:10.1242/jcs.101741

Martyniak K, Masternak MM. 2017. Changes in adipose tissue cellular composition during obesity and aging as a cause of metabolic dysregulation. *Experimental Gerontology* **94**:59–63. doi:10.1016/j.exger.2016.12.007

Mi H, Muruganujan A, Ebert D, Huang X, Thomas PD. 2019a. PANTHER version 14: More genomes, a new PANTHER GO-slim and improvements in enrichment analysis tools. *Nucleic Acids Research* **47**:D419–D426. doi:10.1093/nar/gky1038

Mi H, Muruganujan A, Huang X, Ebert D, Mills C, Guo X, Thomas PD. 2019b. Protocol Update for large-scale genome and gene function analysis with

the PANTHER classification system (v.14.0). *Nature Protocols* **14**:703–721. doi:10.1038/s41596-019-0128-8

Mitteer DR, Greer BD, Fisher WW, Cohrs VL. 2018. Teaching behavior technicians to create publication-quality, single-case design graphs in graphpad prism 7. *Journal of Applied Behavior Analysis* **51**:998–1010. doi:10.1002/jaba.483

Noormohammadi A, Calculli G, Gutierrez-Garcia R, Khodakarami A, Koyuncu S, Vilchez D. 2018. Mechanisms of protein homeostasis (proteostasis) maintain stem cell identity in mammalian pluripotent stem cells. *Cellular and Molecular Life Sciences* **75**:275–290. doi:10.1007/s00018-017-2602-1

Nowicki M, Bzhalava D, Bała P. 2018. Massively parallel implementation of sequence alignment with basic local alignment search tool using parallel computing in Java library. *Journal of Computational Biology* **25**:871–881. doi:10.1089/cmb.2018.0079

Palumbo P, Lombardi F, Siragusa G, Cifone MG, Cinque B, Giuliani M. 2018. Methods of Isolation, Characterization and Expansion of Human Adipose-Derived Stem Cells (ASCs): An Overview. *International journal of molecular sciences* **19**:1897. doi:10.3390/ijms19071897

Perez-Riverol Y, Csordas A, Bai J, Bernal-Llinares M, Hewapathirana S, Kundu DJ, Inuganti A, Griss J, Mayer G, Eisenacher M, Pérez E, Uszkoreit J, Pfeuffer J, Sachsenberg T, Yilmaz Ş, Tiwary S, Cox J, Audain E, Walzer M, Jarnuczak AF, Ternent T, Brazma A, Vizcaíno JA. 2019. The PRIDE database and related tools and resources in 2019: Improving support for quantification data. *Nucleic Acids Research* **47**:D442–D450.

doi:10.1093/nar/gky1106

Qi L, Tsai B, Arvan P. 2017. New Insights into the Physiological Role of Endoplasmic Reticulum-Associated Degradation. *Trends in Cell Biology* **27**:430–440. doi:10.1016/j.tcb.2016.12.002

Salo VT, Belevich I, Li S, Karhinen L, Vihinen H, Vigouroux C, Magré J, Thiele C, Hölttä-Vuori M, Jokitalo E, Ikonen E. 2016. Seipin regulates ER –lipid droplet contacts and cargo delivery . *The EMBO Journal* **35**:2699–2716. doi:10.15252/embj.201695170

Sarjeant K, Stephens JM. 2019. Adipogenesis 1–20.

Schneider CA, Rasband WS, Eliceiri KW. 2012. NIH Image to ImageJ: 25 years of image analysis. *Nature Methods* **9**:671–675. doi:10.1038/nmeth.2089

Serena C, Keiran N, Ceperuelo-Mallafre V, Ejarque M, Fradera R, Roche K, Nuñez-Roa C, Vendrell J, Fernández-Veledo S. 2016. Obesity and Type 2 Diabetes Alters the Immune Properties of Human Adipose Derived Stem Cells. *Stem Cells* **34**:2559–2573. doi:10.1002/stem.2429

Sha H, Sun S, Francisco AB, Ehrhardt N, Xue Z, Liu L, Lawrence P, Mattijssen F, Guber RD, Panhwar MS, Brenna JT, Shi H, Xue B, Kersten S, Bensadoun A, Péterfy M, Long Q, Qi L. 2014. The ER-associated degradation adaptor protein Sel1L regulates LPL secretion and lipid metabolism. *Cell metabolism* **20**:458–470. doi:10.1016/j.cmet.2014.06.015

Spalding KL, Arner E, Westermark PO, Bernard S, Buchholz BA, Bergmann O, Blomqvist L, Hoffstedt J, Näslund E, Britton T, Concha H, Hassan M, Rydén M, Frisén J, Arner P. 2008. Dynamics of fat cell turnover in humans.

Nature **453**:783–787. doi:10.1038/nature06902

Tam CS, Xie W, Johnson WD, Cefalu WT, Redman LM, Ravussin E. 2012. Defining insulin resistance from hyperinsulinemic-euglycemic clamps. *Diabetes care* **35**:1605–1610. doi:10.2337/dc11-2339

Turunen JJ, Niemelä EH, Verma B, Frilander MJ. 2013. The significant other: Splicing by the minor spliceosome. *Wiley Interdisciplinary Reviews: RNA* **4**:61–76. doi:10.1002/wrna.1141

Untergasser A, Cutcutache I, Koressaar T, Ye J, Faircloth BC, Remm M, Rozen SG. 2012. Primer3-new capabilities and interfaces. *Nucleic Acids Research* **40**:1–12. doi:10.1093/nar/gks596

Vandesompele J, De Preter K, Pattyn F, Poppe B, Van Roy N, De Paepe A, Speleman F. 2002. Accurate normalization of real-time quantitative RT-PCR data by geometric averaging of multiple internal control genes. *Genome biology* **3**:RESEARCH0034.

Yi X, Yang Y, Wu P, Xu X, Li W. 2019. Alternative splicing events during adipogenesis from hMSCs. *Journal of Cellular Physiology* **235**:304–316. doi:10.1002/jcp.28970

Yilmaz E. 2017. Endoplasmic Reticulum Stress and Obesity BT - Obesity and Lipotoxicity In: Engin AB, Engin A, editors. Cham: Springer International Publishing. pp. 261–276. doi:10.1007/978-3-319-48382-5_11

Zhang Ying, Qu P, Ma X, Qiao F, Ma Y, Qing S, Zhang Yong, Wang Y, Cui W. 2018. Tauroursodeoxycholic acid (TUDCA) alleviates endoplasmic reticulum stress of nuclear donor cells under serum starvation. *PloS one*

13:e0196785–e0196785. doi:10.1371/journal.pone.0196785

Zhu M, Heydarkhan-Hagvall S, Hedrick M, Benhaim P, Zuk P. 2013. Manual isolation of adipose-derived stem cells from human lipoaspirates. *Journal of visualized experiments : JoVE* e50585–e50585. doi:10.3791/50585

Table 1. Anthropometric and biochemical characteristics of study subjects from cohort 1.

	NG Obese	IR Obese	T2D Obese
N	27	25	17
Gender (female/male)	13 / 14	13 / 12	11 / 6
Post-menopause (n, %)	2 (15)	2 (15)	3 (27)
Lipid-lowering therapy (n, %)	0 (0)	5 (20)	4 (24)
Antidiabetic therapy (n, %)	0 (0)	3 (12)	8 (47)
Antihypertensive therapy (n, %)	1 (4)	6 (24)	5 (29)
Age (years)	43 ± 3	43 ± 2	46 ± 2
Weight (kg)	140.4 ± 7.0	153.4 ± 10.0	145.4 ± 7.5
Height (m)	1.67 ± 0.03	1.69 ± 0.02	1.65 ± 0.03
Body mass index (kg/m^2)	50.2 ± 2.1	52.8 ± 2.9	52.9 ± 1.9
Fat mass (%)	43.1 ± 1.9	41.2 ± 2.0	42.1 ± 1.7
Lean mass (%)	39.1 ± 3.2	36.1 ± 1.1	35.0 ± 1.0
Water mass (%)	23.0 ± 3.5	22.7 ± 1.6	22.9 ± 1.3
Waist circumference (cm)	144.2 ± 5.9	156.1 ± 8.1	149.9 ± 4.6
Systolic pressure (mm/Hg)	128.1 ± 2.3	127.0 ± 3.5	122.1 ± 2.6
Diastolic pressure (mm/Hg)	78.5 ± 4.4	75.5 ± 3.1	71.5 ± 2.6
Fasting glucose (mg/dL)	88.9 ± 1.8	105.2 ± 2.4 ^{aaa}	159.2 ± 10.0 $^{aaa, bbb}$
Fasting glucose (mmol/L)	4.93 ± 0.10	5.84 ± 0.13 ^{aaa}	8.83 ± 0.56 $^{aaa, bbb}$
Fasting insulin (mU/L)	15.4 ± 1.8	25.9 ± 2.9 ^{aa}	17.9 ± 2.7 ^{b}
HbA1c (%)	5.45 ± 0.06	6.25 ± 0.11 ^{a}	8.51 ± 0.56 $^{aaa, bbb}$
HbA1c (mmol/mol)	32.2 ± 0.6	41.0 ± 1.2 ^{a}	65.7 ± 6.1 $^{aaa, bbb}$
HOMA-IR (units)	3.42 ± 0.44	6.77 ± 0.74 ^{aa}	6.74 ± 1.05 ^{aa}
Total cholesterol (mg/dL)	167.4 ± 10.0	181.6 ± 8.3	198.1 ± 8.6
LDL cholesterol (mg/dL)	122.9 ± 11.1	112.9 ± 6.6	124.2 ± 8.5
HDL cholesterol (mg/dL)	39.5 ± 3.3	36.3 ± 2.1	36.7 ± 1.6
Triglycerides (mg/dL)	108.2 ± 7.0	132.7 ± 12.2	152.0 ± 12.9 ^{a}
Free fatty acids (mmol/L)	66.7 ± 6.3	74.4 ± 7.2	83.5 ± 6.2
C-reactive protein (mg/L)	9.61 ± 1.68	11.4 ± 2.3	17.4 ± 5.3
Uric acid (mg/dL)	6.30 ± 0.32	7.03 ± 0.36	6.85 ± 0.68

NG, normoglycemic; **IR**, insulin-resistant; **T2D**, type 2 diabetes; **LDL**, low-density lipoprotein; **HDL**, high-density lipoprotein; **HbA1c**, glycated hemoglobin; **HOMA-IR**, homeostasis model assessment of insulin resistance. ^{a}P<0.05, ^{aa}P<0.01, ^{aaa}P<0.001 *vs.* NG Obese; ^{b}P<0.05, ^{bbb}P<0.001 *vs*. IR Obese. One-way ANOVA with Tukey's multiple comparisons test or Kruskal-Wallis with Dunn's multiple

comparisons test (for parametric or non-parametric data, respectively, determined by Shapiro-Wilk normality test) were used.

Figure legends

Figure 1. Comparative proteomic analysis of subcutaneous (SC) and omental (OM) preadipocytes from obese subjects with type 2 diabetes (T2D) *vs.* normoglycaemia (NG). Data correspond to individuals from cohort 1. (**A**) Venn diagrams showing overlap of differentially regulated proteins between T2D *vs.* NG obese subjects in SC and OM preadipocytes (left panel). Up-regulated and down-regulated proteins are indicated in the right panel. (**B**) Top10 over-represented canonical pathways in T2D *vs.* NG obese subjects in SC preadipocytes and (**C**) in OM preadipocytes according to Ingenuity Pathway Analysis. Blue and red bars indicate down-regulated and up-regulated pathways, respectively, in T2D *vs.* NG obese subjects. Numbers indicate the number of identified proteins/total proteins annotated to the pathway. Black line indicates -Log_2(*P value*). The online version of this article includes the following figure supplements for Figure 1: ***Figure 1*—Figure supplement 2** and ***Figure 1*—Figure supplement 3**.

Figure 2. Downregulation of the splicing machinery in subcutaneous (SC) preadipocytes is associated with obesity-related insulin resistance (IR) and type 2 diabetes (T2D). (**A**) Hierarchical clustering dendrogram heatmap analysis of splicing-related genes in SC (green) and OM (red) preadipocytes from normoglycemic (NG), IR, and T2D morbidly obese subjects (cohort 1) (n=6) measured by qPCR dynamic array. Rows stand for splicing-related genes (white, mayor spliceosome; grey, minor spliceosome; black, splicing factors), while

columns stand for subject groups. The scale in the colour bar represents -Log_2(Fold Change). (**B**) mRNA levels of *PRPF8* in SC and OM preadipocytes from NG, IR, and T2D morbidly obese subjects (n=6) measured by qPCR dynamic array. (**C**) Representative blot and protein level quantification of PRP8 in SC and OM preadipocytes from NG, IR and T2D morbidly obese subjects (n=6). *****P<0.05, ******P<0.01 *vs.* NG and/or IR subjects, $^{\#\#}$P<0.01 *vs*. SC preadipocytes from the same subjects. (**D**) *PRPF8* mRNA levels and area under the curve (AUC) during *in vitro* differentiation of SC and OM preadipocytes from NG and IR morbidly obese subjects (n=6). *****P<0.05, *******P<0.001 *vs. PRPF8* mRNA levels at Day 0; $^{\#\#\#}$P<0.001 *vs. PRPF8* mRNA levels at Day 3; $^{\$}$P<0.05, $^{\$\$}$P<0.01, $^{\$\$\$}$P<0.001 *vs.* NG. (**E**) mRNA levels of *PRPF8* in SC and OM preadipocytes from lean, and NG and T2D subjects with simple obesity from cohort 2 (n=5-11). *****P<0.05 *vs.* lean and/or NG obese subjects, $^{\#}$P<0.05 *vs*. SC preadipocytes from the same subjects. Data are presented as mean ± standard error of the mean (S.E.M.). One-way ANOVA with Tukey's multiple comparisons test or Kruskal-Wallis with Dunn's multiple comparisons test (for parametric or non-parametric data, respectively, determined by Shapiro-Wilk normality test) were used for B, C, and E; two-way ANOVA was used for D. The online version of this article includes the following figure supplements for Figure 2: ***Figure 2*—Figure supplement 4** and ***Figure 2*—Figure supplement 5**.

Figure 3. *PRPF8* silencing impairs adipogenesis and adipocyte function. (**A**) *PRPF8* mRNA levels in SGBS cells during adipogenesis. (**B**) Representative blot and protein quantification of PRP8 content in SGBS cells during adipogenesis. **ND**, non-detected. *****P<0.05, ******P<0.01, *******P<0.001 vs. preceding differentiation days. (**C**) Representative confocal micrographs of SGBS adipocytes three days

post-transfection (differentiation day 7) with control or *PRPF8*-siRNA stained with Oil Red-O (lipid droplets, red) and DAPI (nucleus, blue). Morphometric analysis of lipid droplets was carried out using ImageJ software. Scale bar = 10 µm. mRNA levels of splicing variants of the transcription factors, *PPARG* and *SREBF1* (**D**), and representative blot and protein level quantification of PPARγ1 and PPARγ2 (**E**), and of the lipid droplet-related proteins, *BSCL2*, *CIDEB*, and *CIDEC* (**F**), in SGBS adipocytes 3 days post-transfection. *****P<0.05, ******P<0.01, *******P<0.001 *vs.* control; $^{\#\#}$P<0.01 *vs. PRPF8*-siRNA; $^{\$}$P<0.05 *vs. PRPF8*-pcDNA3.1. (**G**) Representative blots and protein level quantification of ADRP, BiP, PSMB8, CHOP, DGAT2, FAS, PLIN1, pHSL$^{(Ser563)}$, HSL, Pro-caspase3, and Caspase-3 in SGBS adipocytes 3 days post-transfection. *****P<0.05, ******P<0.01 *vs.* control-siRNA. (**H**) Representative blots and protein level quantification of pAKT$^{(Ser473)}$ and AKT in SGBS adipocytes 3 days post-transfection treated with/without insulin (100nmol/L, 15min). *******P<0.001 *vs.* Control-siRNA -Insulin; $^{\#\#\#}$P<0.001 *vs.* control-siRNA +Insulin. (**I**) Representative confocal micrographs of SGBS adipocytes five days post-transfection (differentitaion day 10) with control, *PRPF8*-siRNA or *PRPF8*-pcDNA3.1 alone, or in combination (*PRPF8* Recovery) stained with Oil Red-O (lipid droplets, red) and DAPI (nucleus, blue). Morphometric analysis of lipid droplets was carried out using ImageJ software. Scale bar = 10 µm. *****P<0.05, ******P<0.01, *******P<0.001 *vs.* control; $^{\#}$P<0.05, $^{\#\#}$P<0.01, $^{\#\#\#}$P<0.001 *vs. PRPF8*-siRNA; $^{\$}$P<0.05. $^{\$\$}$P<0.01 *vs. PRPF8*-pcDNA3.1. (**J**) Schematic representation of the proposed mechanism of action of PRP8 on adipocyte differentiation. PRP8 mediates alternative splicing events regulating the expression and/or isoform balance of the master regulators of adipogenesis, *SREBP1* and *PPARγ* (solid arrows), likely through a direct action on the

corresponding pre-mRNAs. This, in turn, would result in changes in the expression of adipogenic genes down-stream *SREBP1* and *PPARγ* (dashed arrows), yet a direct action of PRP8 on *CIDEB* splicing is also plausible. The observed down-regulation of PRP8 in SC preadipocytes from IR/T2D obese individuals would contribute to the impaired adipogenic capacity of these cells. The model is based on published molecular mechanisms, *in silico* analysis of ENCORI and HumanBase databases, and the main findings shown in this article. This figure was created using graphical elements from Servier Medical Art repository (SMART; https://smart.servier.com/). Data are presented as mean ± standard error of the mean (S.E.M.). One-way ANOVA with Tukey's multiple comparisons test or Kruskal-Wallis with Dunn's multiple comparisons test (for parametric or non-parametric data, respectively) were used for A and B; unpaired t test or Mann Whitney test (for parametric or non-parametric data, respectively) were used for C-G and I; and two-way ANOVA was used for H. Normality distribution was determined by Shapiro-Wilk normality test. The online version of this article includes the following figure supplements for Figure 3: ***Figure 3*—Figure supplement 6** and ***Figure 3*—Figure supplement 7**.

Figure 4. Unbalanced Unfolded Protein Response (UPR) in preadipocytes is associated with obesity-related insulin resistance (IR) and type 2 diabetes (T2D). Data correspond to individuals from cohort 1. Representative blots and protein level quantifications of BiP (**A**), ATF6α^{p90} and ATF6α^{p50} (**B**), pPERK$^{(Thr980)}$ and PERK (**C**), pEIF2α$^{(Ser51)}$ and EIF2α (**D**), CHOP (**E**), pIRE1α$^{(Ser724)}$ and IRE1α (**F**), and PDI and GRP94 (**H**) in subcutaneous (SC) and omental (OM) preadipocytes from normoglycemic (NG), IR and T2D obese subjects (n=6-12). (**G**) mRNA levels of *XBP1s* and *XBP1u* in SC and OM preadipocytes from NG, IR and T2D

obese subjects (n=12). *****P<0.05, ******P<0.01, *******P<0.001 *vs.* NG and/or IR subjects; #P<0.05, ##P<0.01, ###P<0.001 *vs.* SC preadipocytes from the same subjects. Data are presented as mean ± standard error of the mean (S.E.M.). One-way ANOVA with Tukey's multiple comparisons test or Kruskal-Wallis with Dunn's multiple comparisons test (for parametric or non-parametric data, respectively, determined by Shapiro-Wilk normality test) were used.

Figure 5. Activation of Endoplasmic Reticulum-Associated Degradation (ERAD) in preadipocytes is associated with obesity-related insulin resistance (IR) and type 2 diabetes (T2D). Data correspond to individuals from cohort 1. mRNA levels of *BIP* (**A**), *DERL1*, *SEC61A1*, *STT3A* and *STT3B* (**B**), *HRD1*, *RNF185* and *SEL1L* (**C**), and *RAD23A* and *UBQLN1* (**D**), in subcutaneous (SC) and omental (OM) preadipocytes from normoglycemic (NG), IR and T2D obese subjects (n=12). *****P<0.05, ******P<0.01, *******P<0.001 *vs.* NG and/or IR subjects; #P<0.05, #P<0.01, ###P<0.001 *vs.* SC preadipocytes from the same subjects. (**E**) Hierarchical clustering dendrogram heatmap analysis of ERAD-related genes in SC (green) and OM (red) preadipocytes from NG, IR and T2D obese subjects. Rows stand for ERAD-related steps (white, recognition; light grey, retrotranslocation; dark grey, ubiquitination; black, targeting to proteasome), while columns stand for subject groups. The scale in the colour bar represents -Log_2(Fold Change). (**F**) mRNA levels of ERAD-related genes in SGBS preadipocytes exposed during 30 h to high glucose (4.5 g/L)/high insulin (100 nmol/L) (HGHI; white), 5 nM TNFα (light grey), 500 μM Oleate (dark grey) or 500 μM Palmitate (black). *****P<0.05, ******P<0.01 *vs.* corresponding control. (**G**) Hierarchical clustering dendrogram heatmap analysis of ERAD-related genes in SGBS preadipocytes in control (green) and after exposure to HGHI, TNFα,

Oleate or Palmitate (red). Rows stand for ERAD-related steps (white, recognition; light grey, retrotranslocation; dark grey, ubiquitination; black, targeting to proteasome), while columns stand for subject groups. The scale in the colour bar represents -Log_2(Fold Change). (**H**) Chymotrypsin-like peptidase activity of the 26S proteasome (+ATP) and 20S proteasome (+SDS). mRNA levels of ERAD (**I**) and adipogenesis-related (**K**) genes, and representative dot-blot and protein quantification of ubiquitin-conjugated proteins (**J**) in SGBS preadipocytes exposed 14 h to 0.5 mg/mL TUDCA (TUDCA, grey), 30 h to HGHI conditions (white), or a combination of both (TUDCA+HGHI, black). **ND**, non-detected; *****P<0.05, ******P<0.01. *******P<0.001 *vs.* control; $^{\#}$P<0.05, $^{\#\#}$P<0.01, $^{\#\#\#}$P<0.001 *vs.* HGHI; $^{\$}$P<0.05, $^{\$\$}$P<0.01 *vs.* TUDCA. Data are presented as mean ± standard error of the mean (S.E.M.). One-way ANOVA with Tukey's multiple comparisons test or Kruskal-Wallis with Dunn's multiple comparisons test (for parametric or non-parametric data, respectively) were used for A-D; unpaired t test or Mann Whitney test (for parametric or non-parametric data, respectively) were used for F-K. Normality distribution was determined by Shapiro-Wilk normality test. The online version of this article includes the following figure supplements for Figure 5: ***Figure 5*—Figure supplement 8**, ***Figure 5*—Figure supplement 9**, and ***Figure 5*—Figure supplement 10**.

Legends to Figure supplements

Figure 1—Figure supplement 1. (**A**) Cell size of subcutaneous (SC) and omental (OM) mature adipocytes from morbidly obese subjects (hereinafter referred to as obese) with normoglycemia (NG), insulin resistance (IR), or type 2 diabetes (T2D) (cohort 1) (n=6-8). *****P<0.05, *******P<0.001 *vs.* NG and/or IR obese

subjects; ##P<0.01, ###P<0.001 *vs.* SC preadipocytes from the same subjects. (**B**) Representative blot and protein level quantification of DLK1/PREF1, CD45, and CD14 in the stromal-vascular fraction (SVF) and preadipocytes (PreAds) from SC and OM adipose tissue. ***P<0.001 *vs.* SVF. (**C**) mRNA levels of preadipocyte markers in the preadipocyte cultures obtained after 3-4 passages of SVFs isolated from SC and OM adipose tissue samples. (**D**) *m*RNA levels of *KI67* in SC and OM preadipocytes from NG, IR, and T2D obese subjects (n=6). *P<0.05, ***P<0.001 *vs.* NG and/or IR obese subjects; ##P<0.01 *vs.* SC preadipocytes from the same subjects. (**E**) Proliferation rate of SC and OM preadipocytes from NG, IR, and T2D obese subjects (n=20-22). #P<0.05, ##P<0.01 *vs.* SC preadipocytes from the same subjects. (**F**) Representative phase-contrast microscopy images (x100 magnification and zoom) during *in vitro* differentiation of SC and OM preadipocytes from NG, IR and T2D obese subjects. (**G**) mRNA levels of *FABP4*, *ADIPOQ*, and *PPARG* during *in vitro* differentiation of SC and OM preadipocytes from NG and IR obese subjects; the values of the area under the curve (AUC) are also shown (n=6). *P<0.05, **P<0.01, ***P<0.001 *vs.* previous days; #P<0.05, ##P<0.01, ###P<0.001 *vs.* NG Obese. Data are presented as mean ± standard error of the mean (S.E.M.). One-way ANOVA with Tukey's multiple comparisons test or Kruskal-Wallis with Dunn's multiple comparisons test (for parametric or non-parametric data, respectively) were used for A, D, and E; unpaired t test or Mann Whitney test (for parametric or non-parametric data, respectively) were used for B and AUC values; and two-way ANOVA was used for G. Normality distribution was determined by Shapiro-Wilk normality test.

***Figure 1*—Figure supplement 2.** Characterization of the human preadipocyte proteome. Analysis of the proteins identified by iTRAQ-LC-MS/MS in the

proteome of preadipocytes isolated from morbidly obese subjects (cohort 1; hereinafter referred to as obese subjects). (**A**) Proteins were categorized according to biological processes using GO PANTHER classification system (http://www.pantherdb.org/). (**B**) The bar chart represents the GO classification and fold enrichment of significantly over- and under-represented Biological Processes ($p \leq 0.05$ Bonferroni test) in preadipocyte proteome. The black line represents the number of identified proteins per each GO term and the red line represents $-Log_2$(*P value*).

Figure 1—Figure supplement 3. (**A**) Venn diagrams showing overlap of differentially regulated proteins between SC and OM preadipocytes from NG and T2D obese subjects (cohort 1). Over-represented canonical pathways in SC *vs.* OM preadipocytes from NG (**B**), and T2D (**C**) obese subjects according to Ingenuity Pathway Analysis. Blue and red bars indicate down- and up-regulated pathways, respectively, in SC *vs.* OM preadipocytes. Numbers indicate the number of identified proteins/total proteins annotated to the pathway. Black line indicates $-Log_2$(*P value*).

Figure 2—Figure supplement 4. mRNA levels of components of the major spliceosome (**A**), minor spliceosome (**B**), and splicing factors (**C**) in SC and OM preadipocytes from NG, IR, and T2D obese subjects (n=6; cohort 1) measured by qPCR array. Only the genes from the microarray that were significantly regulated are represented (27 out of 42; *PRPF8* is shown in ***Figure 3B***). *****P<0.05, ******P<0.01, *******P<0.001 *vs.* NG and/or IR subjects; $^{\#}$P<0.05, $^{\#\#}$P<0.01, $^{\#\#\#}$P<0.001 *vs.* SC preadipocytes from the same subjects. Data are presented as mean ± standard error of the mean (S.E.M.). One-way ANOVA with Tukey's multiple comparisons test or Kruskal-Wallis with Dunn's multiple comparisons

test (for parametric or non-parametric data, respectively, determined by Shapiro-Wilk normality test).

Figure 2—Figure supplement 5. mRNA levels of components of the major spliceosome (**A**), minor spliceosome (**B**), and splicing factors (**C**) in SC and OM preadipocytes from NG, IR, and T2D obese subjects (n=6) measured by RT-PCR. *****P<0.05, ******P<0.01, *******P<0.001 *vs.* NG and/or IR subjects; $^{\#}$P<0.05, $^{\#\#}$P< 0.01, $^{\#\#\#}$P<0.001 *vs.* SC preadipocytes from the same subjects. Data are presented as mean ± standard error of the mean (S.E.M.). One-way ANOVA with Tukey's multiple comparisons test or Kruskal-Wallis with Dunn's multiple comparisons test (for parametric or non-parametric data, respectively, determined by Shapiro-Wilk normality test).

Figure 3—Figure supplement 6. mRNA levels of *PRPF8* in SGBS adipocytes at day 3 and at day 5 post-transfection (D7 and D10 of differentiation, respectively) (**A**), and representative blot and protein level quantification of PRP8 in SGBS adipocytes at day 5 post-transfection (**B**) with control, *PRPF8*-siRNA or *PRPF8*-pcDNA3.1, alone or in combination (*PRPF8* Recovery). Cell viability of SGBS adipocytes at day 3 and day 5 post-transfection (**C**). mRNA levels of splicing variants of the transcription factors, *PPARG* and *SREBF1* (**D**), representative blot and protein level quantification of PPARγ1 and PPARγ2 (**E**), and mRNA levels of splicing variants of the lipid droplet-related proteins, *BSCL2*, *CIDEB*, and *CIDEC* (**F**) in SGBS adipocytes 5 days post-transfection with control, *PRPF8*-siRNA or *PRPF8*-pcDNA3.1, alone or in combination (*PRPF8* Recovery). *****P<0.05, ******P<0.01, *******P<0.001 *vs.* control; $^{\#}$P<0.05, $^{\#\#}$P<0.01, $^{\#\#\#}$P<0.001 *vs.* *PRPF8*-siRNA; $^{\$}$P<0.05, $^{\$\$}$P<0.01, $^{\$\$\$}$P<0.001 *vs.* *PRPF8*-pcDNA3.1. Representative blots and protein level quantification of ADRP and BiP (**G**), and

mRNA levels of the adipokines, *FABP4* and *ADIPOQ* (**H**), in SGBS adipocytes at day 5 post-transfection. *****P<0.05 *vs.* control. Representative blot and protein level quantification of pAKT$^{(Ser473)}$ and AKT in SGBS adipocytes 5 days post-transfection treated with/without insulin (100 nmol/L, 15 min) (**I**). *******P<0.001 *vs*. without Insulin; $^{###}$P<0.001 *vs.* control-siRNA +Insulin*.* Data are presented as mean ± standard error of the mean (S.E.M.). One-way ANOVA with Tukey's multiple comparisons test or Kruskal-Wallis with Dunn's multiple comparisons test (for parametric or non-parametric data, respectively, determined by Shapiro-Wilk normality test) were used for A-G; and two-way ANOVA was used for I.

Figure 3—Figure supplement 7. (**A**) mRNA levels of *PRPF8* in hADSCs cells during differentiation (days 0-13). (**B**) mRNA levels of *PRPF8* in hADSCs cells transfected with *PRPF8*-siRNA or Control-siRNA at day 1 of differentiation and observed at days 3-6-10 of differentiation; the values of the area under the curve (AUC) are also shown. (**C**) Cytotoxicity assay of hADSCs cells transfected with *PRPF8*-siRNA or Control-siRNA. (**D**) Representative micrographs of hADSCs cells transfected with *PRPF8*-siRNA or Control-siRNA after staining with BODIPY (lipid droplets, red) and Hoechst (nucleus, blue). mRNA levels of splicing variants of the transcription factors, *PPARG* and *SREBF1* (**E**), and of the lipid droplet-related proteins, *BSCL2*, *CIDEB,* and *CIDEC* (**F**) in hADSCs cells transfected with *PRPF8*-siRNA or Control-siRNA. *****P<0.05, ******P<0.01, *******P<0.001 *vs.* day 3 of differentiation; $^{\#}$P<0.05, $^{\#\#}$P<0.01, $^{\#\#\#}$P<0.001 *vs.* day 6 of differentiation; $^{\$}$P<0.05, $^{\$\$}$P<0.01, $^{\$\$\$}$P<0.001 *vs.* Control-siRNA of the same day of differentiation. Data are presented as mean ± standard error of the mean (S.E.M.). One-way ANOVA with Tukey's multiple comparisons test or Kruskal-Wallis with Dunn's multiple comparisons test (for parametric or non-parametric

data, respectively) were used for A; two-way ANOVA was used for B-F; and Unpaired t test or Mann Whitney test (for parametric or non-parametric data, respectively) were used for AUC values. Normality distribution was determined by Shapiro-Wilk normality test.

Figure 5—Figure supplement 8. mRNA levels of ERAD-related genes during *in vitro* differentiation of SC and OM preadipocytes from NG and IR obese individuals (cohort 1). Area under the curve (AUC) is also shown. *****P<0.05, ******P<0.01, *******P<0.001 *vs.* day 0 of differentiation; $^{\#}$P<0.05, $^{\#\#}$P<0.01, $^{\#\#\#}$P<0.001 *vs.* day 3 of differentiation; $^{@@@}$P<0.001 *vs.* day 6 of differentiation; $^{\$}$P<0.05, $^{\$\$}$P<0.01, $^{\$\$\$}$P<0.001 *vs.* NG Obese. Data are presented as mean ± standard error of the mean (S.E.M.). Two-way ANOVA was used for A; one-way ANOVA with Tukey's multiple comparisons test or Kruskal-Wallis with Dunn's multiple comparisons test (for parametric or non-parametric data, respectively) were used for B; and Unpaired t test or Mann Whitney test (for parametric or non-parametric data, respectively) were used for AUC values. Normality distribution was determined by Shapiro-Wilk normality test.

Figure 5—Figure supplement 9. Representative phase-contrast microscopy (x100 magnification and zoom) and confocal micrographs of SGBS preadipocytes exposed during 30 h to a combination of glucose (4.5 g/L) and insulin (100 nM) (HGHI; white bars), 5 nM TNFα (grey bars), 500 µM Oleate (dark grey bars), or 500 µM Palmitate (black bars) (**A**). Cells were stained with Oil Red-O (lipid droplets) and DAPI (nucleus). Lipid droplet number and size in untreated and treated SGBS preadipocytes were assessed by morphometric analysis using ImageJ software (**B**). *****P<0.05, ******P<0.01, *******P<0.001 *vs.* corresponding control. Representative blots and protein level quantification of pAKT$^{(Ser473)}$ and AKT in

SGBS preadipocytes after exposure to insulin (100 nM, 15 min) or medium alone (**C**). ******P<0.01, *******P<0.001 *vs.* corresponding control with insulin. Data are presented as mean ± standard error of the mean (S.E.M.). Unpaired t test or Mann Whitney test (for parametric or non-parametric data, respectively, determined by Shapiro-Wilk normality test) were used.

Figure 5—Figure supplement 10. mRNA levels of ERAD (**A**) and adipogenesis-related genes (**B**) in SGBS preadipocytes overexpressing BiP (pCMV-BIP, white), exposed 14 h to 0.5 mg/mL TUDCA (TUDCA, grey), or a combination of both (TUDCA+pCMV-BIP, black). *****P<0.05, ******P<0.01. *******P<0.001 *vs.* control; $^{\#}$P<0.05, $^{\#\#}$P<0.01, $^{\#\#\#}$P<0.001 *vs.* pCMV-BIP; $^{\$}$P<0.05, $^{\$\$}$P<0.01, $^{\$\$\$}$P<0.001 *vs.* TUDCA. Data are presented as mean ± standard error of the mean (S.E.M.). One-way ANOVA with Tukey's multiple comparisons test or Kruskal-Wallis with Dunn's multiple comparisons test (for parametric or non-parametric data, respectively, determined by Shapiro-Wilk normality test) were used.

Legends to Source data

Figure 1—Source data 1. Common pathways of normoglycemic (NG) and with type 2 diabetes (T2D) obese subjects (cohort 1) in the subcutaneous (SC) *vs.* omental (OM) preadipocytes proteome according to Ingenuity Pathway Analysis (IPA).

Figure 1—Source data 2. Fat depot-specific canonical pathways in the type 2 diabetes (T2D) *vs.* normoglycemic (NG) obese subjects' (cohort 1) proteome according to Ingenuity Pathway Analysis (IPA).

Figure 3—Source data 3. Analysis of CLIP_Seq data (target binding sites and related pathways) from PRPF8-silenced HepG2 and K562 cells provided by The Encyclopedia of RNA Interactomes (ENCORI) database.

Figure 3—Source data 4. Adipose tissue-specific network of the functional interactions of PRPF8 according to HumanBase tool database.

Supplement files

Supplemental file 1. Lineal regression analyses of subcutaneous (SC) and omental (OM) preadipocytes proliferation rate and anthropometric and biochemical parameters.

	SC Preadipocytes		OM Preadipocytes	
	r	***P value***	**r**	***P value***
Age (years)	-0.024	0.875	0.240	0.113
Weight (kg)	-0.373	0.023 *	-0.461	0.004 **
Height (m)	-0.147	0.386	-0.152	0.369
BMI (kg/m^2)	-0.518	0.001 ***	-0.593	<0.0001 ***
Fat mass (%)	-0.585	0.024 *	-0.714	0.004 **
Lean mass (%)	-0.093	0.741	0.696	0.005 **
Water mass (%)	-0.161	0.567	0.436	0.105
Waist circumference (cm)	-0.201	0.341	-0.204	0.352
Systolic pressure (mm/Hg)	-0.617	0.001 **	-0.127	0.553
Diastolic pressure (mm/Hg)	-0.468	0.021 *	-0.053	0.805
Fasting glucose (mg/dL))	-0.324	0.028 *	-0.406	0.005 **
Fasting insulin (mU/L)	-0.418	0.019 *	-0.427	0.017 *
HbA1c (%)	-0.417	0.007 **	-0.442	0.004 **
HOMA-IR (units)	-0.546	0.002 **	-0.512	0.003 **
Total cholesterol (mg/dL)	0.112	0.474	0.075	0.632
LDL cholesterol (mg/dL)	0.160	0.365	0.074	0.679
HDL cholesterol (mg/dL)	0.030	0.865	0.116	0.514
Triglycerides (mg/dL)	-0.170	0.281	-0.337	0.029 *
Free fatty acids (mmol/L)	0.239	0.262	0.431	0.036 *
C-reactive protein (mg/L)	-0.225	0.259	-0.530	0.004 **
Uric acid (mg/dL)	0.047	0.782	0.107	0.527

r=Spearman's correlation coefficient. *P<0.05, **P<0.01, ***P<0.001.

Supplemental file 2. Anthropometric and biochemical characteristics of study subjects from cohort 2.

	Lean	NG Obese	T2D Obese
N	18	15	10
Gender (female/male)	10 / 8	9 / 6	6 / 4
Antidiabetic therapy (n, %)	0 (0)	0 (0)	7 (70)
Age (years)	51 ± 13	54 ± 14	60 ± 8
Weight (kg)	65.6 ± 8.7	92.2 ± 10.7 [aaa]	90.0 ± 11.7 [aaa]
Height (m)	1.68 ± 0.07	1.66 ± 0.10	1.68 ± 0.12
Body mass index (kg/m^2)	23.3 ± 2.1	33.6 ± 2.7 [aaa]	32.1 ± 2.9 [aaa]
Systolic pressure (mm/Hg)	125.1 ± 17.3	138.7 ± 17.5	142.2 ± 15.0
Diastolic pressure (mm/Hg)	74.2 ± 8.3	76.2 ± 9.8	81.6 ± 12.3
Fasting glucose (mg/dL)	88.0 ± 13.2	97.3 ± 15.3	121.6 ± 41.4 [aa, b]
Fasting glucose (mmol/L)	5.51 ± 0.96	5.84 ± 0.80	8.24 ± 5.61 [aa, b]
Fasting insulin (mU/L)	11.4 ± 2.2	12.7 ± 6.7	18.4 ± 1.3
HOMA-IR (units)	2.82 ± 0.94	3.28 ± 1.81	6.91 ± 5.08
Total cholesterol (mg/dL)	184.7 ± 33.6	192.8 ± 51.8	172.2 ± 24.6
LDL cholesterol (mg/dL)	104.1 ± 37.1	124.8 ± 43.9	98.7 ± 10.5
HDL cholesterol (mg/dL)	54.0 ± 11.0	49.7 ± 16.1	43.0 ± 14.0
Triglycerides (mg/dL)	106.7 ± 62.1	142.3 ± 60.1	226.6 ± 162.5 [aa]
Urid acid (mg/dL)	4.65 ± 0.68	5.13± 0.97	6.48 ± 0.96 [aa, b]

NG, normoglycemic; **T2D**, type 2 diabetes; **LDL**, low-density lipoprotein; **HDL**, high-density lipoprotein; **HOMA-IR**, homeostasis model assessment of insulin resistance. [aa]P<0.01, [aaa]P<0.001 *vs.* Lean; [b]P<0.05 *vs*. NG Obese. One-way ANOVA with Tukey's multiple comparisons test or Kruskal-Wallis with Dunn's multiple comparisons test (for parametric or non-parametric data, respectively, determined by Shapiro-Wilk normality test) were used

Supplemental file 3. Sequences and transcript sizes of primers used for RT-PCR studies.

	Primer sequences (5' → 3')		
Gene (NCBI reference)	**Forward**	**Reverse**	**Size (bp)**
Hsa ACTB (NM_001101.3)	ACTCTTCCAGCCTTCCTTCTT	CAGTGATCTCCTTCTGCATCC	176
Hsa ADIPOQ (NM_009605.4)	TGGAGAAGCCGCTTATGTGT	GTCCCGGAATGTTGCAGTAG	159
Hsa BiP (X87949.1)	CTATGAAGCCCGTCCAGAAA	GTCGAGCCACCAACAAGAAC	85
Hsa BSCL2-1 (NM_001122955.3)	TCAGATCCTGGAGCATACCAA	CAGGCAGTGAACTAGCGACA	94
Hsa BSCL2-2/3 (KU178595.1)	GCCTCCTGCTATTTGGCTTT	TCTTCAGGGCTCTCACCATC	309
Hsa CCL2 (NM_002982.4)	CTGGACAAGCAAACCCAAAC	GGGGAAAGCTAGGGGAAAA	90
Hsa CIDEB-1 (NM_001318807.2)	GCCTACAGCCTGCCTCTTTT	TTGTGTTTGAGGTGGGGTCT	72
Hsa CIDEB-2 (NM_014430.3)	GGGCCTACAGGACACAGAAA	TGGACGTGACAGAGATGTGAA	237
Hsa CIDEC-5 (NM_001321142.2)	GAGGCTGTGAGGGGGAGAA	CTTGTCAGCTGGACTGCGTT	154
Hsa CIDE$_{total}$ (NM_001321142.2)	ATGGGAGAGAGGAGGCTTTG	CACTGACACATGCCTGGAGA	147
Hsa DERL1 (NM_001134671.2)	AAGACAAGCAGCGGATGAAG	AGGAAACAAACACCCAGCAA	175
Hsa FABP4 (NM_001442.3)	TGCAGCTTCCTTCTCACCTT	GGCAAAGCCCACTCCTACTT	134
Hsa FABP5 (DN991192)	GAAGGAGCTAGGAGTGGGAATAG	TCTCTCCCAGGGTACAAGAAAA	146
Hsa GAPDH (NM_002046.5)	AATCCCATCACCATCTTCCA	AAATGAGCCCCAGCCTTC	122
Hsa HPRT (S79316.1)	TAATCCAGCAGGTCAGCAAAG	CTGAGGATTTGGAAAGGGTGT	157
Has HRD1 (AB085847.1)	TGATGGGCAAGGTGTTCTTT	GCCAGTGGAAACATTTGAGG	177
Hsa KI67 (NM_002417)	GACATCCGTATCCAGCTTCCT	GCCGTACAGGCTCATCAATAAC	233
***Hsa γORF4* (Aprile et al., 2014)**	AAACCCAAAACAACTTCCCG	CTTGCAGTGGGGATGTCTCA	279
Hsa PDGFRA (NM_006206.6)	CCTTTTTGTGACGGTCTTGG	AAAGGCTACATCTGGGTCTGG	148
***Hsa PPARG-1* (Aprile et al., 2014)**	CGAGGACACCGGAGAGGG	TGTGGTTTAGTGTTGGCTTCTT	69
Hsa PPARG-2 (NM_015869.4)	AGGAGTGGGAGTGGTCTTCC	TTTTAACGGATTGATCTTTTGC	255
Hsa PPARG-3 (NM_138711.3)	TGGGTGTGTAGTCGTGGTACTTT	CTCGGTTACTCCCCGTTTCT	82
Hsa PPARG-4 (NM_005037.6)	GCCGTGGCCGCAGAAA	CCACGGAGCTGATCCCAAAG	76
***Hsa PPARG$_{total}$* (Aprile et al., 2014)**	ATGGCCACCTCTTTGCTCT	GAGAAGGAGAAGCTGTTGGC	272
Hsa RAD23A (D21235.1)	TGGCCCAAATCTTTCCATC	TGAGCTGATGTTAGCCCTTCTC	100
Hsa RNF185 (NM_152267.3)	CAACAGGACCCCAGAGAGAA	CCACCATCTCCAAATCCAAA	101
Hsa SEC61A1 (NM_013336.3)	GAGTGGACCTGCCAATCAAG	AGCTGAGAGCATTTGGGAGA	146
Hsa SEL1L (AF052059.1)	CCTGCCACTTCCCTTTTCTT	CCATTTCTGCTTCCTGCATC	180
Hsa SREBF1-1 (NM_001005291.3)	GACCGACATCGAAGGTGAAG	GGTCAAATAGGCCAGGGAAG	158
Hsa SREBF1$_{total}$ (NM_001005291.3)	AGCTCAAGGATCTGGTGGTG	TGTGTTGCAGAAAGCGAATG	93
Hsa STT3A (NM_001278503.1)	AGCTATGGCAAACCGAACAA	CCTCCAAAAATGACCAGCAC	153
Hsa STT3B (NM_178862.2)	CCCTCCTCCTTTTTCTTCCTC	ACGACTTGTGCTTGCTCTCC	153
Hsa TGFB2 (NM_000660.6)	GCAACAATTCCTGGCGATAC	CTAAGGCGAAAGCCCTCAA	136
Hsa UBQLN1 (NM_013438.4)	CAACACACCAGGAATGCAGA	CTTCTCATGTAGGGGGCAGA	90
Hsa UPK3B (NM_030570.3)	TGCACTCAGGAGGGTTTAGG	ATGGTGGAGCAGGAGAGACA	135
Hsa XBP1s (NM_001079539.1)	TGGATGCCCTGGTTGCT	CACCTGCTGCGGACTCA	87
Hsa XBP1u (NM_005080.3)	CGCAGCACTCAGACTACGTG	CTGGGTCCAAGTTGTCCAGA	147
Mmu PRPF8 (NM_138659.2)	TACATGACGGCCAAGAACAA	TGCAATCCCAGTACAAGCAA	146

bp, base pairs**.**

1619 **Appendix 1—key resource table**

Reagent type (species) or resource	Designation	Source or reference	Identifiers	Additional information
Cell line (*Homo sapiens*)	Human preadipocytes from SC and OM adipose tissue	This paper	N/A	Primary cell line
Cell line (*Homo sapiens*)	Human adipose-derived stromal cells (hADSCs)	This paper and previous work from Dr. Mikael Rydén group	(***Gao et al., 2017***, ***2014***)	SC adipose tissue from a male donor (16 years old, BMI 24 kg/m^2)
Cell line (*Homo sapiens*)	Simpson-Golabi-Behmel syndrome (SGBS) cell line	Gift from Prof. Dr. José Manuel Fernández-Real (Institut d'Investigació Biomèdica; Girona, Spain)	N/A	
Biological sample (*Homo sapiens*)	Human SC and OM adipose tissue from NG, IR and T2D morbid obese individuals (cohort 1)	General and Digestive Surgery Unit and the Lipids and Atherosclerosis Unit of the Reina Sofía University Hospital (Córdoba, Spain)	Reina Sofía University Hospital Research Ethical Committee (439/2010)	
Biological sample (*Homo sapiens*)	Human SC and OM adipose tissue from lean, NG and, T2D obese individuals (cohort 2)	Endocrinology ad Surgery Departments at the University Hospital Joan XXIII (Tarragona, Spain)	(Ejarque et al., 2017; Serena et al., 2016)	
Antibody	ADRP (B-6) (mouse monoclonal)	Santa Cruz Biotechnology	sc-377429, N/A	(1:1000)
Antibody	AKT (rabbit polyclonal)	Cell Signaling Technology	9272, AB_329827	(1:1000)
Antibody	ATF6α (H-280) (rabbit polyclonal)	Santa Cruz Biotechnology	sc-22799, AB_2242950	(1:1000)
Antibody	CASPASE-3 (8G10) (rabbit monoclonal)	Cell Signaling Technology	9665, AB_2069872	(1:1000)
Antibody	CD14 (M-305) (rabbit polyclonal)	Santa Cruz Biotechnology	sc-9150, AB_2074171	(1:1000)
Antibody	CD45 (H-230) (rabbit polyclonal)	Santa Cruz Biotechnology	sc-25590, AB_2174143	(1:1000)
Antibody	CHOP (L63F7) (mouse monoclonal)	Cell Signaling Technology	2895, AB_2089254	(1:1000)
Antibody	DGAT2 (goat polyclonal)	Novus	NB100-57851, AB_921135	(1:1000)
Antibody	DLK/PREF1 (H-118) (rabbit polyclonal)	Santa Cruz Biotechnology	sc-25437, AB_2292943	(1:1000)
Antibody	eIF2α (3A7A8) (mouse monoclonal)	Santa Cruz Biotechnology	sc-517214, N/A	(1:1000)
Antibody	FAS (C-20) (goat polyclonal)	Santa Cruz Biotechnology	sc-16147, AB_2101097	(1:1000)
Antibody	BiP/GRP78 (A-10) (mouse monoclonal)	Santa Cruz Biotechnology	sc-376768, N/A	(1:1000)
Antibody	GRP94 (rabbit polyclonal)	Cell Signaling Technology	2104, AB_823506	(1:1000)
Antibody	HSL/LIPE (rabbit polyclonal)	Abcam	ab45422, AB_2135367	(1:1000)
Antibody	IRE1α (B-12) (mouse monoclonal)	Santa Cruz Biotechnology	sc-390960, N/A	(1:1000)
Antibody	PDI (C81H6) (rabbit monoclonal)	Cell Signaling Technology	3501, AB_2156433	(1:1000)

Antibody	PERK (B-5) (mouse monoclonal)	Santa Cruz Biotechnology	sc-377400, AB_2762850	(1:1000)
Antibody	Phospho-AKT (Ser473) (rabbit monoclonal)	Cell Signaling Technology	4060, AB_2315049	(1:750)
Antibody	Phospho-eIF2α (Ser51) (rabbit polyclonal)	Santa Cruz Biotechnology	sc-101670, AB_2096507	(1:750)
Antibody	Phospho-HSL/LIPE (Ser563) (rabbit polyclonal)	Cell Signaling Technology	4139, AB_2135495	(1:750)
Antibody	Phospho-IRE1α (Ser724) (rabbit polyclonal)	Abcam	ab48187, AB_873899	(1:750)
Antibody	Phospho-PERK (Thr981) (rabbit polyclonal)	Santa Cruz Biotechnology	sc-32577, AB_2293243	(1:750)
Antibody	PLIN1 (guinea pig polyclonal)	Progen	GP29, N/A	(1:1000)
Antibody	PPARγ (D69) (rabbit polyclonal)	Cell Signaling Technology	2430, AB_823599	(1:1000)
Antibody	PRP8 (E-5) (mouse monoclonal)	Santa Cruz Biotechnology	sc-55533, AB_831685	(1:1000)
Antibody	PSMB8/LMP7 (sheep polyclonal)	R&D Systems	AF7710, N/A	(1:1000)
Antibody	UBIQUITIN (rabbit polyclonal)	Cell Signaling Technology	3933, AB_2180538	(1:1000)
Antibody	Goat/Sheep IgG (mouse monoclonal)	Sigma-Aldrich	A9452, AB_258449	(1:2500)
Antibody	Guinea Pig IgG (goat polyclonal)	Sigma-Aldrich	A7289, AB_258337	(1:2500)
Antibody	Mouse IgG (rabbit polyclonal)	Sigma-Aldrich	A9044, AB_258431	(1:2500)
Antibody	Rabbit IgG (goat polyclonal)	Sigma-Aldrich	A8275, AB_258382	(1:10000)
Recombinant DNA reagent	phrGFP-N1	Agilent Technologies	240036	
Recombinant DNA reagent	pcDNA3.1(+)	Invitrogen	V79020	
Recombinant DNA reagent	*PRPF8* (*NM_006445*) in pcDNA3.1(+)	GenScript	OHu19527C	
Recombinant DNA reagent	pCMV-Myc	Clontech	635689	
Recombinant DNA reagent	pCMV-BiP-Myc-KDEL-wt	AddGene	27164	
Sequence-based reagent	Primers for RT-PCR, see ***Supplemental file 3***	This paper	N/A	
Sequence-based reagent	Primers for splicing-machinery components array	(***Gahete et al., 2018***)	N/A	
Sequence-based reagent	*PRPF8* Silencer™ Select Validated siRNA	Ambion	4390824	
Sequence-based reagent	Silencer™ Select Negative Control No. 1 siRNA	Ambion	4390843	
Peptide, recombinant protein	3-Isobutyl-1-methylxanthine (IBMX)	Sigma-Aldrich	I5879	
Peptide, recombinant protein	Antipain	Sigma-Aldrich	A6191	
Peptide, recombinant protein	Biotin	Sigma-Aldrich	B4639	

Peptide, recombinant protein	Bovine Serum Albumin (BSA)	Sigma-Aldrich	A8806, A7030
Peptide, recombinant protein	Chymostatin	Sigma-Aldrich	C7268
Peptide, recombinant protein	Collagenase Type V	Sigma-Aldrich	C9263
Peptide, recombinant protein	Dexamethasone	Sigma-Aldrich	D4902, D1756
Peptide, recombinant protein	Human 3,3',5-Trihydrochloride sodium salt (T3)	Sigma-Aldrich	T5516, T6397
Peptide, recombinant protein	Human FGF2	Sigma-Aldrich	F0291
Peptide, recombinant protein	Human Insulin	Sigma-Aldrich	I2643, I9278
Peptide, recombinant protein	Human Transferrin	Sigma-Aldrich	T8158
Peptide, recombinant protein	Human Tumor Necrosis Factor-α (TNFα)	Sigma-Aldrich	T6674
Peptide, recombinant protein	Hydrocortisone	Sigma-Aldrich	H0135
Peptide, recombinant protein	Leupeptin	Sigma-Aldrich	L2884
Peptide, recombinant protein	MG-132	Calbiochem	474790
Peptide, recombinant protein	N-Succinyl-Leu-Leu-Val-Tyr-7-Amido-4-Methylcoumarin (Suc-LLVY-AFC)	Sigma-Aldrich	S6510
Peptide, recombinant protein	Pepstatin A	Sigma-Aldrich	P4265
Peptide, recombinant protein	Rosiglitazone	Sigma-Aldrich	R2408
Chemical compound, drug	(+)-Sodium L-ascorbate	Sigma-Aldrich	A4034
Chemical compound, drug	1,4-dithiothreitol (DTT)	Thermo Scientific	R0862
Chemical compound, drug	Acetonitrile	Sigma-Aldrich	271004
Chemical compound, drug	Adenosine 5′-triphosphate (ATP) disodium salt hydrate	Sigma-Aldrich	A26209
Chemical compound, drug	BODIPY™ 500/510 C_1, C_{12} (4,4-Difluoro-5-Methyl-4-Bora-3a,4a-Diaza-s-Indacene-3-Dodecanoic Acid)	Invitrogen	D3823
Chemical compound, drug	Calcium chloride ($CaCl_2$)	Sigma-Aldrich	449709
Chemical compound, drug	CHAPS hydrate	Sigma-Aldrich	C3023
Chemical compound, drug	Chloroform	Sigma-Aldrich	C2432
Chemical compound, drug	Clarity Western ECL Substrate	Bio-Rad	1705061
Chemical compound, drug	D-(+)-Glucose	Panreac Applichem / Siga-Aldrich	1413411211, G8270
Chemical compound, drug	DAPI	Sigma-Aldrich	D9542
Chemical compound, drug	Dimethyl sulfoxide (DMSO)	Sigma-Aldrich	D4540

Chemical compound, drug	D-Pantothenic acid hemicalcium salt	Sigma-Aldrich	P5155
Chemical compound, drug	Dulbecco's Phosphate Buffered Saline (D-PBS) Solution	Sigma-Aldrich	D1408
Chemical compound, drug	Dulbecco's Phosphate Buffered Saline (D-PBS) Solution (-) Ca^{2+}, Mg^{2+}	HyClone	SH30028.02
Chemical compound, drug	Dulbecco's Modified Eagle Medium (DMEM)/F-12 (1:1)	Gibco	31330-038
Chemical compound, drug	EDTA disodium salt	Sigma-Aldrich	E5134
Chemical compound, drug	Exonuclease I Reaction Buffer	New England BioLabs	B0293S
Chemical compound, drug	Fluorescence Mounting Medium	Dako	S3023
Chemical compound, drug	Formic acid	Scharlau	AC10760050
Chemical compound, drug	Glycerol	VWR	97063-892
Chemical compound, drug	Ham's F-12 Nutrient Mix	Gibco	21765037
Chemical compound, drug	Hepes Buffer (1M)	Gibco	15630056
Chemical compound, drug	Hoechst 33342, Trihydrochloride, Trihydrate	Invitrogen	H3570
Chemical compound, drug	Immersol™ Immersion Oil	Carl Zeiss	518F
Chemical compound, drug	Iodoacetamide (IAA)	Sigma-Aldrich	I1149
Chemical compound, drug	Isopropanol	Sigma-Aldrich	33539
Chemical compound, drug	iTRAQ™ Reagents	Applied Biosystems	PN4351918
Chemical compound, drug	Lipofectamine 2000 Transfection Reagent	Invitrogen	11668019
Chemical compound, drug	Lipofectamine RNAiMAX Transfection Reagent	Invitrogen	13778150
Chemical compound, drug	Magnesium Chloride ($MgCl_2$)	Merck	5833
Chemical compound, drug	Magnesium Sulfate 7-hydrate ($MgSO_4$)	Panreac Applichem	141404
Chemical compound, drug	Methanol (MeOH)	VWR Chemicals	20864320
Chemical compound, drug	Newborn Calf Serum (NCS)	Gibco	16010159
Chemical compound, drug	Nonfat dried milk powder	Panreac Applichem	Cat# A0830
Chemical compound, drug	Oil Red O	Sigma-Aldrich	O0625
Chemical compound, drug	Oleic acid	Sigma-Aldrich	O1383
Chemical compound, drug	Opti-MEM™ I Reduced Serum Medium	Gibco	11058021
Chemical compound, drug	Paraformaldehyde (PFA)	Bosterbio	AR1068

Chemical compound, drug	Penicillin-Streptomycin (10,000 U/mL)	Sigma-Aldrich / Gibco	P4333, 15140122
Chemical compound, drug	Potassium Chloride (KCl)	Merck	104936
Chemical compound, drug	Ponceau S	Sigma-Aldrich	P3504
Chemical compound, drug	RBC Lysis Buffer	Norgen Biotek Corp.	21201
Chemical compound, drug	RNase-Free DNase Set	Qiagen	79254
Chemical compound, drug	Sodium Chloride (NaCl)	Merk Millipore	7647145
Chemical compound, drug	Sodium Dodecyl Sulfate (SDS)	Sigma-Aldrich	L3771
Chemical compound, drug	Sodium Hydroxide (NaOH)	Sigma-Aldrich	S4085
Chemical compound, drug	Sodium Palmitate	Sigma-Aldrich	P9767
Chemical compound, drug	Sodium Phosphate Monobasic Monohydrate (NaH_2PO_4)	Fisher scientific	BP330-1
Chemical compound, drug	Sodium Phosphate Monobasic Monohydrate Dihydrate ($NaH_2PO_4x2H_2O$)	Sigma-Aldrich	71505
Chemical compound, drug	TE Buffer	Invitrogen	12090015
Chemical compound, drug	Tetraethylammonium Bromide (TEAB)	Sigma-Aldrich	241059
Chemical compound, drug	Thiazolyl Blue Tetrazolium Bromide (MTT)	Sigma-Aldrich	M5655
Chemical compound, drug	Trichloroacetic acid (TCA)	Sigma-Aldrich	T6399
Chemical compound, drug	Triton™ X-100	Sigma-Aldrich	T8787
Chemical compound, drug	Trizma® base (Tris base)	Sigma-Aldrich	T6066
Chemical compound, drug	Trizma® hydrochloride (Tris-HCl)	Sigma-Aldrich	T3253
Chemical compound, drug	TRIzol™ Reagent	Invitrogen	15596018
Chemical compound, drug	Trypan Blue solution	Sigma-Aldrich	T8154
Chemical compound, drug	Trypsin Gold, Mass Spectrometry Grade	Promega	V5280
Chemical compound, drug	Trypsin-EDTA solution	Sigma-Aldrich	T3924
Chemical compound, drug	Tween® 20	Panreac Applichem	A1389
Chemical compound, drug	Urea	Sigma-Aldrich	U1205
Commercial assay or kit	96.96 DNA Binding Dye Sample / Loading Kit	Fluidigm	BMK-M10-96.96-EG
Commercial assay or kit	AllPrep DNA/RNA/Protein Mini Kit	Qiagen	80004
Commercial assay or kit	Cytotoxicity Detection Kit Plus	Roche	4744926001

Commercial assay or kit	GoTaq® qPCR Master Mix	Promega	A6001
Commercial assay or kit	Mycoplasma gel detection kit	Biotools	4542
Commercial assay or kit	NEON™ Transfection System Kit	Invitrogen	MPK10096
Commercial assay or kit	Protein Assay Dye Reagent Concentrate	Bio-Rad	5000006
Commercial assay or kit	RC DC™ Protein Assay	Bio-Rad	5000122
Commercial assay or kit	RevertAid First Strand cDNA Synthesis Kit	Thermo Scientific	K1621
Commercial assay or kit	SsoFast™ EvaGreen® Supermix	Bio-Rad	1725200
Software, algorithm	Biomark & EP1 Software 4.5.2	Fluidigm	https://www.fluidigm.com/software
Software, algorithm	Basic Local Alignment Search Tool (BLAST)	NCBI (Nowicki et al., 2018)	https://blast.ncbi.nlm.nih.gov/Blast.cgi
Software, algorithm	ENCORI: The Encyclopedia of RNA Interactomes	(***Li et al., 2013***)	http://starbase.sysu.edu.cn/index.php
Software, algorithm	GeNorm 3.3	(***Vandesompele et al., 2002***)	https://genorm.cmgg.be/
Software, algorithm	GraphPad PRISM 7	GraphPad Software, Inc. (Mitteer et al., 2018)	https://www.graphpad.com
Software, algorithm	High-Content Screening (HCS) Studio Cell Analysis Software 2.0	Thermo Fisher Scientific	https://www.thermofisher.com/es/es/home/life-science/cell-analysis/cellular-imaging/high-content-screening/hcs-studio-2.html
Software, algorithm	Human Base tool	(***Greene et al., 2015***)	https://hb.flatironinstitute.org/
Software, algorithm	Huygens Professional 2.4.4	Scientific Volume Imaging	https://svi.nl/Huygens-Professional
Software, algorithm	ImageJ 1.50b	National Institute of Health (NIH) (***Schneider et al., 2012***)	https://imagej.nih.gov/ij/
Software, algorithm	Ingenuity Pathways Analysis (IPA) 49309495	Qiagen, provided by the Andalusian Bioinformatics Platform (PAB) center (University of Málaga, Spain; www.scbi.uma.es) (***Krämer et al., 2014***)	www.ingenuity.com
Software, algorithm	LightCycler® 96 1.1.0.1320	Roche Life Science	https://lifescience.roche.com/en_es/products/lightcycler-381711.html

Software, algorithm	Magellan™ software 7.2 SP1	Tecan	https://lifesciences.tecan.com/software-magellan
Software, algorithm	MetaboAnalyst 4.0	(***Chong et al., 2018***)	https://www.metaboanalyst.ca/docs/About.xhtml
Software, algorithm	Primer3 Input 4.1.0	(***Untergasser et al., 2012***)	http://bioinfo.ut.ee/primer3/
Software, algorithm	Protein ANalysis THrough Evolutionary Relationships (PANTHER) classification system 14.1	(***Mi et al., 2019a***, ***2019b***)	http://www.pantherdb.org/
Software, algorithm	Real-Time PCR Analysis Software 3.0	Fluidigm	https://www.fluidigm.com/
Software, algorithm	SoftMax Pro 2.2.1	Molecular Devices	https://www.moleculardevices.com/
Software, algorithm	Statistic R module	Pearl software	https://www.pearlsoftware.com/
Software, algorithm	StepOne™ Real-Time PCR System 2.3	Thermo Scientific	https://www.thermofisher.com/es/es/home.html
Software, algorithm	Stratagene Mx3000p	Thermo Scientific	https://www.thermofisher.com/es/es/home.html
Software, algorithm	Venn Diagram Plotter	Pacific Northwest National Laboratory	https://omics.pnl.gov/software/venn-diagram-plotter

Figure 1

A

T2D Obese *vs.* NG Obese

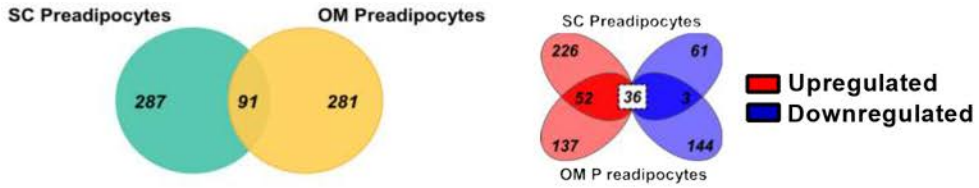

B

T2D Obese *vs.* NG Obese dysregulated pathways in SC Preadipocytes

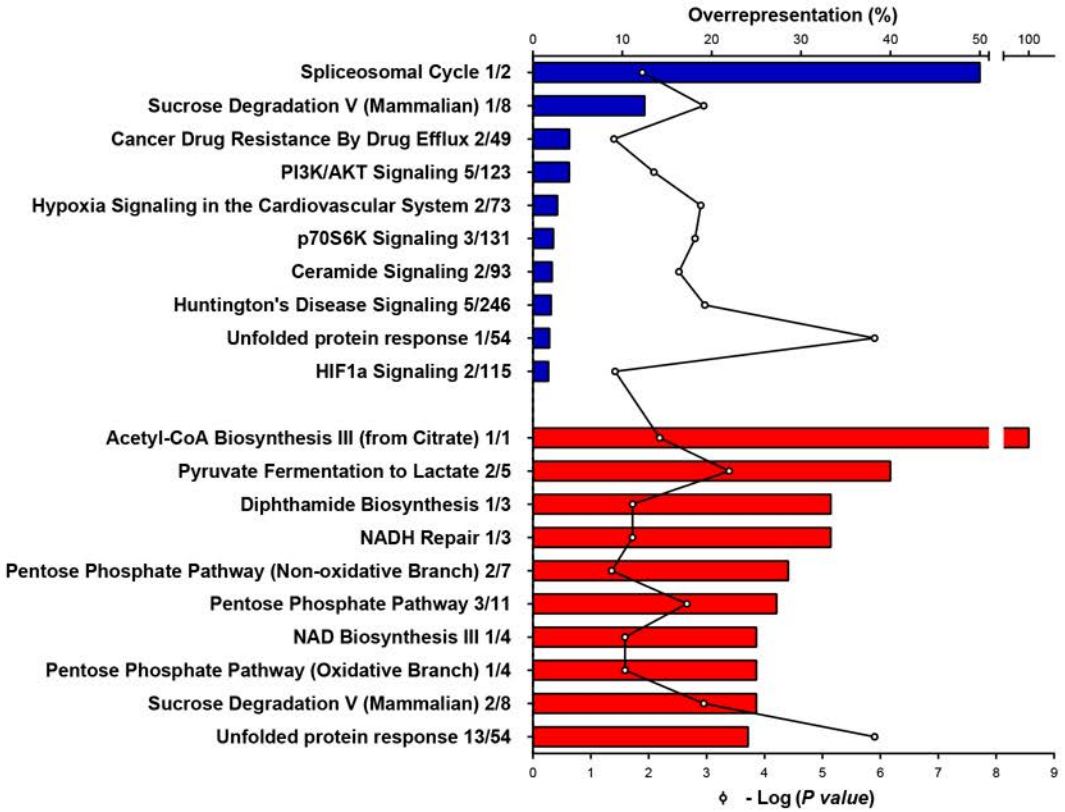

C

T2D Obese *vs.* NG Obese dysregulated pathways in OM Preadipocytes

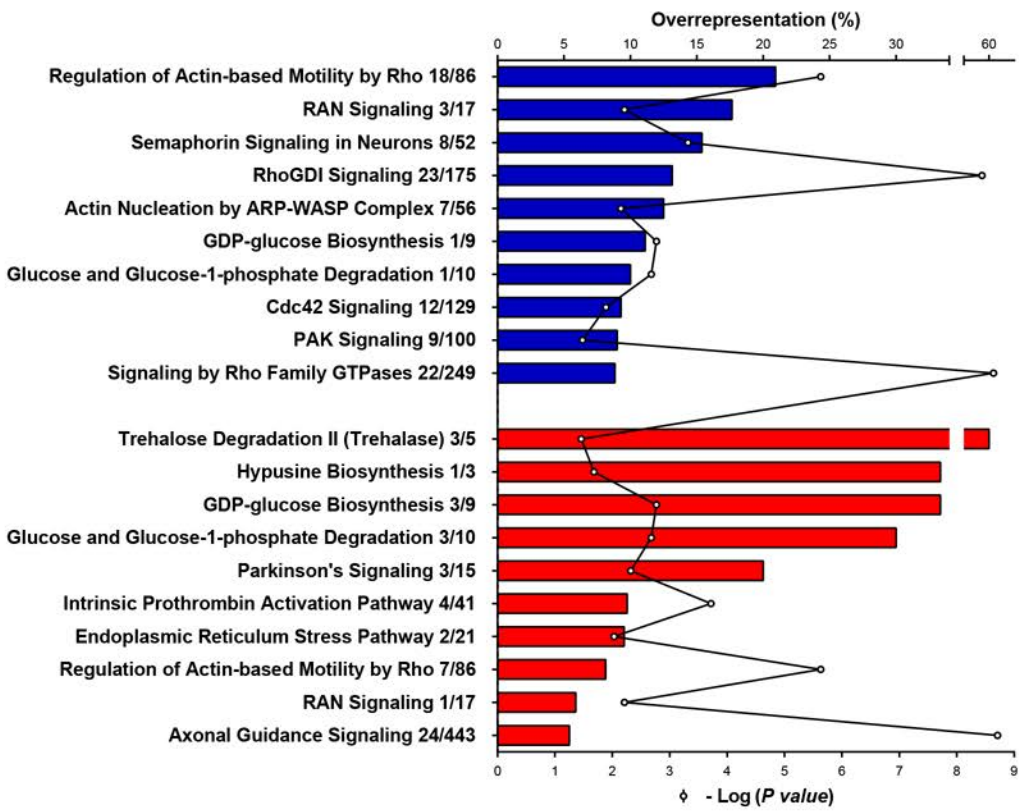

Figure 2

A

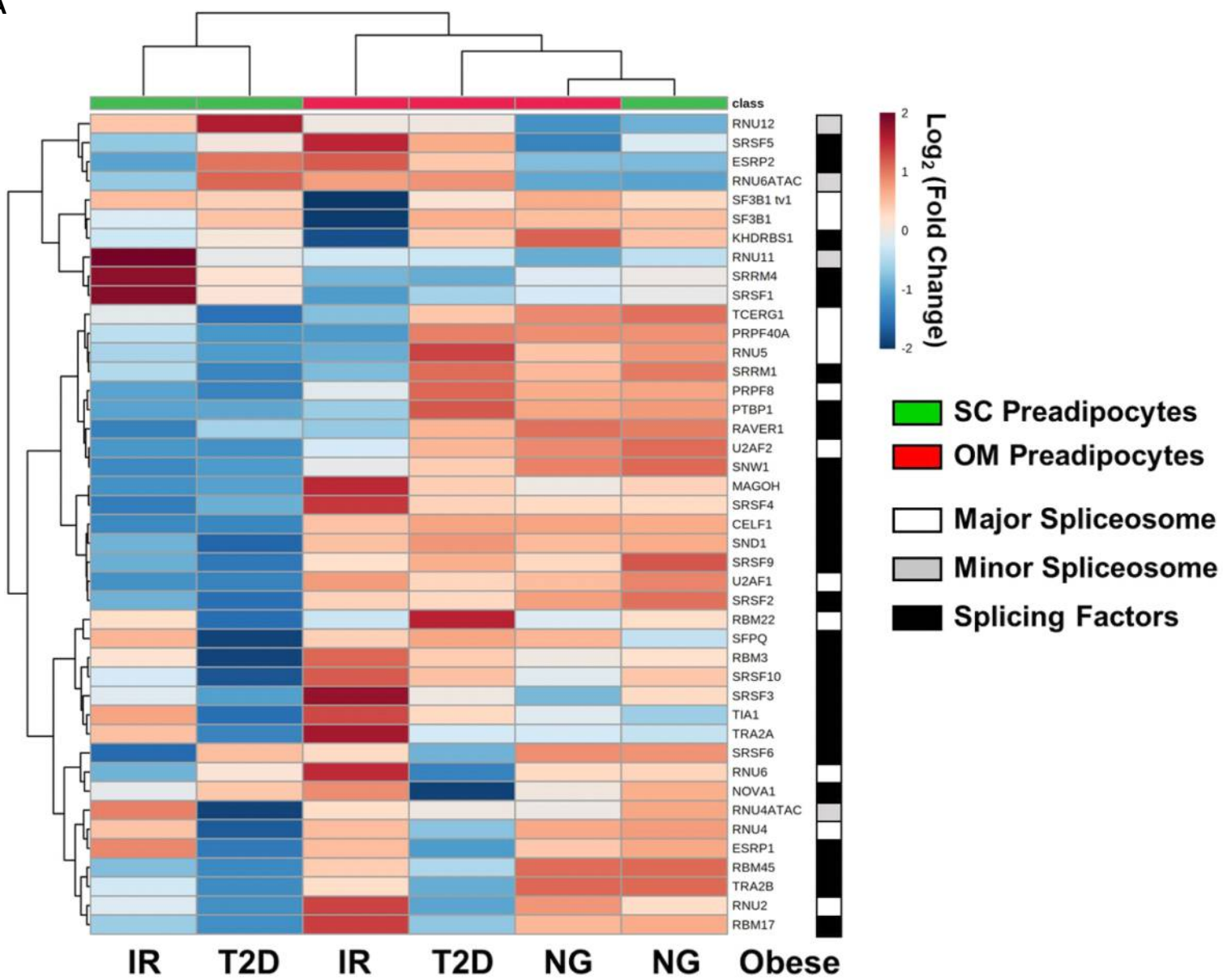

B

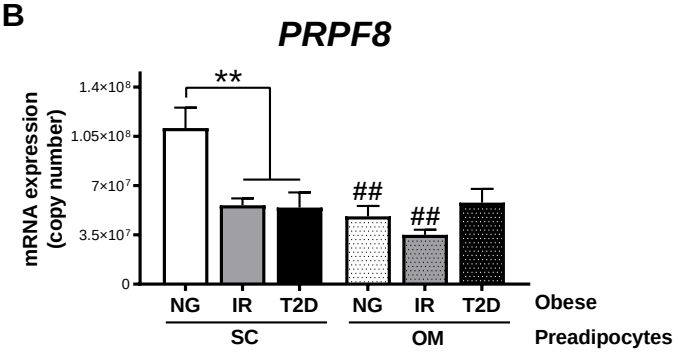

C

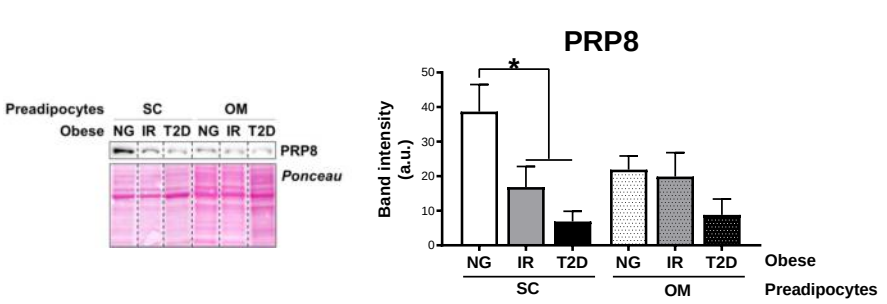

D

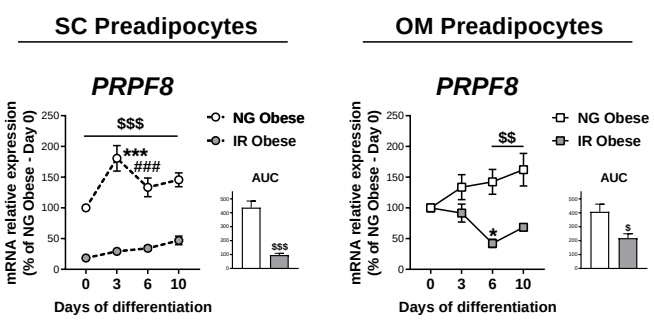

E

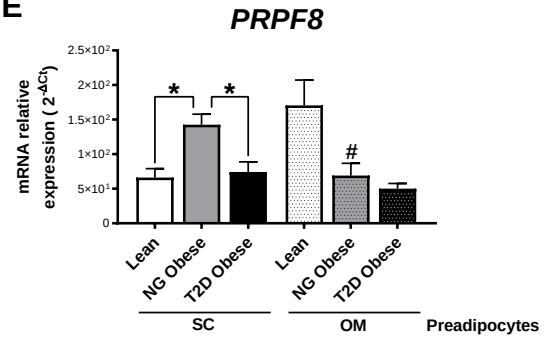

Figure 3

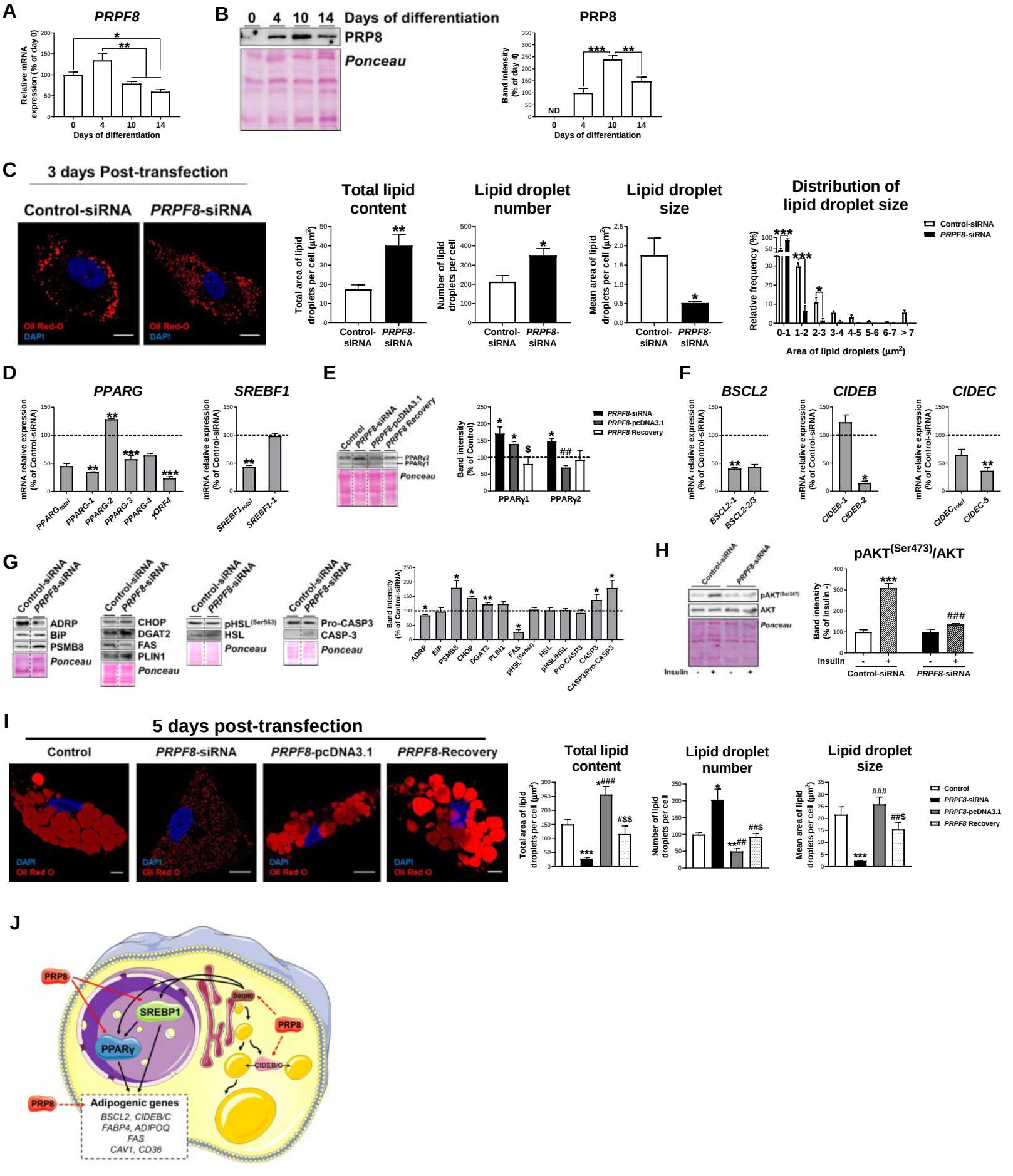
A
PRPF8
Relative mRNA expression (% of day 0)
Days of differentiation
B
0 4 10 14 Days of differentiation
PRP8
Ponceau
Band Intensity (% of day 4)
ND
C
3 days Post-transfection
Control-siRNA
PRPF8-siRNA
Oil Red-O
DAPI
Total lipid content
Total area of lipid droplets per cell (µm²)
Lipid droplet number
Number of lipid droplets per cell
Lipid droplet size
Mean area of lipid droplets per cell (µm²)
Distribution of lipid droplet size
Relative frequency (%)
Area of lipid droplets (µm²)
0-1 1-2 2-3 3-4 4-5 5-6 6-7 > 7
D
PPARG
SREBF1
mRNA relative expression (% of Control-siRNA)
PPARGtotal PPARG-1 PPARG-2 PPARG-3 PPARG-4 γORF4
SREBF1total SREBF1-1
E
Control PRPF8-siRNA PRPF8-pcDNA3.1 PRPF8 Recovery
PPARγ2
PPARγ1
Ponceau
Band intensity (% of Control)
PPARγ1 PPARγ2
PRPF8-siRNA
PRPF8-pcDNA3.1
PRPF8 Recovery
F
BSCL2
CIDEB
CIDEC
BSCL2-1 BSCL2-2/3
CIDEB-1 CIDEB-2
CIDECtotal CIDEC-5
G
Control-siRNA PRPF8-siRNA
ADRP
BiP
PSMB8
CHOP
DGAT2
FAS
PLIN1
pHSL(Ser563)
HSL
Pro-CASP3
CASP-3
Ponceau
Band intensity (% of Control-siRNA)
ADRP BiP PSMB8 CHOP DGAT2 PLIN1 FAS pHSL(Ser563) HSL pHSL/HSL Pro-CASP3 CASP3 CASP3/Pro-CASP3
H
Control-siRNA PRPF8-siRNA
pAKT(Ser347)
AKT
Ponceau
Insulin
pAKT(Ser473)/AKT
Band intensity (% of Insulin -)
Control-siRNA PRPF8-siRNA
I
5 days post-transfection
Control
PRPF8-siRNA
PRPF8-pcDNA3.1
PRPF8-Recovery
DAPI
Oil Red O
Total lipid content
Total area of lipid droplets per cell (µm²)
Lipid droplet number
Number of lipid droplets per cell
Lipid droplet size
Mean area of lipid droplets per cell (µm²)
Control
PRPF8-siRNA
PRPF8-pcDNA3.1
PRPF8 Recovery
J
PRP8
SREBP1
PPARγ
Seipin
CIDEB/C
Adipogenic genes
BSCL2, CIDEB/C
FABP4, ADIPOQ
FAS
CAV1, CD36

Figure 4

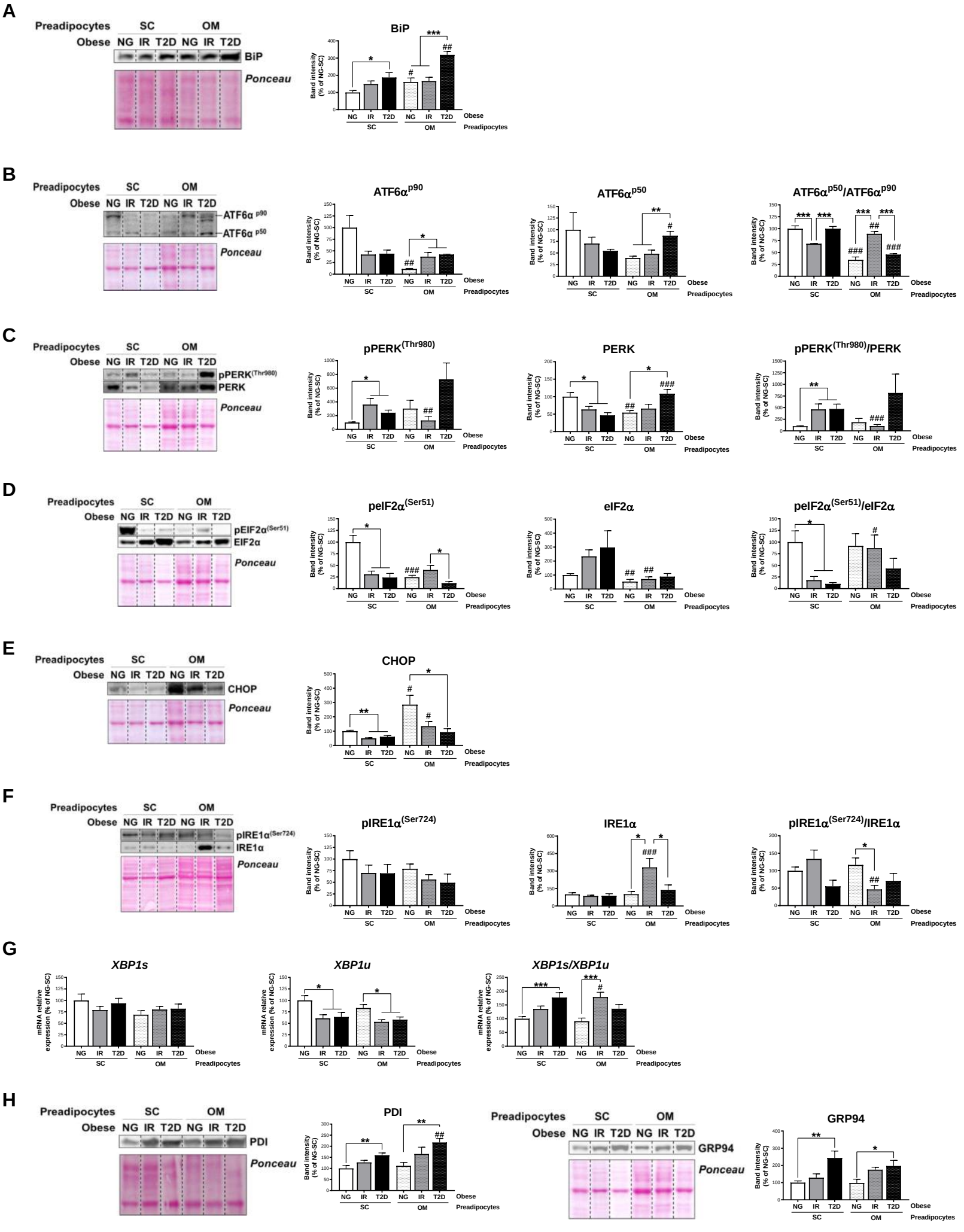
A
Preadipocytes SC OM
Obese NG IR T2D NG IR T2D
BiP
Ponceau
BiP
Band intensity (% of NG-SC)
B
ATF6α p90
ATF6α p50
ATF6α p50/ATF6α p90
C
pPERK(Thr980)
PERK
pPERK(Thr980)/PERK
D
peIF2α(Ser51)
EIF2α
peIF2α(Ser51)/eIF2α
E
CHOP
F
pIRE1α(Ser724)
IRE1α
pIRE1α(Ser724)/IRE1α
G
XBP1s
XBP1u
XBP1s/XBP1u
mRNA relative expression (% of NG-SC)
H
PDI
GRP94
Obese
Preadipocytes

Figure 5

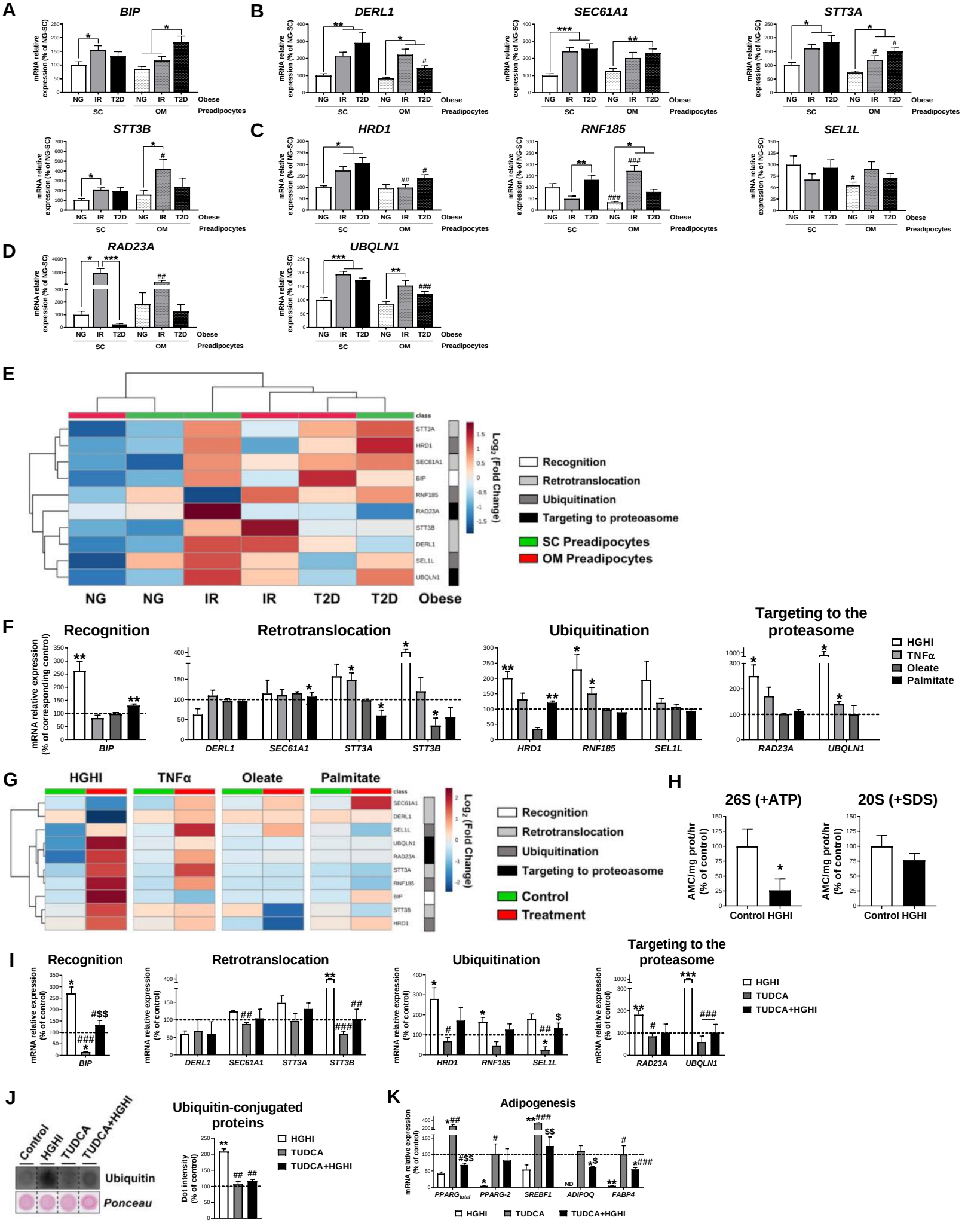
A
BIP
B
DERL1
SEC61A1
STT3A
STT3B
C
HRD1
RNF185
SEL1L
D
RAD23A
UBQLN1
mRNA relative expression (% of NG-SC)
NG IR T2D NG IR T2D
Obese
SC OM
Preadipocytes
E
class
STT3A
HRD1
SEC61A1
BIP
RNF185
RAD23A
STT3B
DERL1
SEL1L
UBQLN1
Log2 (Fold Change)
Recognition
Retrotranslocation
Ubiquitination
Targeting to proteoasome
SC Preadipocytes
OM Preadipocytes
NG NG IR IR T2D T2D Obese
F
Recognition
Retrotranslocation
Ubiquitination
Targeting to the proteasome
mRNA relative expression (% of corresponding control)
HGHI
TNFα
Oleate
Palmitate
G
HGHI
TNFα
Oleate
Palmitate
Control
Treatment
H
26S (+ATP)
20S (+SDS)
AMC/mg prot/hr (% of control)
Control HGHI
I
Recognition
Retrotranslocation
Ubiquitination
Targeting to the proteasome
mRNA relative expression (% of control)
HGHI
TUDCA
TUDCA+HGHI
J
Control
HGHI
TUDCA
TUDCA+HGHI
Ubiquitin
Ponceau
Ubiquitin-conjugated proteins
Dot intensity (% of control)
K
Adipogenesis
mRNA relative expression (% of control)
PPARGtotal
PPARG-2
SREBF1
ADIPOQ
FABP4
ND

Figure supplement 1

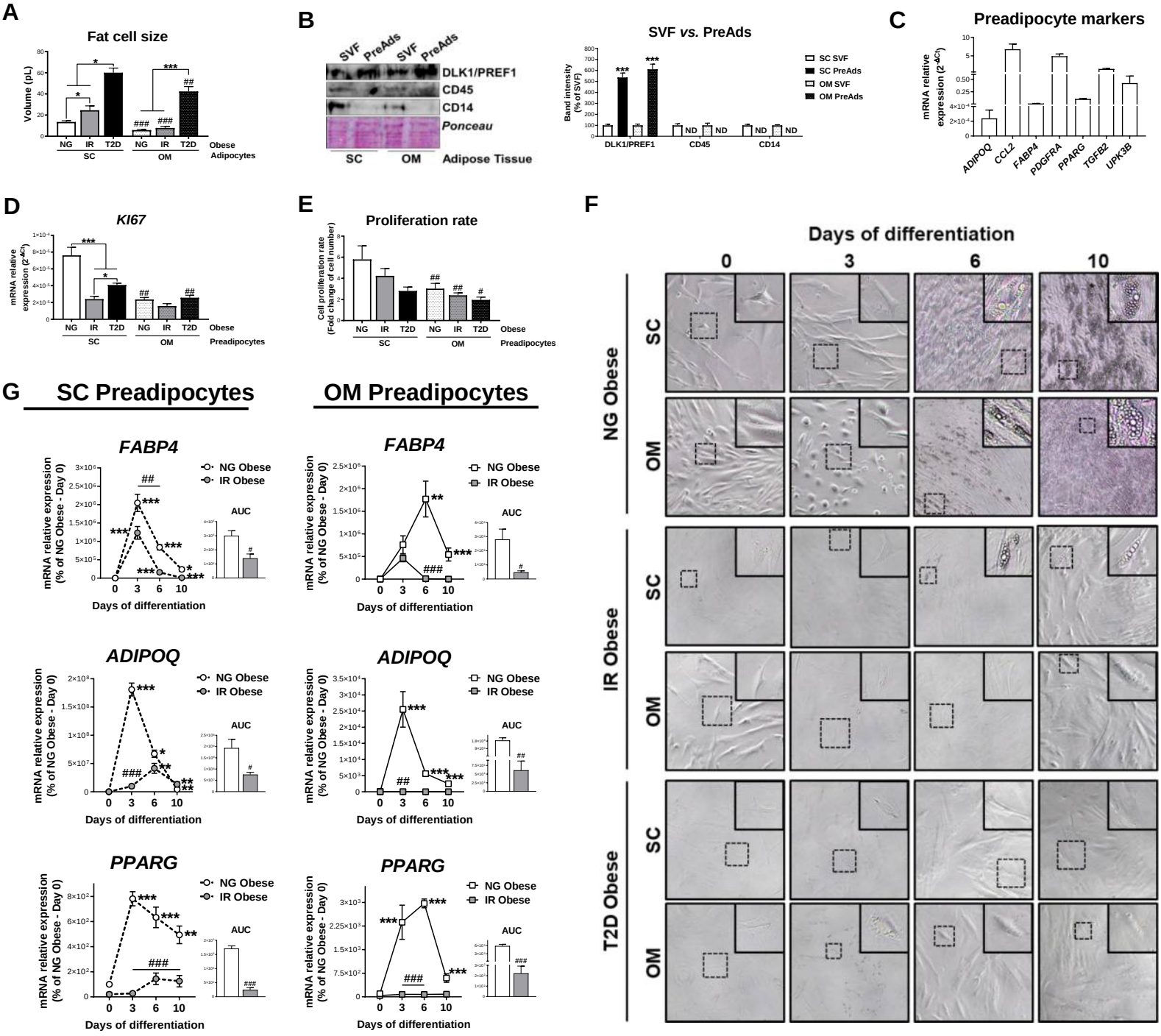

Figure supplement 2

A

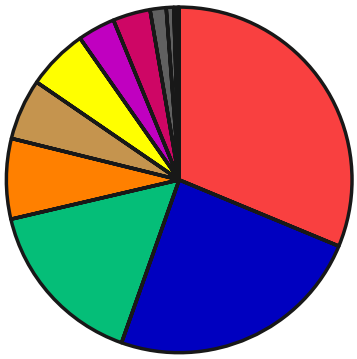

- 31.3% **Cellular Process** *(GO:0009987)*
- 24.2% **Metabolic Process** *(GO:0008152)*
- 15.9% **Cellular Component or Biogenesis** *(GO:0071840)*
- 7.5% **Localization** *(GO:0051179)*
- 5.7% **Biological Regulation** *(GO:0065007)*
- 5.7% **Response to Stimulus** *(GO:0050896)*
- 3.5% **Multicellular Organismal Process** *(GO:0032501)*
- 3.5% **Developmental Process** *(GO:0032502)*
- 1.5% **Immune System Process** *(GO:0002376)*
- 0.7% **Biological Adhesion** *(GO:0022610)*
- 0.4% **Locomotion** *(GO:0040011)*
- 0.3% **Reproduction** *(GO:0000003)*

B

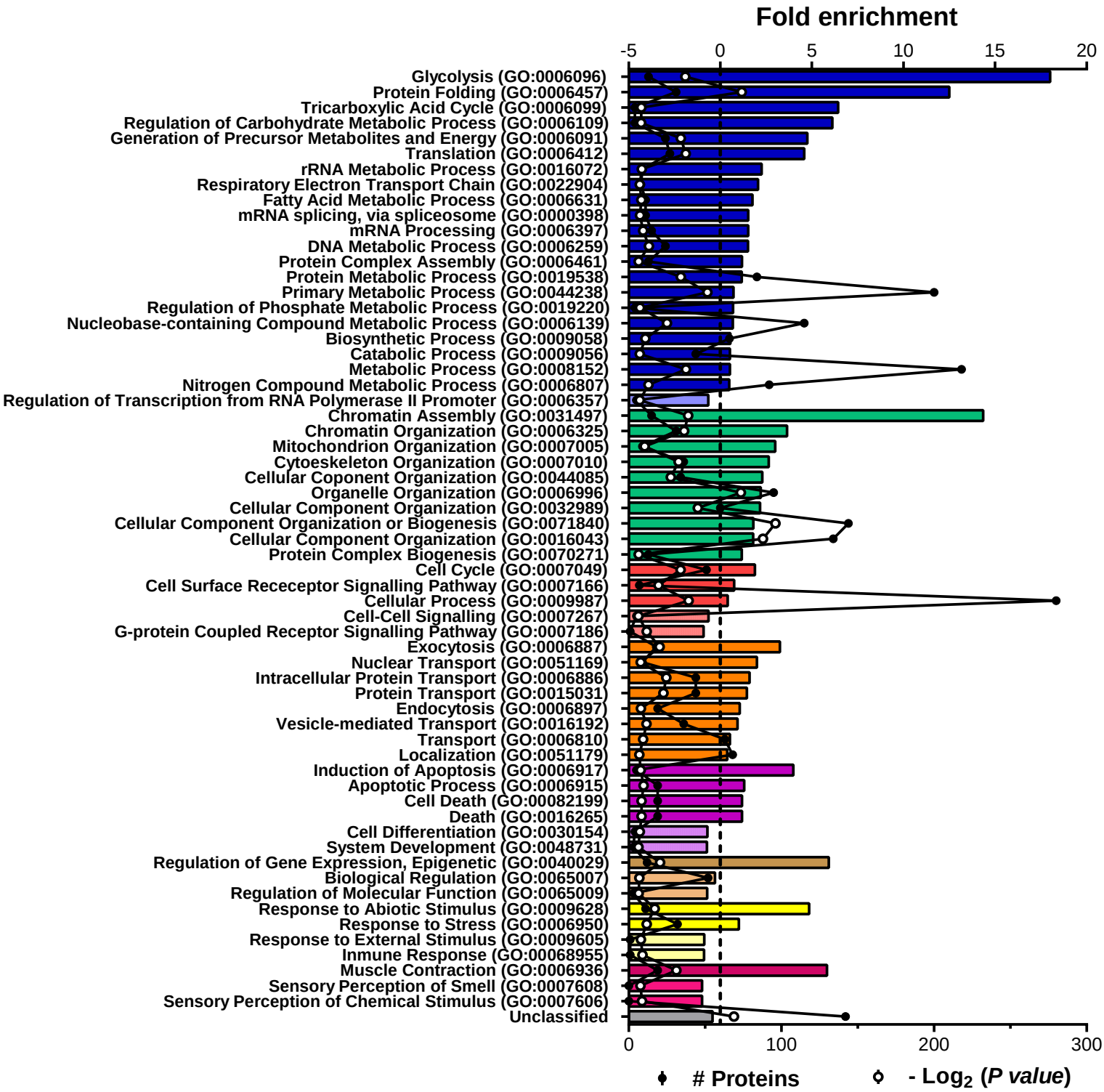

Figure supplement 3

A **SC Preadipocytes *vs.* OM Preadipocytes**

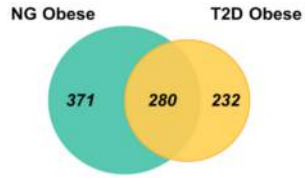

B **SC Preadipocytes *vs.* OM Preadipocytes dysregulated pathways in NG Obese**

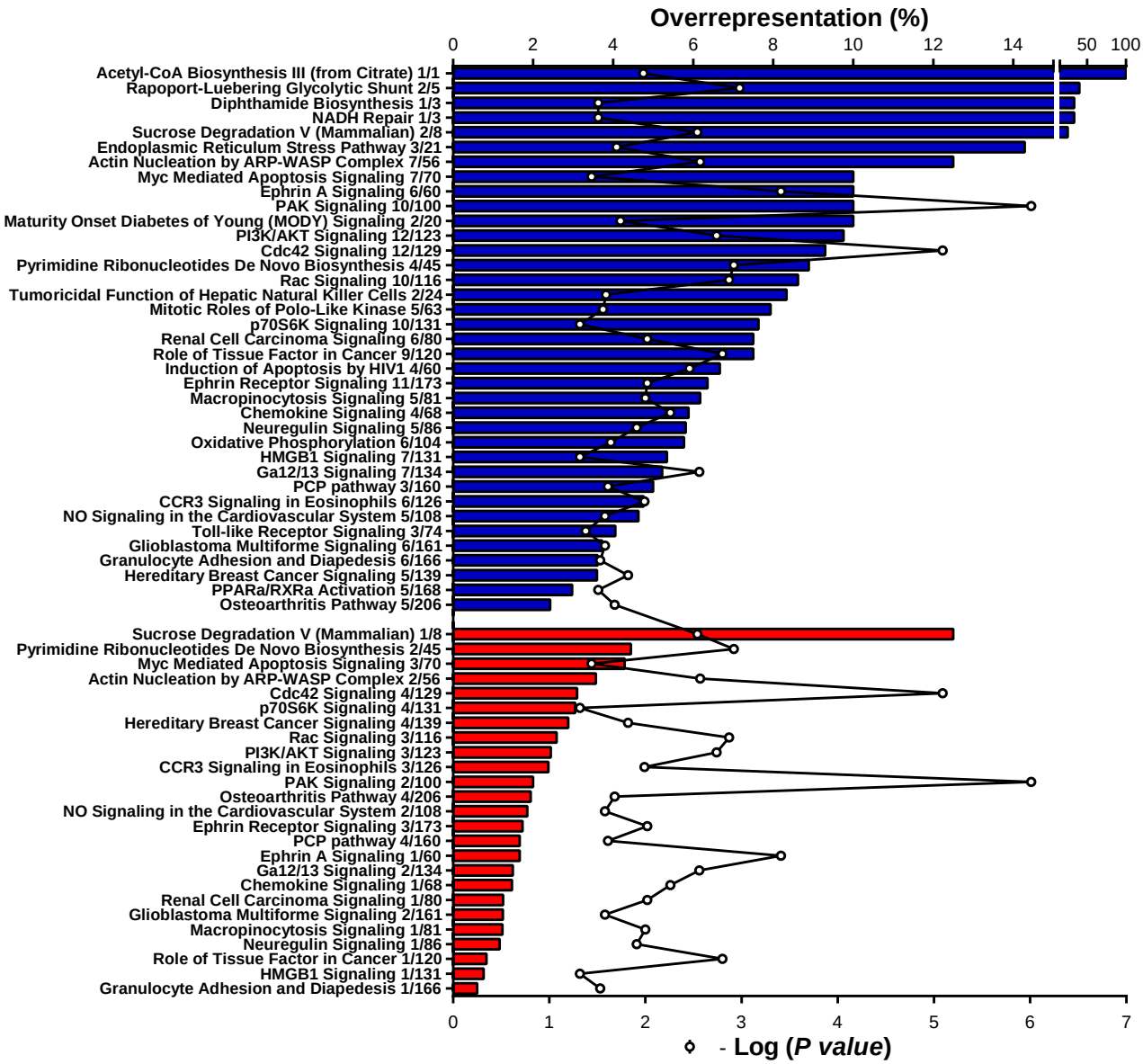

C **SC Preadipocytes *vs.* OM Preadipocytes dysregulated pathways in T2D Obese**

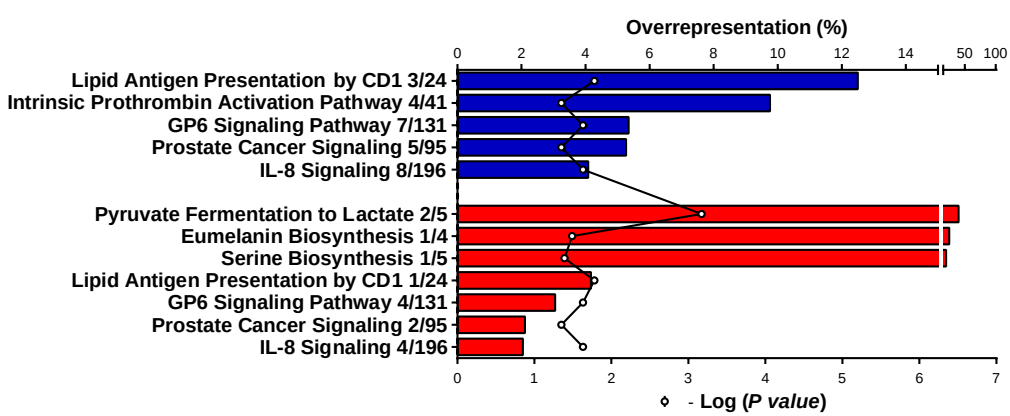

Figure supplement 4

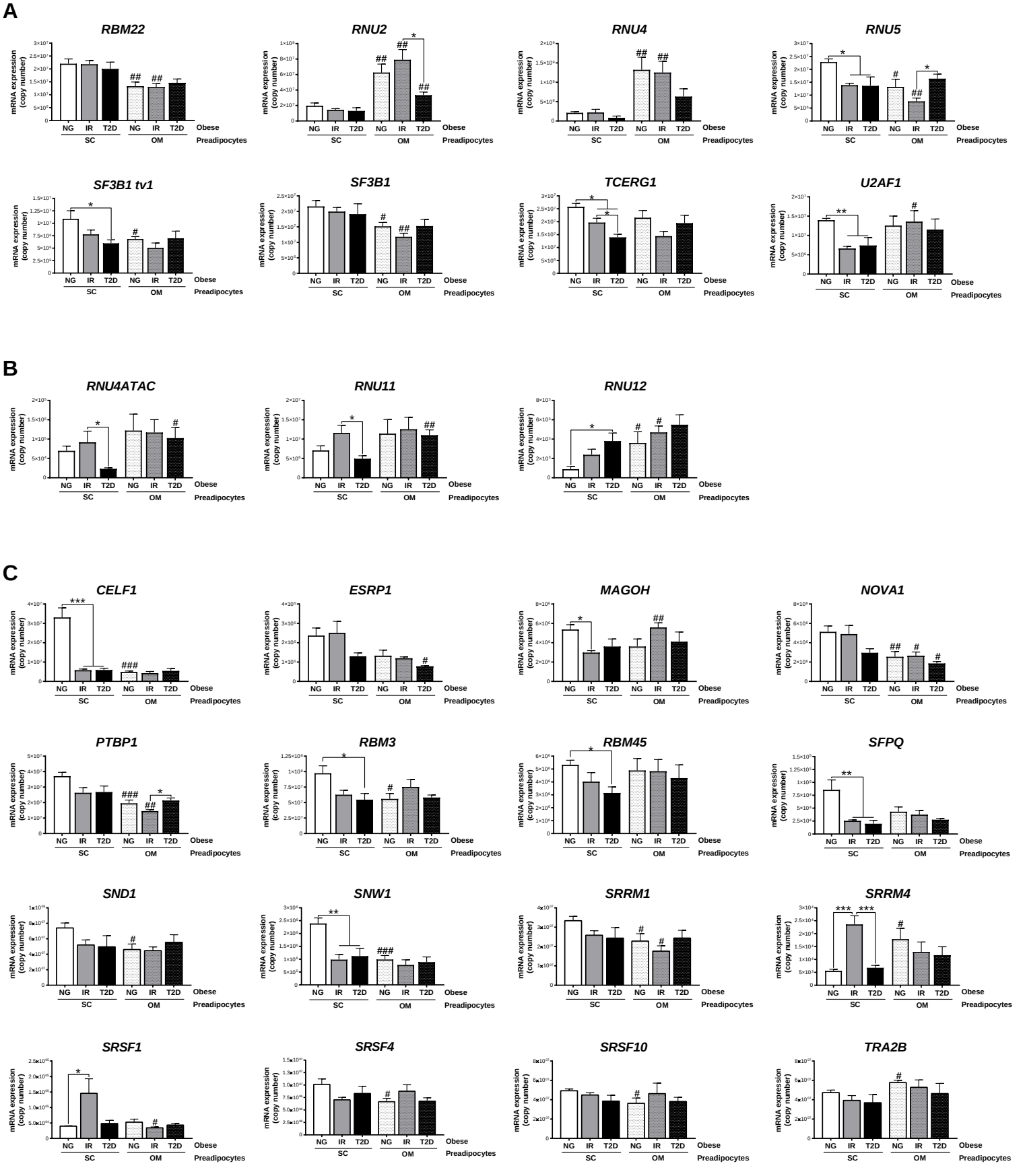

Figure supplement 5

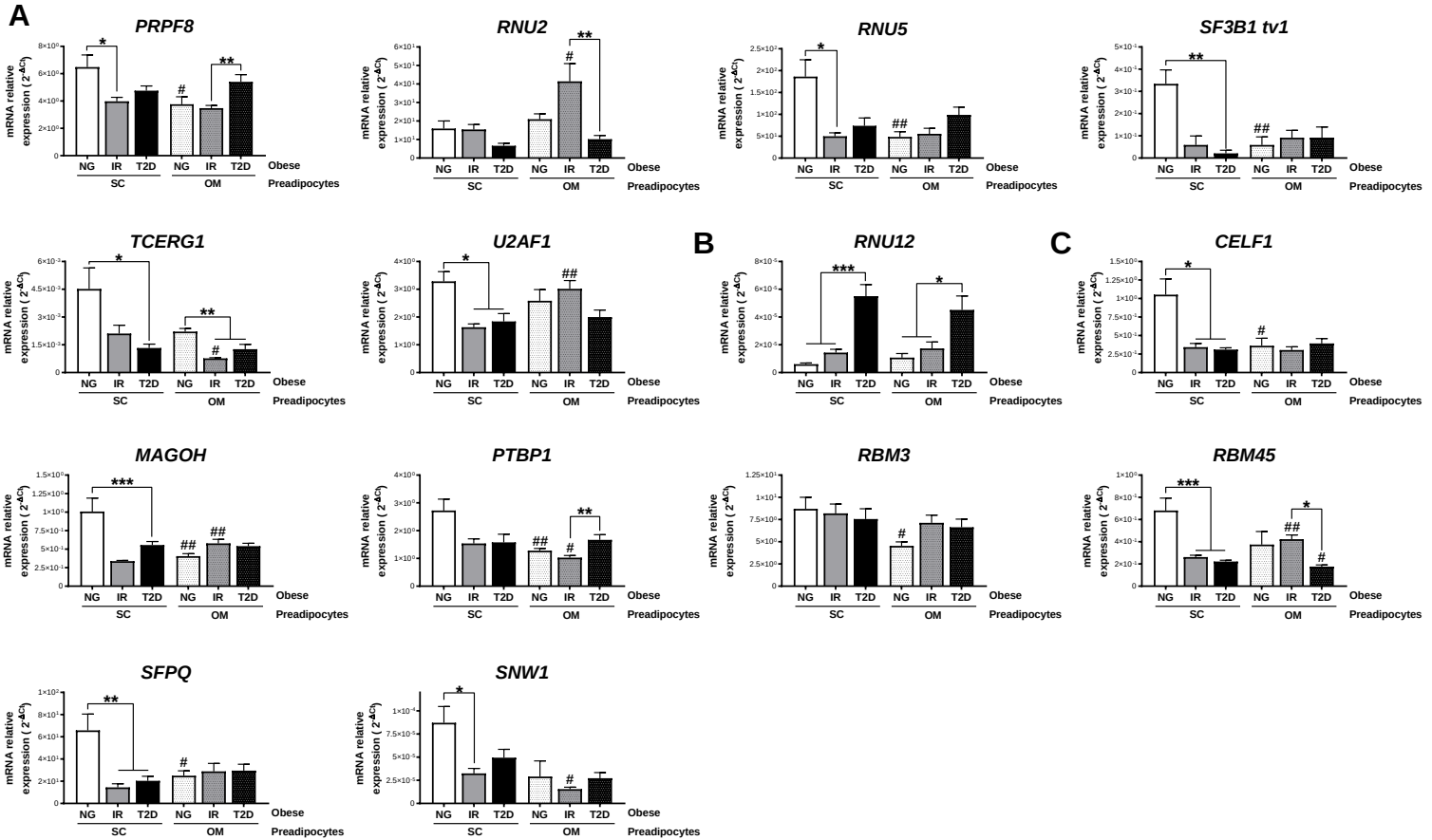

Figure supplement 6

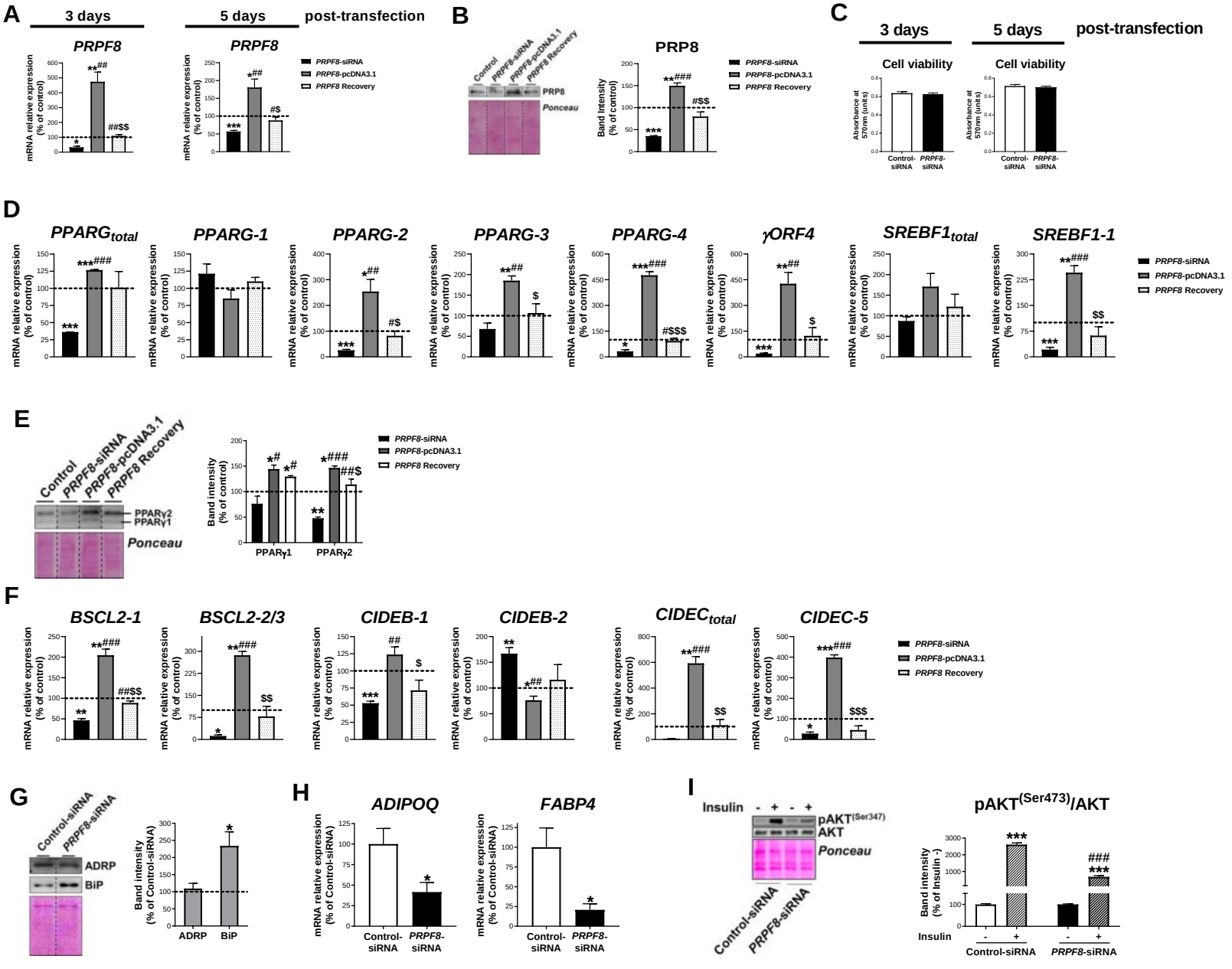

Figure supplement 7

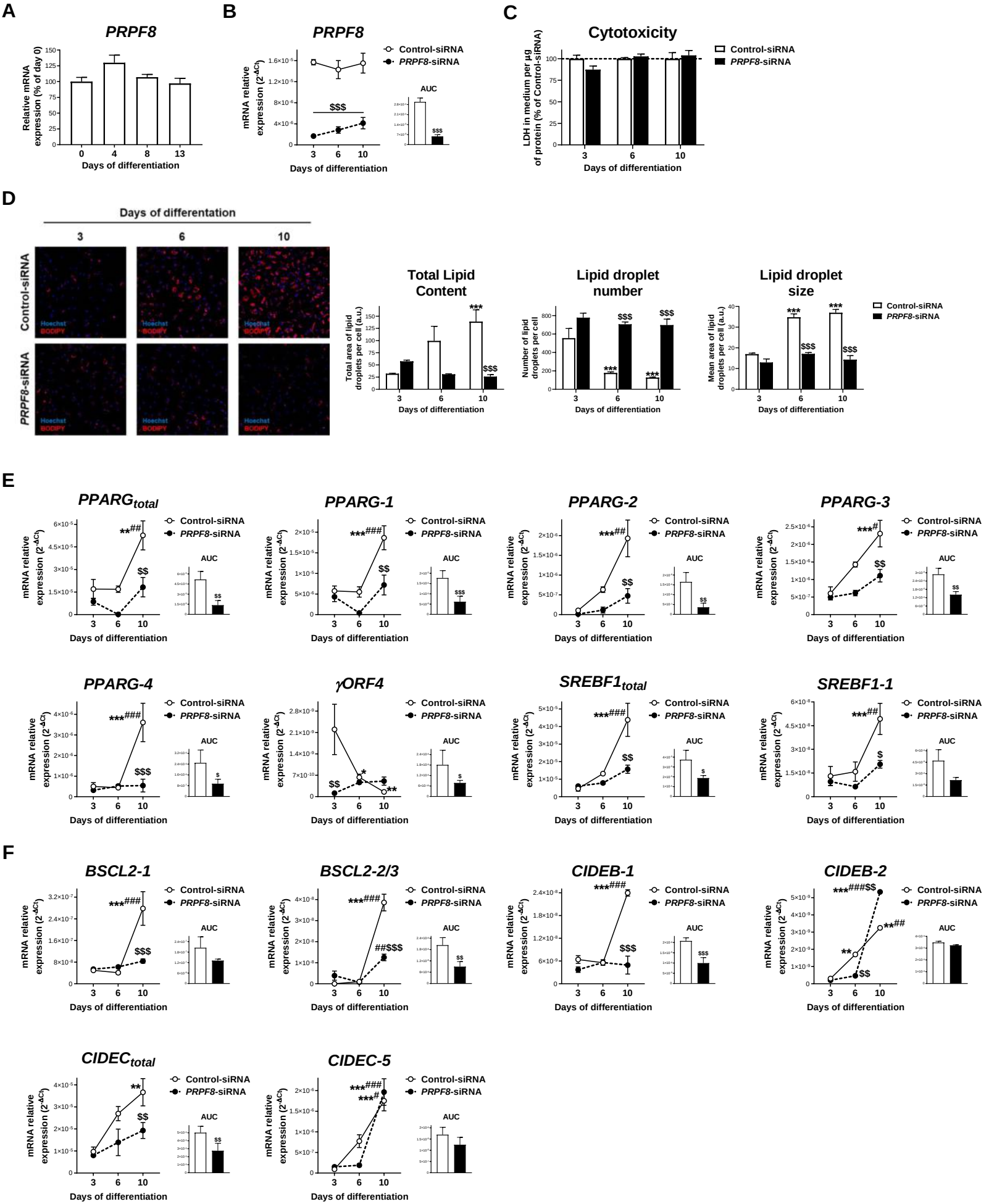

Figure supplement 8

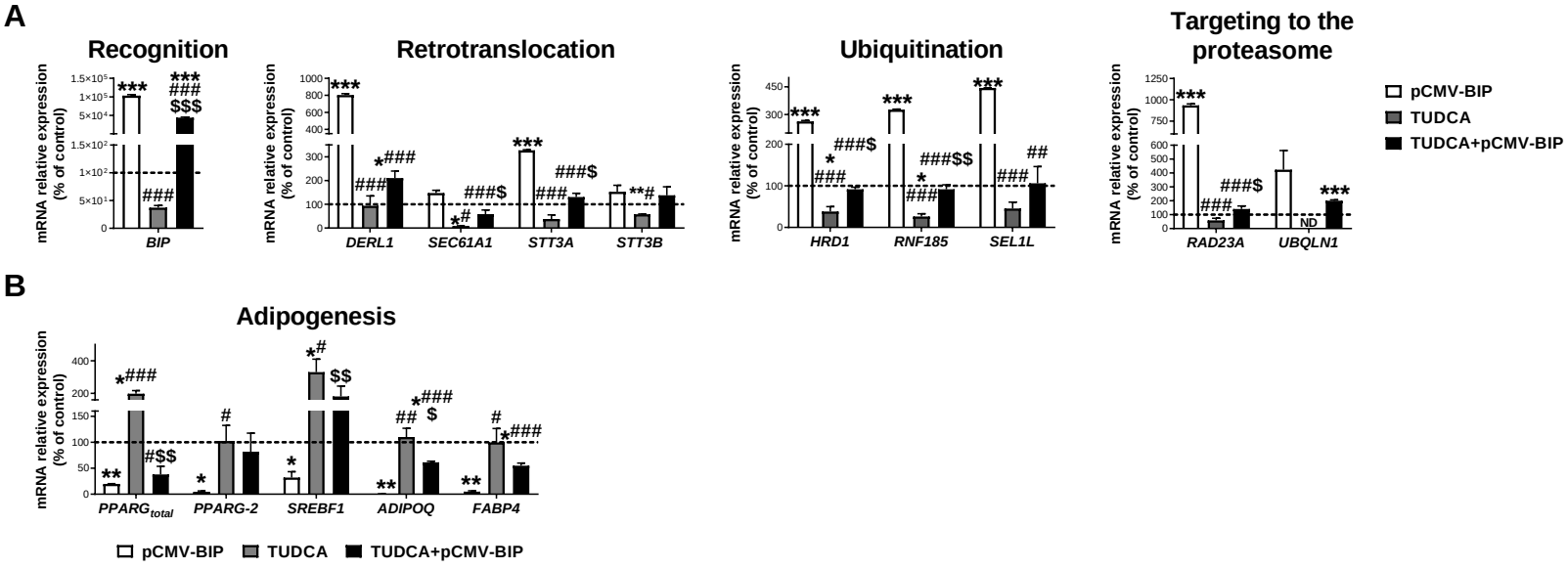

Figure supplement 9

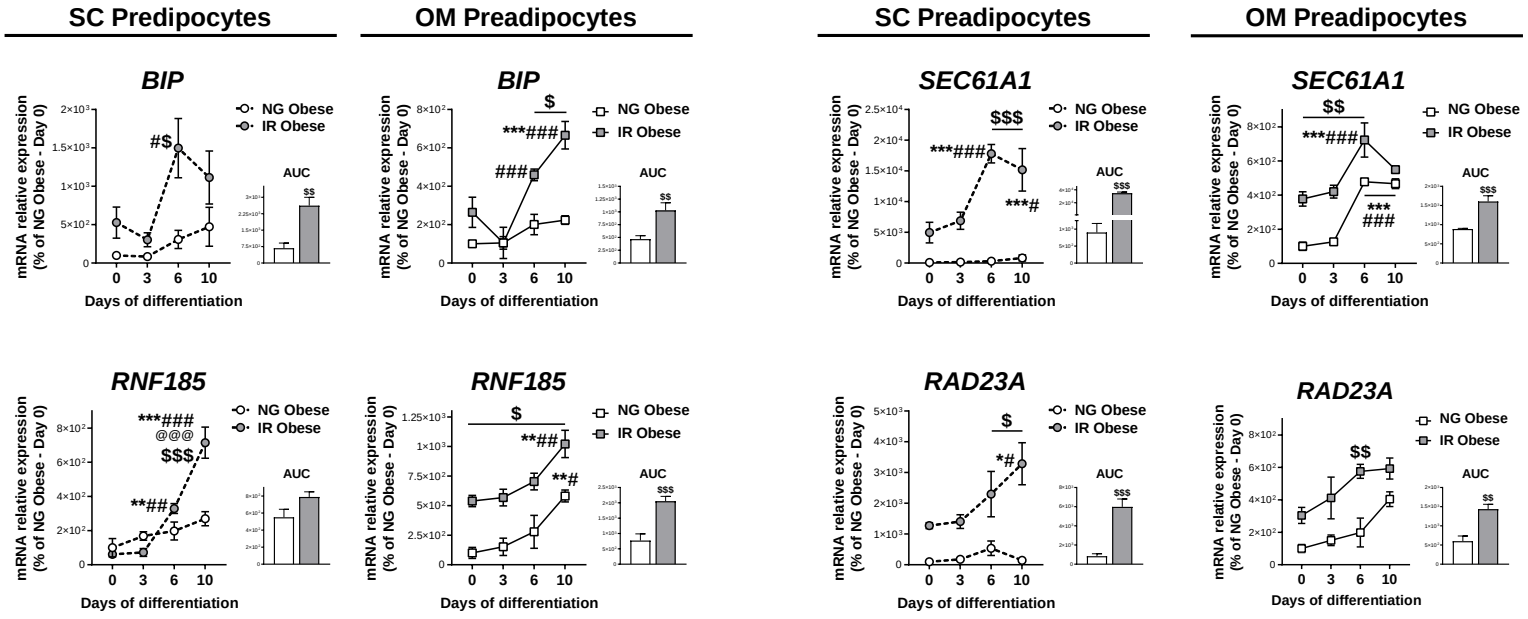

Figure supplement 10

A

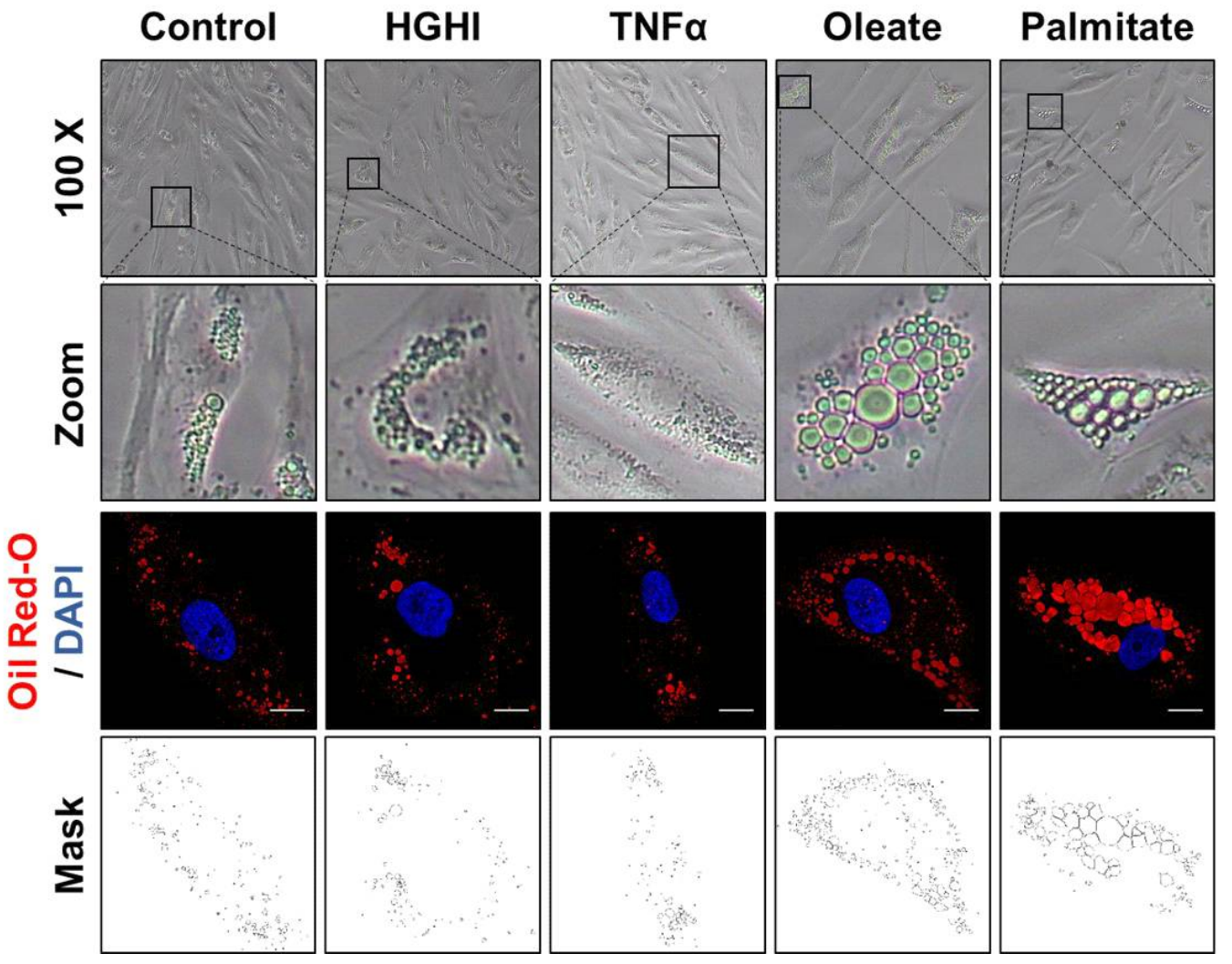

B

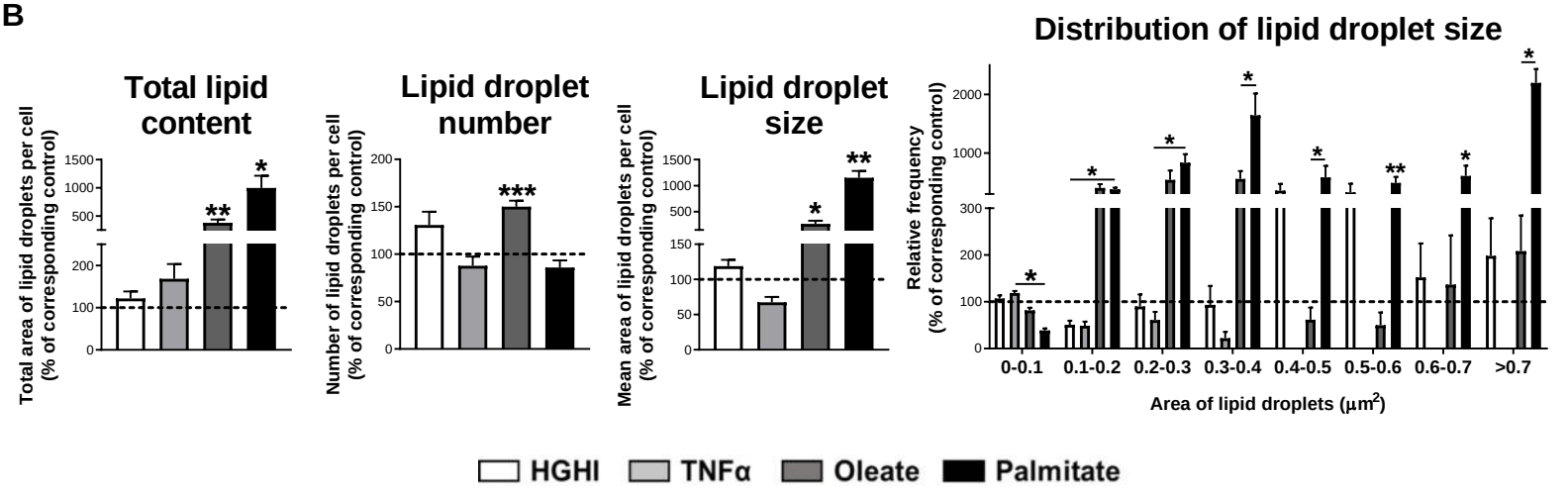
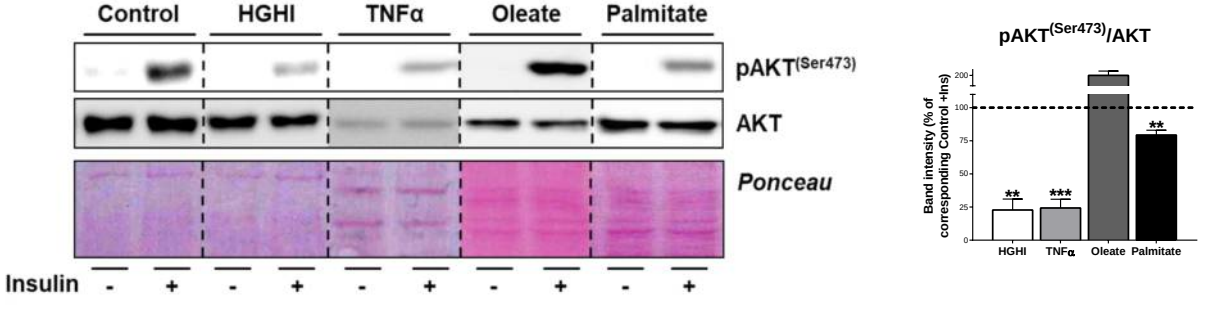
C